Seagrass mapping and monitoring along the coasts of Crete, Greece

Lemenkova Polina
March, 2011

Course Title:	Geo-Information Science and Earth Observation for Environmental Modelling and Management
Level:	Master of Science (MSc)
Course Duration:	September 2009 – March 2011
Consortium partners:	University of Southampton (UK) Lund University (Sweden) University of Warsaw (Poland) University of Twente, Faculty ITC (The Netherlands)

Seagrass mapping and monitoring along the coasts of Crete, Greece

by

Lemenkova Polina

Thesis submitted to the University of Twente, Faculty of Geo-Information Science and Earth Observation (ITC), in partial fulfilment of the requirements for the degree of Master of Science in Geo-information Science and Earth Observation for Environmental Modelling and Management

Thesis Assessment Board

Chair:	Prof. Dr. Andrew K. Skidmore
External Examiner	Dr. Małgorzata Roge-Wisniewska
First supervisor:	Mr. Valentijn Venus
Second supervisor:	Dr. Albertus G. Toxopeus

UNIVERSITY OF TWENTE.
ITC
FACULTY OF GEO-INFORMATION SCIENCE AND EARTH OBSERVATION

Disclaimer

This document describes work undertaken as part of a programme of study at the University of Twente, Faculty ITC. All views and opinions expressed therein remain the sole responsibility of the author, and do not necessarily represent those of the university.

I herewith certify that although I conferred with other researchers while preparing this document, and used a range of various research and literature resources, cited in the text, the content of this MSc Thesis document remains my own, original work, written by me personally.

Signed.................................(Lemenkova Polina)
Enschede, The Netherlands.
18th February 2011.

List of Acronyms

4AOP	Automatized Atmospheric Absorption Atlas Operational Release
6SV1	Second Simulation of a Satellite Signal in the Solar Spectrum, Version 1
ASCII	American Standard Code for Information Interchange
ANOVA	ANalysis of VAriance
ASTER	Advanced Spaceborne Thermal Emission and Reflection Radiometer
BRDF	Bidirectional Reflectance Distribution Function
CASI	Compact Airborne Spectrographic Imager
CDOM	Coloured Dissolved Organic Matter
CRTM	Community Radiative Transfer Model
CNES	Centre National d'Etudes Spatiales (of France)
CRTM	Community Radiative Transfer Model
CRTM	Community Radiative Transfer Model
CZCS	Coastal Zone Color Scanner
ENVISAT	ENVIronmental SATellite
ESA	European Space Agency
FOV	Field Of View
GDAL	Geospatial Data Abstraction Library
GIS	Geographic Information System
GPS	Global Positioning System
GRASS	Geographic Resources Analysis Support System
GRETL	GNU Regression, Econometrics and Time-series Library
HCMR	Hellenic Centre for Marine Research
GUI	Graphical User Interface
HyMap	Hyperspectral Mapper
ILWIS	Integrated Land and Water Information System
iPAQ	internet Pocket PC by CompAQ
KOPRA	Karlsruhe Optimized and Precise Radiative transfer Algorithm
LAD	Least Absolute Deviations
LAI	Leaf Area Index
Landsat TM	Landsat Thematic Mapper
Landsat ETM+	Landsat Enhanced Thematic Mapper Plus
MERIS	MEdium Resolution Imaging Spectrometer
MIPAS	Michelson Interferometer for Passive Atmospheric Sounding
MODIS	Moderate Resolution Imaging Spectroradiometer
NASA	National Aeronautics and Space Administration

NIR	Near-Infra-Red
NOAA	National Oceanic and Atmospheric Administration
OBC	On Board Calibration
OLS	Ordinary Least Squares
Olympus ST	Olympus Stylus Tough
RRTM	Rapid Radiative Transfer Model
RTTOV	Radiative Transfer for TIROS Operational Vertical Sounder
RTM	Radiative Transfer Model
SAM	Scanning Acoustic Microscope
SCUBA	Self Contained Underwater Breathing Apparatus
SeaWiFS	Sea-viewing Wide Field-of-view Sensor
SPOT	Satellite Pour l'Observation de la Terre
SPSS	Statistical Package for the Social Sciences
STDEV	Standard Deviation
SWIR	Short Wave InfraRed
TIR	Thermal InfraRed
TIROS	Television and Infrared Observation Satellite
Trios-RAMSES	RAdiance Measurement SEnSor
UML	Unified Modelling Language
USGS	U.S. Geological Survey
UV	UltraViolet (10 nm to 400 nm)
UVA	UltraViolet A, or long wave (315 nm-400 nm)
UVB	UltraViolet B, or medium wave (280 nm-315 nm)
VIS	VISible
VNIR	Visible and Near-InfraRed
WASI	WAter colour SImulator
WLS	Weighted Least Squares

Abstract

The seagrasses, a unique group of aquatic plants, create complex, extremely diversified and productive ecological systems in the littoral coastal zones. The only flowering plant in the world that is able to live completely submerged, seagrasses play vital role in the marine ecosystems of the World Ocean. Seagrasses are the most important component in the environmental food chain of the coastal ecosystems, being a vital food source for various marine species (e.g. fish, dugongs, turtles, swans), and a producer of organic matter, which is the very basis of the food web.
The *P.oceanica* seagrass is an endemic for the Mediterranean region, and a main species in the marine coastal environment of Greece. Meadows of *P.oceanica* are subjected to the human activities, because they occur in coastal areas, where they are affected both by anthropogenic and by climatic and environmental factors. Nowadays *P.oceanica* is in the alarming state of regression, because of the deterioration of the environment in the Mediterranean Sea. Due to these reasons, *P.oceanica* is a protected species since 1988 in some European countries (France). Monitoring *P.oceanica* is therefore an important contribution to the saving and protecting the environment of Mediterranean region.
The current MSc thesis focuses on the monitoring of seagrass *P.oceanica* along the northern coasts of Crete Island, Greece, and investigates the application of the remote sensing techniques for the seagrass mapping.
This research was articulated in two parts, where the first one involves an ecological approach to the seagrass distribution in various regions around the globe and the experience of seagrass monitoring nowadays. The second part of this work has technical character and investigates the application of the remote sensing techniques towards seagrass mapping. It, furthermore, focuses on the optical properties of the *P. oceanica* and other seafloor cover types, and studies distinguishability of various seafloor cover types. Studies of the optical characteristics of separate seafloor cover types were made with purpose to clarify, whether their spectral properties change with varying environmental conditions.
Special attention has been drawn on the role of environmental factors on the distribution of *P.oceanica* along the coasts of Crete, and in particular, how the optical properties of the seafloor cover types, i.e. spectral reflectance, are being changed under varying external conditions, e.g. water column, amount of suspended particles and sediments in the seawater, and water temperature. For this purpose we studied differences in the spectral reflectance of *P.oceanica* and other bottom cover types at three distinct depths. The diverse spectral values entail variations in optical properties of the seafloor cover types at changing environmental conditions. We applied WASI simulation techniques for the modelling of the optical parameters of

various seafloor cover types by various spaceborne imaging spectrometers (MERIS, SeaWiFS, CZCS and MODIS), in order to understand their suitability and possible limitations for the seagrass mapping.

Fieldwork research sites were presented by separate locations on the northern coast of Crete region (Ligaria, Agia Pelagia, Xerocampos). The additional measurements of the reflectance spectra of the seawater with and without sediments have been made in aquarium tank in 2009 by means of Trios-RAMSES spectroradiometer. Parallel to the collection of spectra signatures, we captured the imagery for the seagrass mapping, which consists of the aerial images from the Google Earth website and the satellite Landsat TM and Landsat ETM+ scenes.

Document Outline: Structure of the MSc Thesis

Chapter 1 is an introductory section. It describes general background of the research problem, outlines the need and actuality of the problem (including the environmental vulnerability of the seagrasses), and highlights limitations and possibilities of the remote sensing application for the current work. In this chapter we also set up research objectives, put research questions for hypothesis testing and sketch research approach for the proposed work.

In *Chapter 2* we review the existing literature and reported research experience on the similar problem: studies of spectral separability of various seafloor types, limitations and advantages of the remote sensing techniques applied for seagrass mapping seagrass ecology and mapping seagrass environment. We considered not only the Mediterranean environment, but also papers from Australian and Chinese scientists, because seagrass monitoring is most actively developed in the southern regions of our planet. The review of the existing RTM algorithms for the retrieval of the optical parameters, as well as description of various tools for the spectrometric measurements - are given in the same Chapter as well. More close attention has been given to the imaging hyperspectral radiometer Trios RAMSES, used for the data collection.

Chapter 3: Materials and methods deals with the methods and materials used in current work. We start our discussion from the fieldwork area location and describe tools and instruments used during the fieldwork, as well as sampling design. Procedures of the data pre-processing and capturing imagery from the Google Earth are also presented in the same chapter.

Chapter 4: Results presents to the reader the main results of the current MSc work, obtained during the processing fieldwork and other collected data. It starts from the review of the collected data from different sources, then describes the modelling component of the research, namely WASI colour simulation and plotted resulting graphs. We also discuss here the particularities of various sensors, suitable enough for deriving radiometric information to discriminate sand from the seagrass. Furthermore, this chapter includes analysis of the spectral signatures of various seafloor cover types in conditions of changing environment, possibility and limitations for *P.oceanica* spectral discrimination, statistical analysis of the data sets and mapping based on images processing.

Chapter 5: Discussion and conclusions summarizes and briefly discusses again the main results, reported in detail in a previous chapter. This chapter proposes some final discussions to the reader, and comes to the main research outcomes.

Finally, we suggest some recommendations for any further research focusing on the seagrass environment along the coasts of Crete (or other Mediterranean areas) in the final *Chapter 6: "Recommendations"*.

A lot of plotted graphs, statistical outcomes, tables, auxiliary (yet relevant to our research) pictures and images, illustrating our work - are collected in the *Appendices*. Due to the standard editorial limitations of the current MSc work, it was not possible to include all them to the main chapters. However, we tried to make the structure of the *Appendices* most clear and easy-readable as possible, by dividing the *Appendices* into 10 various sub-sections and referencing to them from the main text where necessary.

The *Bibliography* section includes literature and internet resources used for the current work. The cross-referencing and web hyper-referencing are used in the whole document to make reading more quick, effective and informative.

All persons mentioned in the current document are listed in the *Index of People*.

An *Index of Concepts* is placed in the end of the Document to help the reader find what he is looking for.

To my elder brother and best friend, **Peter Lemenkov**

Acknowledgements

This research was carried out at the University of Twente, Faculty of Geo-Information Science and Earth Observation (ITC), Enschede, the Netherlands, under the financial support of the EU Erasmus Mundus Scholarship.

I thank my scientific supervisors, Dr. *Albertus G.Toxopeus* and Mr. *Valentijn Venus* from the ITC, Department of Natural Resources, for our successful scientific collaboration, help and discussions of my research work.
I also express them my most sincere appreciations for our fieldwork on Crete. Besides scientific routine, we had an unforgettable time spent together.
Personally, I would like to mention that I have visited Greece the first time in my life, and I will always remember my Cretan period-2010 and Ligaria beach.

I extend my gratitude to the staff of the Museum of Natural History, the University of Crete, especially to Dr. *Petros Limberakis* and his colleagues, for their assistance during our fieldwork, providing us with all necessary equipment (e.g. SCUBA gear diving, instruments for underwater measurements, etc). I also appreciate their very warm, personal attitude and interest towards our research.

My sincere gratitude goes again to Mr. *Valentijn Venus* for his generous providing me with a lot of spatial data relevant to my research (e.g. such as digital vector layers of Crete island, raster georeferenced maps for the whole island for my GIS project, Excel spreadsheets, etc). Without these vital data the implementation of this project would have hardly been possible. I am also thankful to him for the technical help in Google Earth imagery capturing, using GDAL technologies and assistance during the fieldwork (videometric underwater footage, consultancies in seagrass observation and monitoring, driving boat, etc).

My special thank to his personal, friendly support in various situations on Crete.
I am thankful to Dr. rer. nat. *Peter Gege*, the software developer from the Earth Observation Centre of the German Space Agency, for his generous consultancies concerning the technical question about WASI that arose during my work. I am thankful for all his explanations and articles given to me via e-mail.

My special thanks are addressed to my elder brother, Mr. *Peter Lemenkov*, the software developer from the ipPort, for his priceless numerous advices and constant professional support throughout my career. He encouraged me to use various very useful software and tools, always gave me necessary recommendations and precious help, thus highly contributing to my professional growth.
My special thank for his help with Python scripting. I am also heartfelt thankful to him for his personal friendship and support.

I am grateful to Mr. *Willem Nieuwenhuis*, the software developer from the ITC, Department of Natural Resources, for shared technology of Google Earth aerial imagery grabbing and for his consultancy with ASTER imagery.

I thank Dr. Ir. *Cornelis A.J.M. de Bie* from the Department of Natural Resource, ITC, for his patient sharing of iPAQ knowledge during my Polish fieldwork in summer 2010. I used these skills on Crete.

Many thanks for Dr. *Dingtian Yang* from the South China Sea Institute of Oceanology, our colleague in problem of seagrass monitoring and research, for his handing over the data of spectral reflectance of Thalassia seagrass, which enabled to compare spectra of various seagrass types.

Table of contents

List of figures

List of tables

List of Tools

Software and utilities used in the current work:

- ArcGIS 10.0: mapping, data integration and spatial analysis
- Erdas Imagine: imagery processing and classification
- WASI Water Color Simulator, for modelling optical water properties under changing environment
- iPAQ and GPS for data capture during the fieldwork
- BibTEX, for management of bibliography and reference database
- LATEX, for document typesetting, formatting and performing pdf output
- Python language, for writing auxiliary scripts (e.g. raw data interpolation)
- Gnuplot for plotting graphs
- Open Office : document typesetting, data pre-processing and preliminary statistical evaluation
- Calc2LATEX : converting spreadsheets into LATEX environment
- SPSS (PASW Statistics 18) : statistical data edition and analysis
- Gretl: Gnu Regression, Econometrics and Time-series Library for statistic analysis
- StarUML , Dia , ArgoUML: diagramming flowcharts for work algorithms
- Inkscape: drawing
- Notepad++: auxiliary text editing and raw data formatting
- OpenEV: used for raster Google Earth imagery visualisation and analysis

Keywords

P.oceanica, seagrass, spectral reflectance, remote sensing, WASI, Google Earth

1 Introduction

1.1 Summary

The seagrasses, a unique group of aquatic plants growing submerged in the sea water, with root-like structures (rhizoms) buried in the sediments and vertical elongate leaves. A flowering plant, completely adapted to marine environment, they are however, more closely related to the lily family (*Liliaceae*) than to the true grass, despite their name "*seagrass*", caused by the ribbon-like, grassy leaves [90].

Seagrasses create unique, complex, extremely diversified and productive ecological systems in the littoral coastal zones between 0-50 meters in shallow waters all over the world [58], and serve as valuable environmental indicators for the marine ecosystems health. Seagrasses are closely connected and linked with complex interactions to other vegetation types, e.g. mangroves, coral reefs, etc. An important constructing component of littoral ecosystems, seagrass contributes significantly to their structure and functioning.

The adaptation to the salt waters is evidently influenced the global distribution of the seagrasses, limiting it to shallow coastal areas. A number of critical conditions determine growth of the seagrass, including general climatic characteristics of the area, i.e. temperature, day length, geological and geomorphological conditions, e.g. soft type of sediments (sand or mud), shallow depths, as well as chemical and physical parameters of the water: salinity, waves [85]. The seagrass *Posidonia oceanica* (further *P.oceanica*) is a key species to inhabit littoral of the Mediterranean Sea, see Fig. 1.1

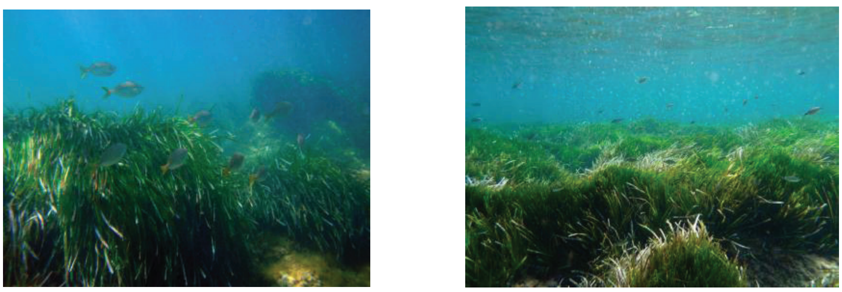

Figure 1.1: Seagrass Posidonia Oceanica

and is widely spread along the coasts of Crete [33] . It plays an important role in a number of geomorphological and ecological processes. Namely, it is a source of food for herbivorous fauna as well as helter zones for fish and other marine organisms; it contributes to the nutrient recycling; it provides sediments stability by reducing the degree of water movements, etc [40].

The purpose of current MSc research work aims to apply methods of remote sensing analysis, including Radiative Transfer Models (RTM), GIS-based spatial analysis, processing and classification of satellite and aerial photos, as well as videometric underwater footage, towards mapping and environmental monitoring of seagrass *P. oceanica* along the selected locations of the northern coasts of Crete island, Greece. The technical implementation is based on WASI RTM software, GIS (ILWIS, Erdas Imagine and ArcGIS), using aerial and satellite images and the results of the underwater videometric measurements.

1.2 Background

1.2.1 Global distribution of the seagrasses

Globally, there are 58 recognized and described seagrass species (Fig. 1.2, Fig.1.4), belonging to two orders (*Hydrocharitales* and *Najadales*), four families (*Hydrocharitaceae, Posidoniaceae, Cymodoceaceae* and *Zosteraceae*), and 12 genera (*Enhalus, Thalassia, Halophila, Posidonia, Syringodium, Halodule, Cymodocea, Amphibolis, Thalassodendron, Zostera, Heterozostera* and *Phyllospandix*) [71].

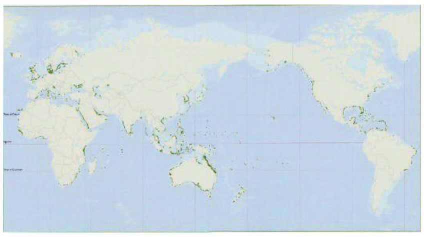

Figure 1.2. Distribution of seagrasses in the world. Source:[48]

The distribution of the seagrasses is strongly influenced by several environmental factors, which include climate (mostly, tropical and temperate areas), bathymetry (shallow shelf zones), hydrological particularities (chemical content of water, nutricient availability and turbidity of waves), and geological characteristics - sedimentation and cover types of the seafloor [88]. There are four European seagrass species in Mediterranean area [12]: *Zostera marina*, *Zostera noltii, Cymodocea nodosa* and *P.oceanica*. In Greece, the common species are *P.oceanica (L.) Delile, Cymodocea nodosa (Ucria) Ascherson, Zostera noltii Hornemann* and *Halophila stipulacea* [3]. These species differ in morphological and phenological features (Fig. 1.3) as well as in structure and dynamics. Thus, *Cymodocea nodosa* is considered the pioneer species of *P.oceanica* beds, the latter species forming the last stage. When *P. oceanica* beds regresses, *C. nodosa* often replaces them [53]; as a result, *P.oceanica, C. nodosa*, and *Z. noltii* do not form mixed persistent stands [16].

1.2.2 Ecological significance of the seagrasses

Seagrass plays vital role in the marine ecosystems of the world ocean. Seagrasses are the only flowering plant in the world that is able to live completely submerged. Seagrass is a habitat for numerous marine fish species [103], source of primary production and food for fish, turtles and other organisms, which gives them special environmental value [104].

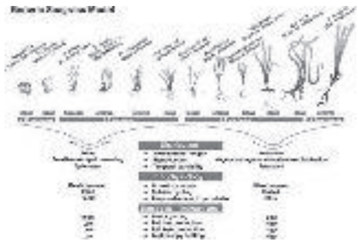

Figure 1.3: Morphology of different types of seagrasses.

Seagrass meadows produce enormous quantities of organic matter (leaves, epiphytes), which constitutes the basis of the food web both within and outside the ecosystem [45].

Finally, seagrasses are an important component in the environmental "food chain" of the coastal ecosystems, being the food source for dugongs, turtles, swans and various fish [18]. Due to their wide distribution, meadows size, easy collection and abundance, sensitivity to the modifications of the coastal zone and their important role in maintaining coastal water quality and clarity, seagrass is perfect indicator and descriptor of the environmental health of marine ecosystems, and is highly suitable for the environmental monitoring [118].

Being often confused with marine “algae”, “seagrasses” are vastly different from them. There are fundamental differences between both marine organisms, the major of them should be briefly mentioned: first, seagrasses are true plants with root system and leaves which photosynthesise, have complex structure and create landscape-similar vast formations on the colonised seafloor areas with soft sediment, whereas algae are simple organisms that can only holdfast; secondly, seagrasses are complex vascular plants with reproductive mechanism such as fruits, seeds and spores, while algae have simple few cell structure with spores and gametes; finally, seagrasses uptake nutrient through root system, while algae nourish directly from the water column [31]. There are other differences between “seagrass” and “algae” but they go beyond the scope of this work.

1.2.3 Environmental vulnerability of the seagrasses

Meadows of P. oceanica are subjected to the human activities, as they occur in coastal areas, where they can be affected both directly [92] or indirectly, through the impact on the quality of waters and sediments [32]. As *P.oceanica* is a long-living plant with a slow growth rate, the anthropogenic modifications of the coastal zone, happening more rapidly than the capacity of the plant to adapt to these changes, reduce its distribution area [95]. One of the main drivers of seagrass decline is, for instance, the location of the fish farming near the seagrass meadows. The negative effects of the sedimentation of waste particles in the farm vicinities on *P.oceanica* meadows are diverse and complex, and may cause benthic deterioration, accumulation of organic matter and seagrass decline [60]. Seagrasses are subject to anthropogenic nutrient (N and P) loading, which may occasionally cause morphological (e.g. leaf length) and physiological (e.g. chlorophyll and nitrogen content of the leaves) responses towards changed environmental conditions [72, 73].

Figure 1.4: Distribution of seagrass in relation to mean ocean temperature. Source: [107]

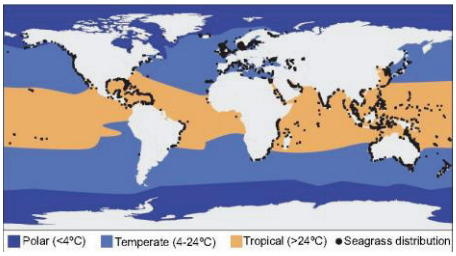

The detailed research of the fish farm-induced decline of the seagrass meadows [29]reports the relationships of fish farm organic and nutrient content in the sediments with dynamics of the key seagrass species (P. oceanica) in the Mediterranean Sea. Nowadays *P.oceanica* is in the alarming state of regression due to the deterioration of the environment in the Mediterranean Sea [122]. Due to these reasons, *P.oceanica* is a protected species since 1988 in some European countries [40], and its presence serves as an indicator of a stable healthy environment. Among other negative factors, affecting both growth and status of the seagrasses the environmental contaminants can be mentioned, e.g. thermal, sewage, dredging and chemical pollution as well as any other kind of maritime works, e.g. trawling and anchoring of boats [122]. Other human activities that cause degrading of the seagrass are recreational boating, commercial overexploitation of coastal resources, eutrophication [88].

Besides anthropogenic factors, various biochemical, climatic and environmental processes can cause negative influence on seagrass distribution. Seagrass is exposed to threats from the global climate and environmental change, i.e. increases in sea surface temperature; sea level rise; increased frequency and intensity of storms and waves; local decrease of water quality, increased sedimentation, contamination and nitrification; desiccation; salinity fluctuations; nutrient changes; suspended sediments [11]. These stress-drivers can alone result in large-scale seagrass degradation, but often seagrass undergo simultaneous affects from several of these factors together. It naturally increases the environmental pressing and leads to drastic loss of very large areas of seagrass globally [107]. In tropical areas, where most of seagrasses are located (Fig.1.4), seagrasses are subject to catastrophic extinction and loss, due to the cyclones, typhoons, storms, regular floods and increased rainfalls. Recovery from such events can take up to several years and often it is only possible by means of the seed reserves from the local environmental surveys [89].

Other threats for seagrasses in tropical areas are increased nutrient availability in the coastal zones, increased eutrophication and invasive macroalgae. These processes have strong affect on the status of the seagrass meadows, and often lead to their complete disappearance [59]. Other environmental threat for the seagrasses arises as a result of the environmental struggle and competition for existence among species. Thus, meadows of *P.oceanica* in the Mediterranean Sea (Fig.1.5) are presently facing invasion by alien algal species, particularly in areas where *P.oceanica* is already degrading, stressed, have gaps and patchy structure in meadows and show other signs of regression [97].

Seagrasses are vulnerable fragile species, important for the marine coastal ecosystems, especially for the protection of the beach structure. However, the facts about seagrass global degrading sound worrying: about 54 percent of the total seagrass meadows have lost any part of their area; the areas, where the seagrass ecosystems are degrading or lost, are not located in a specific area or continent, but registered globally; since 1980s global losses of the seagrasses on our planet is equal to two football fields per hour [94].

1.2.4 General characteristics of *Posidonia oceanica*

Morphology of *P.oceanica*. The endemic Mediterranean seagrass *Posidonia oceanica* (further *P.oceanica*), is a main species in marine coastal environment of Greece, forming, despite its slow growth, the largest, most widespread, homogeneous and dense meadows (Fig.1.1) in the Mediterranean between 5 and 40 m depth [52].

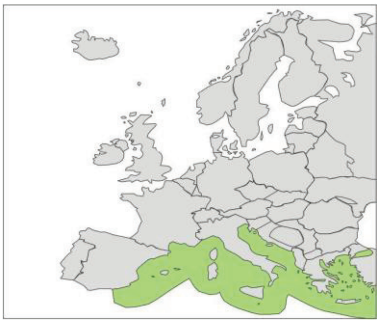

Figure 1.5: Geographical distribution of *P.oceanica*. Source: [12].

The dominant and most productive coastal ecosystem of the Mediterranean, *P.oceanica* is spatially restricted to the Mediterranean area (Fig.1.5), with its extension limited by the western part of the Mediterranean Sea where cold Atlantic waters enter Gibraltar and mix with warm Mediterranean waters, thus decreasing its temperature. Morphologically *P.oceanica* consists of long, 5-12 mm broad, “hairy-like” leaves, 3-4 mm thick roots and short rhizomes (0.5-2.0 mm). The leaves are, perhaps, the most particular characteristics of

P.oceanica, making it highly recognizable and distinguishable from other seagrasses (Fig.1.6): having

usual length of 20-40 cm, in some cases they can reach up to 1 m [12] (Fig.1.8).

Figure 1.6: P.oceanica. Source [77]

Growing *P.oceanica* make a meadows which, in turn, consist of smaller patches, called “matte” (Fig.1.7), a monumental construction made by the growth of rhizomes and leaves with entangled roots and entrapped sediment [39]. Representing one of the most productive Mediterranean ecosystems, *P.oceanica* usually serves as a perfect biological indicator for the assessment of the quality of waters and environmental health [14]. Some authors [49, 96] used status and population dynamics of *P.oceanica* as indicators for the evaluation of the meadow health status. There are several environmental factors, determining the growth of the P.oceanica.

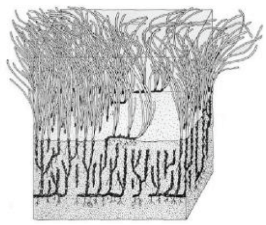

Figure 1.7: Scheme of matte structure of P.Oceanica. Source [116]

Phenology of *P.oceanica* The adaptation to dry-summer subtropical climate reduces its extension to Mediterranean area only (Fig.1.5). Besides, the distribution of the seagrasses changes with water depth: it is noticed [34] that the highest flowering density is usually in the 4-7 m depth. *P.oceanica* flowers appeared in shallow stands in September while in November only in stands deeper than 15 m. This time delay is caused by the different maximum summer temperatures at those depths [16].

The phenology of *P.oceanica* is also affected by the coastal bathymetry: in the isolated meadows in shallow waters plants have shorter and falciform leaves, compared to ones in the deeper and central areas [34]. In *P.oceanica* flower abundance is related to the structure of the meadow with the maximal flower density in the densest stands, while the occurrence of flowering is regulated by environmental factors [16].

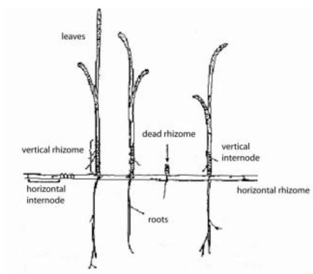

Figure 1.8: Structure and components of P.oceanica. Source [28]

Phenology of the *P.oceanica* undergoes modifications with varying seasons during the year: during the flowering period (ca 3 months long) the number of leaves on the flowering shoots decrease. Changes of the leaf growth also appear in the flowering shoots with longer oldest leaves and shorter and narrower leaves induced during the flowering [46].

1.3 Research problem

Monitoring of the marine benthic ecosystems of seagrasses is essential for the environmental assessment of the coastal zones. It increases our knowledge of the seagrass ecology, highlights threats to the seagrass and preventing them from possible losses and degrading and improves techniques and methods of the underwater-based observations. Mapping the seagrass contributes to the evaluating of the seagrass current distribution, analysis of its dynamics and changes over time, as well as estimations of the degrading of seagrass meadows for the purpose of the coastal management. Precise, correct and up-to-date information about the distribution of *P.oceanica* is necessary for the sustainable conservation of the marine environment and ecosystems in Mediterranean area, being an important contribution to the environmental coastal zone management [117]. However, mapping the seagrass has limitations due to the specific location and characteristics of the research object. The remote sensing techniques have traditionally been widely used for the seagrass monitoring.

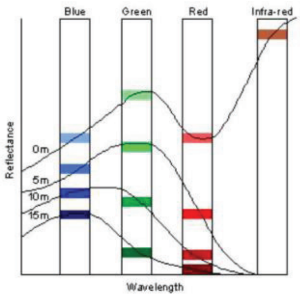

Figure 1.9: Spectra of the seagrass on different depths (0 - 15m). Source [35]

The general overview of the application of various remote sensing data types (colour, infrared, and black and white images) for the seagrass monitoring shows its high suitability and potential as a research method [112, 84]. The using of the aerial photographs as base maps for the seagrass meadows mapping is, perhaps, the most traditional application [86, 68, 111] . The results of the image processing of colour aerial photographs for the monitoring of littoral environment with seagrass beds have been reported by several authors [67, 138, 47] . Satellite imagery processing has also being used for the seagrass monitoring, due to their accuracy, repeatability and information value as a source of data [27], enabling regular temporal coverage over the large remote areas and providing a cost-effective approach for the mapping of the remotely located feature, such as underwater vegetation [64]. Satellite images provide with detailed information on seagrass canopy and other environmental indicators [41]. Various research papers report successful application of the image processing for the seagrass mapping [20, 26, 38, 47, 62, 64, 68, 78, 82, 83, 99, 112, 111, 109, 117, 120, 122, 129, 138]. The application of the remote sensing data towards seagrass mapping is based on the spectral reflectance characteristics of the *P.oceanica* seagrass, which enable its spectral discrimination from spectra of other seafloor types. It is proved [132] that the spectral signatures of different species of tropical seagrasses are well distinguishable from each other.

The application of the methods of images classification for seagrass mapping is based on the classifying the pixels on the image according to their spectral reflectance values (Fig.1.7) [38], so that the seafloor can be divided into several types: sand, rock, *P. oceanica*, other vegetation, etc. Other example of monitoring of *P.oceanica* using remote sensing techniques [20] reports the application of the CZCS images towards the case study of the Italian coast and shows successful results of the neural-based classification using Isodata method of supervised classification. In case of *P.oceanica* meadows aerial and satellite images are particularly suited for the surveying shallow waters [110] enabling to distinguish seagrass formations and dynamics of the temporal evolution of seagrass meadows over the research area [112]. However, using space borne satellite imagery for the seagrass mapping has certain limitations, due to the uncertainties of the spectral signature of the seagrass at higher depths (Fig.1.7), as well as some optical particularities, e.g. light refraction under water, unevenness of the water surface, depths, etc. Some problems can also arise in the images interpretations, as quite different objects may have similar spectral reflectance, e.g. seagrass, dark-coloured bottom patches (mud), macroalgae. The *in-situ* fieldwork including underwater videographic measurements is an important part of the seagrass monitoring, and has been successfully applied towards seagrass mapping [51]. The underwater measurements are used to validate the results and to receive detailed, accurate and precise data for the selected locations. The underwater measurements cannot be applied for the whole research area, however it provides with detailed monitoring along the route of the boat. Therefore, in the selected locations it becomes a useful tool for the assessment of the distribution, density and coverage of the seagrass along the track log. Besides, the underwater observations using scuba diving equipment have been conducted for the measurements of depths.

1.4 Research objective

The current MSc research aims to explore the environmental conditions for the spatial distribution of *P.oceanica* seagrass along the northern coast of Crete Island, based on the remote sensing and GIS techniques, knowledge about the coastal environment in Crete and integration of various data from the following sources:

i. spectra of *P.oceanica*, carbonate sand, silt and other seafloor types
ii. satellite imagery: Landsat TM, Landsat ETM+
iii. aerial photos: Google Earth
iv. *in-situ* fieldwork data of underwater videographic measurements
v. vector GIS layers.

Although there are a variety of environmental factors that contribute to the spectral reflectance, the most important ones are water column height and seafloor fraction. It is because spectra of the seagrass *P.oceanica* vary qualitatively over the depths interval of 0.5–4 m, and secondly, the content and cover fraction of the seafloor have the most distinctive effect on the spectral reflectance of the water. In the environmental conditions of Crete Island, *P.oceanica* may grow at depths up to six meters; however, the most usual depth is four meters, which caused our decision to focus on depths up to 4 meters and use these depths for further WASI modelling. Therefore, in the current research we focus on these two major factors, and study the response of the water reflectance towards changing conditions of the water column depth and seafloor bottom cover fraction (seagrass and carbonate sand).

The research aims to explore the limitations of the application of the Radiative Transfer Models (further RTMs) and remote sensing techniques towards the study of the environmental properties of the *P.oceanica* meadows distribution over the selected locations of northern Crete. The main research objective is monitoring the seagrass *P.oceanica* in selected areas of Crete and analyzing the environmental conditions for the growth of *P.oceanica*.

This research is supported by the *in-situ* measurements in two selected locations of the northern coast of Crete (Ligaria beach in Agia Pelagia district and Xerocampos), using following methods of the remote sensing techniques: spectral modelling by means of the RTM Water Colour Simulator WASI, underwater videometric measurements made by Olympus camera, aerial Google Earth and satellite images from different sources, spatial GIS and statistical analysis.

1.4.1 General objective

The main objective of this study is to analyse the optical properties of the seagrass P.oceanica and other seafloor types, and to apply the remote sensing techniques towards the investigation of the seagrass distribution in selected locations along the northern coast of Crete. General objectives:

1) Analysing spectral reflectance of *P.oceanica* and other seafloor cover types by means of radiative transfer model tools (RTMs), using WASI.
2) Mapping spatial distribution of the seagrass *P.oceanica* over selected locations along the northern coasts of Crete Island.

1.4.2 Specific objectives

a) To study narrow-band spectral reflectance properties of *P.oceanica* and other seafloor cover types (sand and silt) using WASI water colour simulation software
b) To use methods of the *in situ* diving observations and underwater videometric measurements by Olympus camera in order to receive large-scale imagery of the *P.oceanica* mattes

c) To apply remote sensing data (Google Earth aerial images, Landsat TM and ETM+ satellite images) for the monitoring of the seagrass meadows distribution
d) To perform supervised images classification for the thematic mapping of the *P.oceanica* seagrass distribution along the selected locations over the coasts of northern Crete.

1.5 Research questions

1. Is *P.oceanica* spectrally distinct from carbonate sand with varying *in-situ* environmental conditions?
2. Do broadband and hyperspectral sensors provide enough radiometric information for spectral discrimination of seagrass, and therefore, can be used for mapping of *P.oceanica*?

1.6 Hypotheses

A statistical testing will be used to compare between the spectral responses of the different seafloor cover types (i.e. sand and *P. oceanica*), whether it is spectrally distinct and at least one pair is statistically different at every spectral band.

For the research question 1 the Hypothesis Ho claims: seagrass types are not spectrally distinct from other seafloor types with varying *in-situ* conditions, which means Ho: $\mu1 = \mu2 = \mu3 = ... = \mu n$. The alternative Hypothesis Ha claims the opposite statement: seagrass is spectrally distinct with varying *in-situ* conditions, Ho: $\mu \neq \mu2 \neq \mu3 \neq ... \neq \mu n$.

For the research question 2 the Hypothesis Ho claims: broadband and hyperspectral remote sensing data cannot be used for the mapping of *P.oceanica,* because they do not provide enough radiometric information to discriminate sand from seagrass, which means Ho: $\mu1 = \mu2 = \mu3 = ... = \mu n$. The alternative Hypothesis Ha claims the opposite statement: broadband and hyperspectral sensors do prove to provide enough radiometric information to discriminate sand from seagrass, Ho: $\mu \neq \mu2 \neq \mu3 \neq ... \neq \mu n$, and can therefore be used for the seagrass mapping..

The distribution of the spectral responses at every spectral band is assumed to be normal, as well as the equality of the statistical variances. The hypothesis testing is suggested to be carried out using the ANOVA statistical test. The purpose of ANOVA test is to visualize in an effective and quick way the spectral differences between seagrass species and their spatial distribution. Thus, the key hypotheses of the research will be tested to prove whether the results of the research are accurate, reasonable and correct.

1.7. Assumptions

The general research assumption, used in this work, in order to make feasible application of the remote sensing methods, includes some statements about the in-situ atmospheric conditions, viewing angle, wave backscattering and other optical properties of the environment. They all definitely play a certain role and impact final results of optical measurements, but for practical reasons we have chosen to ignore their contribution in the spectral separability of seafloor cover types. We briefly list below general research assumptions for the optical properties of the environmental variables used in this study.

Weather conditions for the measurements are assumed to be perfect: clear, sunny, windless days. Otherwise wind roughens water surface causing sun glitter, and values of spectral reflectance may contain disturbances. Sky radiance might be influenced by multiple reflectances between the sea surface albedo and the atmosphere and in general, the sky radiance increases rapidly while viewing zenith angle is near to 90º (i.e. in the evening hours). Therefore, ideally measurements should be done at noon, with as low zenith angle (Fig. A.3) as possible; otherwise, if the solar zenith angle is too high (e.g. approaching 60-70 degrees), received data may contain noise. For WASI simulations reflection factor of sky radiance is taken as 0.0201 with simulated ideal conditions: viewing angle (0º = nadir). The interval of water temperature taken as default lies in the diapason 17-25 degrees as to simulate the conditions of the Mediterranean Sea. However, in real time conditions the sun zenith angle of 45º has been accepted as suitable.

The anisotropy factor of upwelling radiation or the quality (Q-) factor, showing the directionally dependency of the radiance, is taken as 5. We accepted some values of model-specific optical parameters as default values at WASI simulator which are shown in the Table 3.1. Thus, the concentration of phytoplankton is accepted at the interval of 0.035 – 0.089 mg-1 and concentration of large suspended particles is given to 8. Reference wavelength for CDOM (Gelbstoff) absorption is equal to 440. The backscattering is accepted to be 0.00144m-1. The coefficient of attenuation remains equal to 1.0546, as set up by default at WASI.

We also assume that concentration of non-chlorophyll particles (absorption at $\lambda 0$) as well as concentration of small suspended particles is equal to zero, so we do not count them in this work. Exponent of CDOM (Gelbstoff) absorption is accepted as 0.0140. Finally, the BDRF of bottom reflectance (sand), which defines the reflection of light is at an opaque surface (Fig.A.7), is assumed to be 0.318 sr -1.

1.8. Research approach

Seagrass consistent monitoring and mapping is necessary and important for the sustainable coastal development and conservation measures. Earlier, many seagrass meadows have been destroyed by human activities in the coastal zone, mainly due to the ignorance of their existence, because information on the seagrass bed exact location was not available [22]. Well-time seagrass observations and mapping enables precise control of its spatial distribution, detection of any changes in the seagrass landscapes, highlights potential environmental threats in the coastal zone (e.g. declining of meadows) before they become unmanageable for the coastal management services. Choosing the right and most effective approach method for the seagrass monitoring is essential. Remote sensing methods alone, though having evident advantages, are insufficient, because satellite images of underwater habitats are notoriously difficult to identify and interpret. The best research method should be based on the integrated approach, well described in various scientific works [13, 98, 70] , which includes combination of various techniques of the seagrass monitoring, i.e. remote sensing imagery classification of aerial and satellite images, GIS-based spatial analysis and ground *in-situ* surveys.

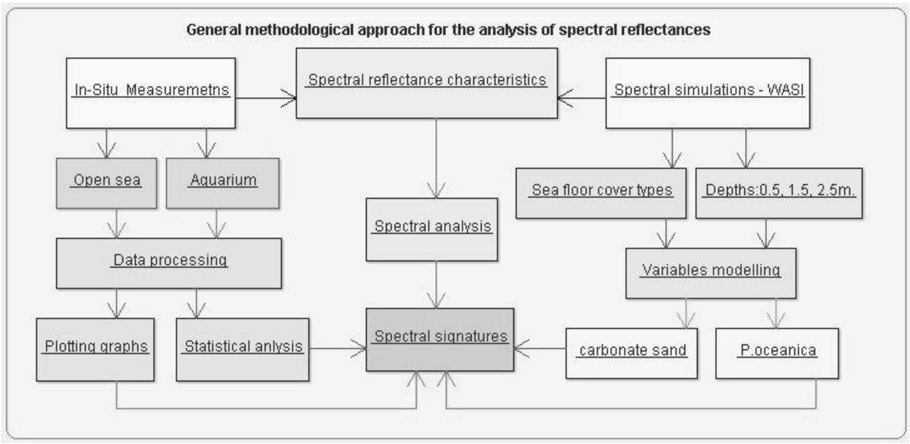

Figure 1.10: General methodological approach for the analysis of spectral signatures. ArgoUML.

The current study is based on the application of the remote sensing data, broadband satellite imagery, aerial images and the results of the underwater videographic measurements towards seagrass mapping (Fig.A.51 Image classification is based on the principle of the differentiation between the spectral signatures of various seafloor cover types (Fig.1.8). The spectrum of light coming up from the ocean surface in shallow waters keeps information on the optical properties of the seawater components and benthic substrate which can be read from their spectral signatures [139]. The pre-processing of the images includes imagery corrections for atmospheric noises and effects of the water column. Reflectance spectra of the seagrass canopy at different depths of the water-column are analysed for the discrimination of their spectral signatures, enabling to separate various seafloor types during classification. The results of the of imagery classification are analysed for the detection of the dynamics in *P.oceanica* seagrass distribution along the northern coasts of Crete. Aerial imagery from Google Earth with high spatial resolution (Fig.A.52), suitable for the large-scale detailed mapping of seagrass mattes, is used for the improvement of the accuracy of large seagrass meadows and separate mattes within the meadows. The *in situ* underwater videometric measurements of the seafloor are collected during the fieldwork in Crete, for the validation of the classification results and to determine the exact current distribution of the *P.oceanica* meadows. The image processing includes steps of the remote sensing techniques, i.e. calibration, masking from land and cloud, atmospheric correction, sea surface glint and depth effects correction as recommended [83]. During the image classification working step the training sites for the supervised classification methods are designed, as well as its control and trials of different classification approaches (Unsupervised, K-means or Isodata; Supervised, Maximum Likelihood).

2 Seagrass monitoring: overview of literature and research resources

2.1 Seagrass global monitoring: history and perspectives

Mapping and monitoring the seagrass is important for the environmental assessment of the marine ecosystems in coastal areas. Regular tracking of current distribution of seagrass meadows, based on correct information and cartographic visualization of seagrasses, is a preventive environmental management, which helps to analyse potential environmental risks of coastal areas, decrease of the number of species, loss of meadows and patches of the seagrasses. The tradition of global seagrass mapping though has not a very long history comparing to the terrestrial cartography, due to the technical difficulties of underwater observations.

However, nowadays is has become a rapidly developing, increasingly popular and challenging research branch. Regular observations and monitoring of the seagrasses are known since 1960s, mainly in tropical regions (Australia). Since that time traditional methods of the seagrass monitoring and common recommendations are being elaborated. The development of the underwater SCUBA diving equipment and devices enabled to conduct underwater detailed measurements and observations largely contributed to the improvement of the traditional in-situ observations of seagrass. From the other side, development of the remote sensing methods and data acquisition from space contributed to the new methods of seagrass mapping, using distance approach and generally based on images classification.

Various global seagrass survey organizations organize and provide regular monitoring of the seagrass species distribution, health and environmental sustainability. We list below the most known seagrass research institutions:

- ✓ Global-scaled: Global Seagrass Monitoring Network and the World Seagrass Association; The World Atlas of Seagrasses is published by the UNEP.
- ✓ Australian Seagrasswatch (perhaps, the best organization, regularly publishing informative reports)
- ✓ European: the Mediterranean association Seagrass-2000, the Mediterranean Institute for Advanced Studies and Seagrasses.org;
- ✓ US American seagrass recovery campaign by the Seagrassgrow, Seagrass Ecosystems Research Laboratory in South Florida, Seagrass.LI and Florida Seagrass organisation;
- ✓ Asian: UNEP/GEF South China Sea Project, Marine Conservation Cambodia and Sosmalaysia.org.

All these organizations aim at the global seagrass monitoring, providing with research results and reporting guidelines and manuals with standardized methods and recommendations, specific for the seagrass research and monitoring. There are also university marine centres and research institutes conducting seagrass monitoring and as a particular part of their research and reporting various approaches for the monitoring and mapping of the seagrasses, including remote sensing applications. Their reports and guidelines were used for references in the current research.

2.2 Measuring optical properties of benthic vegetation: hyperspectral radiometers

The application of the remote sensing data for seagrass mapping is based on our knowledge of the spectral reflectance properties of the target objects, and using it for the classification of these objects on the image. In case of seagrasses it is spectral reflectance of the seafloor cover types, which can be analysed using measurements of optical properties of sea water: radiance and irradiance. Optical remote sensing methods can get through the clear waters to approximately 15–30 m [102]. When sunlight enters the waters and goes down into the water column, parts of the electromagnetic energy are absorbed and scattered, which is determined by the optical and physical properties of the water, e.g. concentration of suspended particles, chlorophyll, coloured dissolved organic matter (Gelbstoff) that make up the water content [1]. Besides, light is strongly dependent on wavelengths, i.e. it is greater in blue wavelengths (400 nm) than in others.

(a) RAMSES-ACC-UV - Hyperspectral UVA/UVB Irradiance Sensor: 280-500 nm *(b) RAMSES-ARC - Hyperspectral UV-VIS Radiance Sensor: 320-950 nm.*

Figure 2.1: RAMSES Hyperspectral Sensors. Source: Trios

The optical properties of the sea water vary with different environmental conditions and reflect current chemical content and physical specifics of the water, revealing the variability and distribution of colour of the sea waters, determined by the material in the water, e.g. chlorophyll, as well as its physical properties, e.g. water absorption, attenuation, backscattering [80].

Shallow waters generally contain more dissolved substances and suspended particles, which directly influences the transparency and colour of the waters of shelf zones [65]. Being highly dynamic environments, coastal waters experience a variety of processes which alter their optical properties incessantly. The effects of these processes influence application of the hyperspectral remote sensing and reinforce other processes [81]. Thus, waves and tides increase sedimentation processes, which in turn, may change micro relief properties and topology.

The optical properties of the water are best reflected in the values of its radiance and irradiance, which can be converted into spectral reflectance, or reflectivity. The spectral irradiance (E) is a radiant flux of the electromagnetic solar radiation energy, received per surface unit area in a given time ($W \cdot m^{-2} \cdot nm^{-1}$), while radiance (L) characterizes total emission or reflection that passes through or is emitted from a particular area ($W \cdot sr^{-1} \cdot m^{-2}$). Therefore, the spectral reflectance, or the reflectivity of the object, can be estimated by the direct mathematical division of these first two characteristics, and is expressed in percentage. The irradiance and radiance of the water thus should be measured, in order to estimate spectral reflectance of the various seafloor cover types.

The optical measurements of the irradiance and radiance of the sea water and bottom cover types of the seafloor can be received by the means of the optical sensor spectroradiometers. There are several companies producing radiometers with various characteristics and adjusted for different purposes, e.g. portable and miniature spectrometers from StellarNet, Hyperspectral Ocean Colour Radiometer (HyperOCR) sensor by Satlantic, traceable spectroradiometers by Orbotronix and lots of others. Among other radiometers there are ones designed by the Trios company producing optical sensors, GER-Series Field portable spectroradiometers from SpectraPartners, etc. Trios-RAMSES hyperspectral radiometers (Trios-RAMSES Hyperspectral UVA/UVB Irradiance Sensor and RAMSES-ARC Hyperspectral UV- VIS Radiance Sensor) are small-sized, low power-consuming, flexible for fieldwork yet with high level of precision, specially calibrated for air and for water application as well as colour measurements (Fig.2.1). These products have been used for the radiance and irradiance measurements in Agia Pelagia bay, Crete Island, 2009.

2.3. *Radiative Transfer Models (RTM)* for the simulation of water optical properties: a brief review of existing software tools

Understanding radiance distribution within a water column is necessary for the studies of the underwater visibility, because scattering properties of the water body naturally vary with changing depth, wavelength and environmental conditions. Simulation of the radiance quantities for natural water bodies enables to analyse seafloor color remote sensing properties. Therefore, the artificial modelling of the seawater optical properties by means of the *Radiative Transfer Modelling (*further *RTM)* is used when water optics is studied under changing environment (e.g., depths, sun angle, suspended particles in water column). In such cases a retrieval of water optical parameters from the remote measurements should be tested and analyzed.

We briefly list below the most effective *RTM* software and algorithms, suitable for underwater radiance simulations, from a range of various best-known up-to-date tools.

a) The *Second Simulation of a Satellite Signal in the Solar Spectrum, version 1* (6SV1) (http://6s.ltdri.org/) is a US atmospheric correction algorithm, developed in the University of Maryland; adjusted for the NASA MODIS satellite imagery (http://modis.gsfc.nasa.gov/) lookup tables. The 6S algorithm has been implemented by the GRASS software for the atmospheric correction http://grass.osgeo.org/grass64/manuals/html64_user/i.atcorr.html
b) Another example of the RTM adjusted for a specific imagery is a German KOPRA RTM (http://www.imk-asf.kit.edu/english/312.php), fitted for MIPAS/ENVISAT imagery.
c) The *HydroLight RTM* commercial software is an advanced model for oceanic radiative transfer calculations, developed by the *Sequoia Scientific, Inc.*, USA. It is designed to solve a wide range of problems in optical oceanography and limnology. (http://www.sequoiasci.com/products/Hydrolight.aspx)

d) The British *RTTOV-9 RTM* is a radiative transfer model, developed for nadir viewing atmospheric sounders and imagers. It includes a number of useful tolls, e.g. can compute sea-surface emissivity for each channel, enables, to specify cloudiness for radiance calculations, etc. This program runs under Unix/Linux platforms and is open source. http://research.metoffice.gov.uk/research/interproj/nwpsaf/rtm/
e) The *Rapid Radiative Transfer Model (RRTM)* is one more RTM freeware (http://rtweb.aer.com/), designed in the USA, Massachusetts.
f) The *MODTRAN,* a commercial software (http://www.modtran.org/) from Spectral Sciences Inc., is another example of the *RTM.* Among its newest updates is generation of atmospheric correction data; it also has an option to write spectral output in binary, and convert it to ASCII.
g) The *Community Radiative Transfer Model, CRTM* is designed by the JCSDA, NASA (http://www.jcsda.noaa.gov/projects_crtm.php) and includes Surface Emissivity/Reflectivity Models, Cloud Absorption/Scattering Model and Gaseous Absorption Model.

For our purpose we have chosen the *WASI RTM* software, due to its effectiveness, adaptability for the Mediterranean environment, open source availability, coverage of necessary wavebands and clear, user friendly interface enabling us to adjust various environmental parameters.

2.4. The *in-situ* observations of the seagrass meadows

The traditional methods of *in-situ* seagrass monitoring include in general the following standard scheme [87]. The seagrass is being sampled on the selected sites using transect lines, quadrant frame, single point markers, markers, GPS and other equipment. The seagrass sampling is taken on the regular way with observation points covering the study area with normal distribution (Fig.A.25, Fig.A.24). During the measurement process, the vertical photograph of the measurements frame is taken, and the following points are traditionally estimated: percentage of the seagrass cover within the quadrate, species composition, sediment composition, canopy height, epyphyte abundance, algae percent cover, count of microfauna and a specimen of seagrass is being taken. This scheme, well described by McKenzie [87] is widely used and well-known among the marine biologists and seagrass researchers. Applications of the *in-situ* seagrass observations of the structuring epiphyte community composition in the *P.oceanica* ecosystems in Mediterranean Sea is, for example, described by Villegas [136]. Realization of traditional methods for mapping seagrass usually involves intensive and time-consuming *in-situ* observations during the fieldwork, as, for example, reported by Iverson and Bittaker

[61]. The results of the *in-situ* measurements and observation are usually managed and treated using integrated GIS approach, as, e.g. reported by Schmieder [127].
Other methods of seagrass in-situ monitoring are based on the application of the active hydro-acoustic sonar sensors that send towards a sea floor a signal of energy and then collect the return echoes for the analysis (Fig.A.5). One of the examples of the acoustic sonar sensor designed for seabed classification is the British RoxAnn system, which application for the seafloor mapping is very well described on the OzCoasts website. However, the application of the acoustic methods requires specialized expensive equipment and is mostly used in the deep open waters, combined with bathymetric measurements. Another limitation of the acoustic techniques is that, initially intended for the bathymetric surveying, acoustic equipment is mostly designed for the geomorphological and geological studies of the underwater substratum and are, therefore, more adjusted for the benthic habitat discrimination, and they are not effective for the identifying of the biological species composition or even the presence of aquatic vegetation such as seagrasses and seaweeds [139]. The current study is based on the application of the remote sensing optical measurement techniques, due to their effectiveness, non-destructive nature and availability of necessary tools: spectral radiometers and RTM.

2.5. Application of the remote sensing data towards seagrass mapping

Various methods and approaches have been applied towards mapping of the seagrasses, based on digitized aerial photographs, GPS data, remote sensing and SCUBA-based fieldwork measurements. SCUBA-based (Fig.A.54) *in-situ* observations, though providing high resolution and accuracy results in seagrass mapping, is limited in application, because of their time consumption, weather-dependency and unsuitability for the case of monitoring large areas of water for small-scale mapping. The underwater videography with a GPS is a tool of seagrass monitoring which has certain advantages, i.e. high spatial and visual resolution, non-destructive sampling, effectiveness at all depths and rapid data collection in the field [128]. However, it cannot cover large areas for small-scale mapping. Remote sensing techniques offer clear advantages over other methods of *in-situ* field measurements and seagrass observations, mentioned above. Preference of the remote sensing methods consists in their weather-independency, cost-effectiveness, accuracy and spatial coverage, which enables periodic monitoring of the seagrass meadows and gives access to the distant and unapproachable areas. Integrated together with GIS vector layers and maps, remote sensing data enable historical mapping [19, 5] and assessment of change detection. However, application of the remote sensing techniques for mapping of submerged vegetation, seafloor cover types and benthic vegetation, inter alia seagrasses, are still in their development.

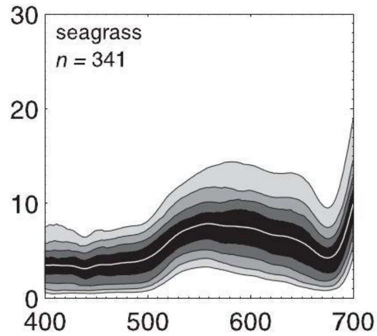

Figure 2.2: In situ optical reflectance spectra of seagrass. Shaded areas - % of spectra lying within the range of reflectance. White lines - mean spectra. Source: [57]

Approaches and methods for the seagrass protection and monitoring still remain location-specific or, at least, nation-specific, depending to large extent on the tools available for the researchers [93]. Universal, international, standardized methods for seagrass directly for seagrasses as such still should be developed. Various case studies have been performed, yet their mostly report methods adjusted for particular areas, without evaluating standard general algorithms that could be extrapolated towards other regions.

Application of the remote sensing towards seagrass mapping is generally based on the assumption that various types of the seafloor bottom have different characteristics of the reflectivity, which is visually expressed in distinct colours of the objects. In its turn, reflectivity of the sediments is affected by the water optical properties and content. For example, Stephens [131] prove that microalgae biomass and community structure affect hyperspectral reflectance of sediments, which enable to estimate total microalgae biomass from measurements of hyperspectral reflectance.

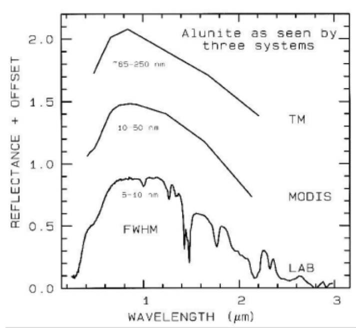

Figure 2.3: Difference between broadband multispectral and hyperspectral resolution of spectral signatures. Source: [23]

Spectral measurements of the target objects are made by means of the radiometers (Fig.2.1), which receive and register the amounts of energy (radiance and irradiance) from the objects. Measuring optical properties of the seawater allows to calculate spectra of the objects and to discriminate them on the aerial and satellite images. Thus, various scientists report success in spectral discrimination of submerged vegetation and other seafloor cover types on imagery using hyperspectral optical properties of the sea water for the assessment of benthic habitats [75, 76, 25, 139]. Studies of spectral reflectance of the different seagrass species comparing to the spectra of sand and other seafloor cover types [134] prove that spectra of green, brown and red benthic macroalgae differ from each other, as well as from sand and deep water reflectance spectra. These differences are well detectable by the means of the remote sensing research methods. Comparing to the terrestrial plants, aquatic vegetation inter alia seagrass cannot be detected using red edge of the spectrum, as these wavelengths are significantly absorbed by water [69], as well as by scattering and absorption by phytoplankton. Some authors [30] also use spectrally based radiative transfer approach to quantitatively estimate shallow-water bathymetry and leaf area index (LAI) of the seagrass. The spectral reflectance in general is the result of the spectral absorption in different bands, typical for each target object. Spectral reflectance of the seagrass (Fig.2.2) is largely influenced by the water depth where it is located, and is generally decreasing in values by increasing depths. The most important spectral diapason for marine mapping of submerged vegetation and, particularly, for seagrass, is 350-800 nm [7]. Using airborne imagery for retrospective data (before 1970s) together with the most recent imagery allows to detect changes in seagrass distribution on over different years and to analyse dynamics of the seagrass distribution [6].

Another important advantage of the application of the remote sensing data for mapping of submerged aquatic vegetation has commercial nature: using remote sensing data and methods enables more low-cost and up-to-date seagrass mapping [100], and is especially useful for the areas where the fieldwork data capturing is unavailable.

Satellite Sensor:	**Landsat**	**SPOT**	**ENVISAT**	**Terra**	**GeoEye**	**Nimbus 7**
Origin	USA	France	Europe (ESA)	USA (NASA)	USA	USA
Instrument	*TM, ETM+*	*Pan, XS*	*MERIS*	*MODIS*	*SeaWiFS*	*CZCS*
Number of channels	8	6	15	36	8	5
Wavelength coverage	185-1700	500-1750	412.5- 900	469-1640	412-865	443-750
Ground resolution (nadir), m	15-pan,30(MS),60 (TIR)	2.5, 5, 10,20	1.2 km/300 m	1.0 km	1.13 km	825 m
Band Width (nm)	0.45-10.4	10,20	2.5,7.5,9,10 14,20	0.18,0.3,0.5,10 - 50	20,40	20,100
Launched	1972, 1999	1986	2002	1999	1997	1978
Recurrent period, days	16	24	35	16	16	16

Table 2.1: Characteristics of selected ocean-colour sensors

Seagrass meadows may reach spatial scales from several up to hundreds of metres, therefore they are susceptible by the means of satellite imagery from remote sensors, both with moderate resolution (e.g., Landsat MSS, Landsat TM, Landsat ETM+, MERIS, ASTER, MODIS) and high resolution as well (e.g., IKONOS, Quickbird, SPOT, CASI). The possibility of their application towards seagrass mapping varies and is limited by the technical characteristics (Table 2.1) and resolution of these sensors (Fig.2.3). In the next paragraphs we briefly discuss limitations and research experience of the using of various imagery for the seagrass mapping.

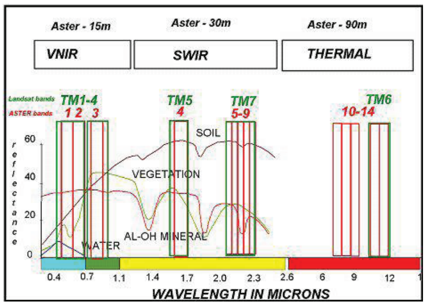

Figure 2.4: Band coverage of ASTER and Landsat channels on the e/m spectrum. Source:[66]

In the next paragraphs (“Review of multispectral imagery...” and “Review of hyperspectral imagery”) we will briefly discuss research experience of the application of satellite imagery towards seagrass mapping, its advantages and limitations, reported by various researchers.

2.5.1 Review of multispectral imagery used for seagrass mapping

Seagrass mapping using remotely sensed data from multispectral sensors is based on the classification and discrimination of the seafloor types using their spectral characteristics in different wavebands. Perhaps, the most known imagery, widely used in the remote sensing mapping, is received from the group of Landsat sensors, known for its historical, pioneer role in the satellite industry. Being the longest running satellite system, lunched in 1972, Landsat is the only source of archival data going back to 1984 at a sufficient spatial resolution [27], which makes its data desirable for historical mapping or environmental analysis of change detection of the seagrass landscapes. The Landsat TM and Landsat ETM+ data, with the most recent from sensor Landsat 7 – an advanced and multispectral scanning, launched in 1999, prove to be feasible and useful for the mapping of submerged vegetation, such as seagrasses or coral reefs. The successful applications of the imagery Landsat TM towards the seagrass mapping, were reported in numerous research works [108, 50, 137, 10, 36, 121].

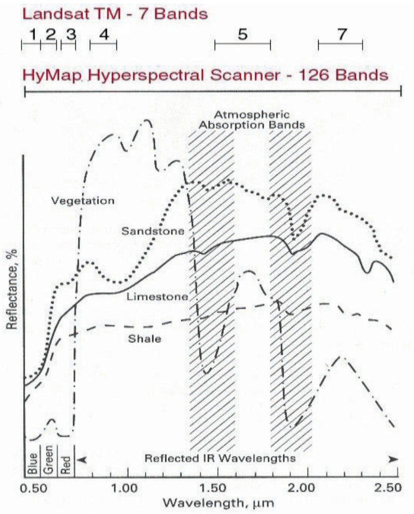

Figure 2.5: Multispectral vs. hyperspectral band coverage. Source: [125]

The Landsat data are particularly suitable for the case of change detection of seagrass landscapes at a decadal scale, because being the main sensor onboard the Landsat satellites, the Thematic Mapper (TM) provides the longest time series available for change detection analysis over submerged vegetation [108].

Another well-known multispectral sensor, SPOT provides multispectral imagery with a spatial resolution of 10 m, covering covers a surface area of 3600 km² (60*60 km swath), 26-day orbital repeat cycle for nadir viewing and imagery with a spatial resolution 20 - 2.5 m [106]. SPOT imagery was used for mapping beds of Posidonia oceanica in the Mediterranean Sea [113] . The IKONOS, offering multispectral and panchromatic imagery, was the first to collect publicly available high-resolution imagery at 1- and 4-meter resolution from Geoeye. IKONOS imagery has been applied for the seagrass mapping due to its high resolution and accessibility. Thus, the results of image classification in case study of shallow-water marine environment [101] made using IKONOS, Landsat TM, and CASI, show that in the blue part of the spectrum, the best results are achieved by the IKONOS and CASI, while Landsat TM has not high enough resolution. It may be caused to some extent by the loss of the radiance contrast, atmospheric Rayleigh scattering and defects of scattering. However, comparing between CASI and IKONOS, the same authors prove that CASI enable to receive still more accurate results of the classification than IKONOS [101]. Another comparative analysis of the application of CASI, Landsat and Quickbird imagery [119] demonstrates high suitability of CASI images for the fine-scale mapping of the seagrass landscapes. Thus, CASI and Quickbird-2 images enable to identify even separate seagrass species with small width and heterogeneous nature of the seagrass patches, which could not be detected using Landsat TM images with their 30*30m resolution.

Advanced Spectrometer for Thermal Emission and Reflection Radiometer (ASTER), launched in 1999 onboard Terra sensor, provides high-resolution images of the Earth in 15 different bands of the electromagnetic spectrum, ranging from visible to thermal infrared light (Fig.2.4). It has diverse subsystems for the visible near infrared (VNIR) with 15 m resolution, shortwave infrared (SWIR), and thermal infrared (TIR) wavelength regions [66]. For each channel there is separate onboard calibration (OBC) system, telescope with independent pointing and different detector technology [4]. This makes ASTER imagery especially suitable for the application towards detailed mapping of surface temperature, emissivity and reflectance of objects and bathymetric elevations as well. Successful application of the ASTER imagery towards mapping of submerged vegetation reported, for example, by Hirose [55].

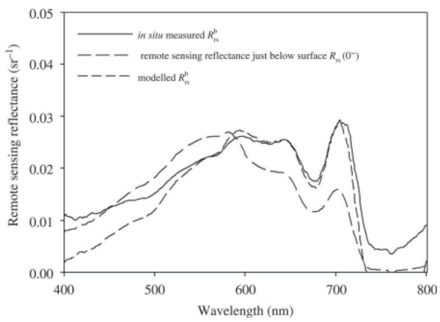

Figure 2.6: Reflectance spectra of sea-Grass Thalassia; Rrs(0-) - subsurface RS reflectance; Rrsb - the bottom reflectance. Source:[140]

Other multispectral images have also been used for the seagrass interpretation. For example, the success of using imagery from the multispectral airborne scanner Daedalus AADS1268 is reported by Heege et al [54] where they aim at classification of macrophytes in shallow waters of the Lake Constance.

In regard to the methods chosen for the image interpretation, the supervised classifications proves to be the most worthy in a majority of case studies [108, 114] .

While often methods of the unsupervised classification are used as a tool for classifying submerged object and features on the multispectral images and aerial imagery [37], it still does not provide common algorithms that can be applied to other images and regions. Thus, the strength of the optical signal coming from the various types of the seafloor is strongly influenced by the effects of the water column, its depth and chemical properties. Yet methods of the unsupervised classification overleap mixed spectral effects of the water column which shift the real values of the spectra, with the pure reflectance from the benthos; as a result, it may cause significant errors [30].

For the accurate assessments of various seafloor cover types, water column depth and its optical properties, methods of supervised classification should be preferably used as being more suitable in classification and interpretations of imagery. However, it is only true if spectrally distinct regions of the spectrum are covered by a space-born sensor and if the atmospheric distortion and viewing geometry is not degrading the radiometric quality at essential wavelengths. While this and other studies [119] demonstrated the advantages and success of the application of multispectral imagery for the spectral discrimination of the seafloor cover types and mapping the submerged landscapes on the basis of pixels classification, the application of data from hyperspectral sensors has better potential due to their higher resolution (Fig.2.5).

2.5.2 Review of hyperspectral imagery used for seagrass mapping

The application of the hyperspectral sensors is most effective and provide more accurate classification results (Fig.2.5), due to their higher spectral resolution [15] with interval narrows to 10 nanometres, while broadband sensors are limited to the spectral width of ca 150 nm (Fig.2.3). Hyperspectral imagery is acquired through the simultaneous acquisition of images in many narrow, contiguous spectral bands from hyperspectral scanners (mostly) cover the 400- to 2500-nm spectral bands [126]. Perhaps, the most advantageous and general characteristics of hyperspectral imagery is its high spectral resolution, desirable for the case of seagrass monitoring. The most suitable scanner fit for detailed seagrass mapping would cover bands of 550-750 nm and have a spectrum resolution of 5-15 nm [42], which exactly characterizes typical airborne and hyperspectral satellite scanners. Important features may be detected in the narrow wavelengths of hyperspectral imagery, while this information can be lost in the broader wavelengths of other sensors. With its 126 spectral bands, HyMap imagery enables to distinguish features of interest, i.e. seagrass types [115], which is the major advantage of the of hyperspectral data for mapping landscapes of the seagrasses. While comparing multispectral imagery with airborne hyperspectral, the last one showed higher overall accuracies [119]. Several, regular and narrow (10 nm) spectral bands, specific for hyperspectral imagery, are strong tool enabling to detect even slight and subtle differences in the spectral reflectance between various seafloor types, e.g. different seagrass species at diverse depths, algae, corals, dark-coloured sands or other types of sediments [56]. Therefore, there is great potential of the application of hyperspectral remote sensing imagery towards seagrass mapping at species level, as long as they are distinguishable spectrally (Fig.2.6) which, for example, has been tested in the case study of Australian marine ecosystems by Fyfe [42]. Application of various classifications methods, inter alia maximum likelihood, minimum distance and means, towards hyperspectral imagery [114], combined with fieldwork measurements ensures accurate mapping results with the maximum likelihood methods producing the best results. Therefore, accurate mapping of the seagrass landscapes and other seafloor types using remote sensing approaches requires application of high-spatial resolution (higher than 5 m) or hyperspectral imagery. Comparative analysis of the application of hyperspectral and multispectral imagery towards the seafloor types classification [56] demonstrates that coral, seagrasses and sand very well distinguishable in their spectra with an overall classification accuracy of 98 percent. However, the use of data from various sensors, both hyperspectral and multispectral, is possible and reasonable, as soon as it meets the research specific objective. Thus, the use of multispectral imagery with high spatial resolution is preferable to using hyperspectral medium resolution data in case of mapping benthic vegetation in areas where the spatial heterogeneity is very high [135].

2.5.3. Comparison of seagrass spectra

The reflectance spectra from different seagrass species reported in various research works demonstrate diverse spectral signatures which are dependent on the mixture of environmental conditions as well as individual characteristics of the seagrass.

In the current work we have compiled an extensive measurements dataset (up to 400 single spectral profiles) of the reflectance spectra from various seafloor cover types (*P.oceanica* and carbonate sand) in the coastal waters of Crete Island, which is partly visualized on the plotted graphs (Fig. 4.2, 4.6, A.27, A.28, A.30, A.35, A.36.

Having analyzed reflectance spectra received in previous works by other researchers and compared them with our results, obtained in the current work, we noticed some general trends in the character of reflectance spectra of various seafloor cover types. We mention below some general conclusions and observed tendencies in the profiles and patterns of spectra of *P.oceanica* and carbonate sand (as for Crete Island).

Measured remote sensing spectral reflectance is highly variable with changing environmental conditions, such as water physical content (amounts of suspended particles and organic matter, salinity, chemical content), water column depth, atmospheric conditions (incl. sun zenith angle) and individual features on the plant, e.g. morphology and colour pigmentation of the leaves, differed in various plant's health and age conditions.

The maximal values of the spectral reflectance of *P.oceanica,* received both in the current work and by previous researchers, lies in wavelength interval of 500-600 nm, as, for example, shown on Fig.2.2, Fig.2.6, and can be clearly seen in our results as well (Fig. 4.2, 4.6, 4.8, A.35). Comparison f the remote sensing reflectance spectra of various seagrass species, e.g. *P.oceanica* (Fig. 4.4) and *Thalassia testudinum* (Fig.2.6), sows that P.oceanica is in generally brighter in the wavelength interval 500-600 nm which can be caused by various colour pigmentation. The plotted graphs with spectra of the seagrasses *P.oceanica* and *Thalassia testudinum* demonstrate that the dip in the spectral reflectance after ca 600 nm is more pronounced in case of *P.oceanica* seagrass beds (Fig.4.4) than in those with *Thalassia testudinum* (Fig.2.6), due to absorption caused by pigment of green leaves. The remote sensing of the bottom albedo of *P.oceanica* and carbonate sand (Fig.4.7) shows clear difference between the carbonate sand and *P.oceanica*, which is evidently much darker. To estimate and further analyze particularities of the *P.oceanica* remote sensing reflectance spectra over regions with different bathymetry (0.5, 1.5 and 2.5 meters column depth) we used WASI RTM software, which incorporates measurements of the seafloor reflectance and water column optical properties.

3 Materials and methods

In the section Seagrass monitoring: overview of literature and research resources we briefly discussed main existing cartographic methods and tools for seagrass mapping. In the current research we try to combine various techniques from mentioned above for the assessment of the seagrass distribution in the Mediterranean environment, for the case study of Crete. We mentioned in the List of Tools the software that we used for logically separated research sections, which required various approach. Thus, for example, spectral analysis and assessment of spectral signatures is technically based on WASI, statistical analysis of series of experimental raw data has been made by means of statistical software, such as Gretl and SPSS; mapping has been made using ArcGIS; images processing and classification were made using Erdas Imagine software by means of Google Earth and Landsat imagery. ArcGIS 10.0 software is used for the spatial analysis, general mapping and cartographic layout presentation; the raster processing techniques are applied for the detection of seagrass spatial distribution using supervised classification. The research data include Google Earth aerial images and scenes from the Landsat TM and ETM+ covering research period of 10 years in the same year time, taken from USGS, GloVis, NOAA and The Earth Science Data Interface. The satellite imagery provides vital information of the most recent changes in *P.oceanica* within the coastal areas, as well as the condition (poor or destroyed). The raster processing includes making mosaic-like covering for the whole research area. The Google Earth images are most appropriate for the detailed mapping than satellite than Landsat or ASTER enabling to produce accurate maps with correct results. Therefore, the main set of images for the current work is Google Earth aerial images. The Landsat images are used for the general overview. Besides aerial and satellite photographs, data acquired during the fieldwork (three weeks in September - October) are necessary addition to the mapping helping to solve problems of interpretation during the images classification [109]. Therefore, this work includes sampling of the *in-situ* measurements of the seagrass distribution. The sampling stations were located in two candidate places on the northern (Ligaria) and southern (Xerokampos) parts of Crete island, as these regions are well suitable for the seagrass, due to the annual mean water temperatures and geological factors, i.e. seafloor conditions and sediments. The field campaign has been carried out during the September-October period 2010. The information about the location of the seagrass (mostly represented by the *P.oceanica* species) is useful for the understanding of the relationship between the spatial distribution of the seagrass and the environment of the selected areas of Cretan beaches. The results of the videographic measurements are used for the seafloor types detection, because the objects represented on the photos can be well distinguished and classified according to the following well-known characteristics [17]: size (yet some measurements are necessary for the similar-looking objects); shape (the general form is most reliable evidence for identification); colour (common and reliable object indicator); texture (when changes in tone are too small to be distinguishable, texture may assist identification, e.g., stippled, granular, rough, smooth, etc.); associated features (those usually found near other objects, e.g., rocks and soil).

3.1 Study area

General area: Island of Crete, Greece (Fig.3.1). The study area of the current MSc research is located in the shallow areas of the Ligaria beach, Agia Pelagia and Xerocampos, Crete island, Greece (Fig.3.2).

Figure 3.1: Study area: Crete Island

These shelf areas have maximal depth of four meters. Seagrass sampling has been performed at two stations at a depth of 4 meters, in the following selected areas:

1. Ligaria beach (Agia Pelagia district), 36°20′N 22°59′E
2. Xerokampos, 35°12′N 26°18′E 3. Agia Pelagia, 36°20′N 22°59′E.

3.2 Fieldwork data collection

Seagrass sampling has been performed at two research stations at Crete island - Ligaria beach (36°20′N 22°59′E) and Xerokampos (35°12′N 26°18′E), at depths lesser than 4 meters.

Figure 3.2: Study area: Ligaria beach, Crete Island

The Ligaria Beach is a narrow, sandy and pebble beach (Fig.3.2), located ca 15 km north-west from Heraklion. The *in-situ* measurements were conducted during the fieldwork in the period 21.09.2010-11.10.2010. The fieldwork on seagrass monitoring included visual estimations and photo- and video footage of the above-ground seagrass patches, sediment seafloor cover types, species compositions, water depth and geographic locations recorded using GPS.

3.2.1 Fieldwork equipment

The research materials and equipment were provided by the Natural History Museum of Crete, the University of Crete and the ITC, and included the following items (Fig.3.3): 1) three iPAQs (Fig.3.3a); 2) three GPS (Fig.3.3c); 3) Three underwater video cameras, Olympus ST 8000 (Fig.3.3d), suitable for photographing up to up to 33 foot depths and high-resolution 12.0-Mpixel image sensor; 4) Markers and cords for the depths measurements (Fig.A.56); 5) Waterproof plastic Otterbox (Fig.3.3b) for keeping the iPAQ dry; 6) SCUBA Diving equipment, taken from the Ligaria Diving Centre; 7) Boat (Fig.3.4);

(a) iPAQ, HP *(b) Waterproof Otterbox* *(c) GPS* *(d) Olympus waterproof camera*

Figure 3.3: Fieldwork equipment

A GPS and iPAQ have been used for detection of the geodetic coordinates and keeping the tracklogs along the boat route for GIS project.

Figure 3.4: Boat used for the fieldwork measurements on Crete Island. 2010

3.2.2 Sampling design

The sampling design of the fieldwork was aimed at surveying of the spatial distribution of the meadows of P.oceanica, and spatial pattern of the seagrass meadows consisted from separate patches. The fieldwork included several routes of the boat in the Ligaria beach sampling site, nine routes in total, in the directions parallel to the coastline, ca 180-200 m long each one, thus enabling the course plot to cover the area of growing seagrass: shelf areas not deeper than four meters. The measurements of the seafloor cover types have been made using underwater video cameras Olympus ST 8010 (Fig.3.3(d)), mounted under the boat to capture video footage and imagery (Fig.A.53). The data records were made along each path using

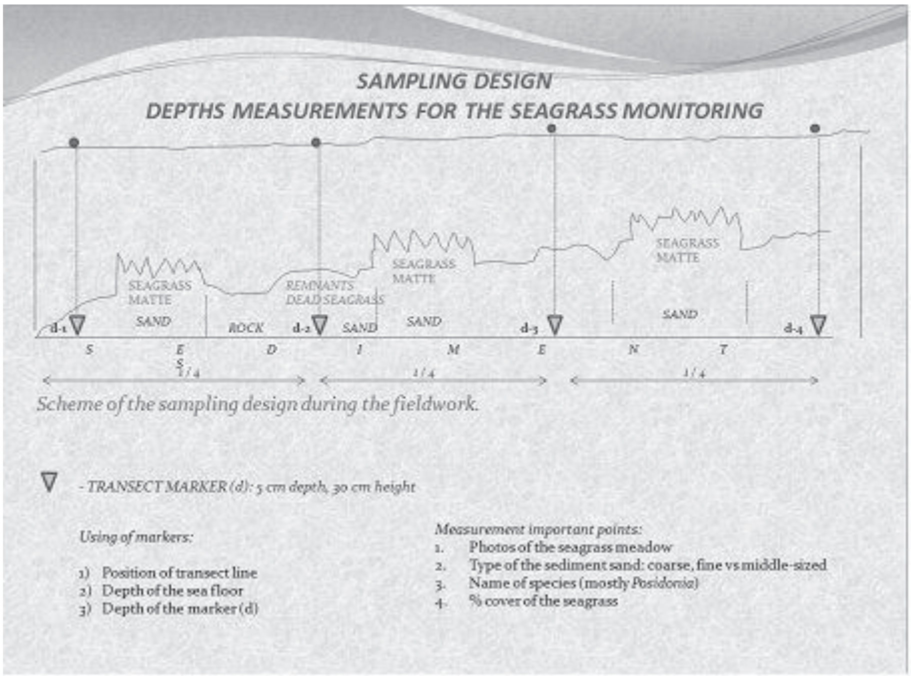

Figure 3.5: Scheme of the depths measurements; fieldwork on Ligaria beach.

these cameras. A videographic approach, tested previously [105], was applied during the fieldwork on Crete island, for collecting information on benthic cover types and distribution of the seagrass patches from photo transects, in order to use for the calibration of mapping approaches.

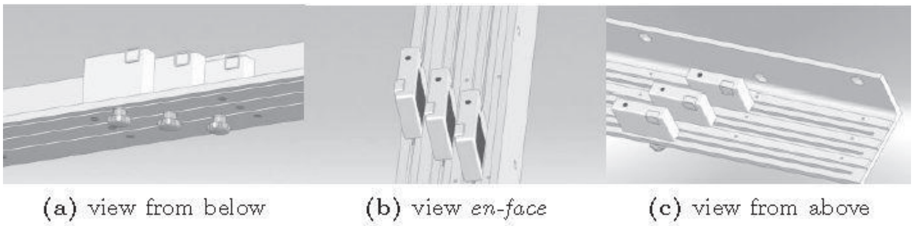

Figure 3.6: Scheme of placements of the Olympus cameras during the measurements

Three underwater video cameras, located on the bottom of the boat (Fig.A.53), provided videometric measurements of the seafloor during the track (Fig.A.9), and resulted in a series of consequent overlapping images of the sea bottom under the boat path. The general locations of the sampling sites and routes were selected on the basis of the visual examination of the seagrass beds during snorkelling and SCUBA diving (Fig.A.54, Fig.A.55), recommendations from the Greek collaborators of the *Natural History Museum of Crete*, and available maps covering the research area. To ensure even and objective selection of sampling sites we used transect sampling method, i.e. photographs were taken along the research path.

Transect method (Fig.3.5) is a common sampling technique in studies of the seagrass monitoring [130], enabling the occurrences of the seagrass meadows to be recorded and counted in a systematic and accurate way, detect spatial distribution of the single seagrass mattes to be properly identified, without location bias (Fig.A.12).

The videographic measurements and photos, enabling to detect types of the seafloor, were captured by means of three underwater digital video cameras Olympus ST 8000 (Fig.3.3d), at five minutes interval along the tracklog path (Fig.A.9). research sampling design also included measurements of depths (Fig.3.5), because bathymetry is one of the most determining factors for the seagrass locations. Measurements of depths were performed during the fieldwork using cord, iPAQs, and markers (Fig.A.57) in order to assure that the videometric measurements are taken at depths not more than four meters, in the shelf area. As a result, nine transects were established of one m wide and 20 m long track, to cover seagrass beds with videographic measurements.

The GPS allowed to capture measurement locations on the iPAQ, encapsulated in a plastic waterproof Otterbox (Fig.3.3b). The camera were adjusted horizontally by a leveller and mounted under the bottom of the boat (Fig.A.53) to capture video footage and imagery (Fig.3.6). The data were taken at proper weather conditions: sunny, serene and cloud-free days with glassy sea state. The locations of the route were randomly selected in the areas of the Ligaria beach, to ensure most dense coverage of the seagrass meadows in the research area. The underwater measurements of the seagrass coverage were carried out by taking video footage and photos of ca 0.5 m2 size each (Fig.A.12, Fig.A.57). The results of the underwater videometric measurements include series of digital images helping to classify seafloor cover types (Fig.A.58) and seagrass meadows, according to the differences in the structure, colour, texture and shapes of the depicted objects. There are several types of the seagrass landscapes along Ligaria beach, namely, seagrass meadows continuously covering vast areas (Fig.A.38 (a)), aggregated seagrass patches, represented by separate mattes with short irregular channels between them (Fig.A.8 (b)) and isolated seagrass patches, or mattes, which located separately from broad meadows (Fig.A.8 (c), Fig.A.58). The results of the underwater videometric measurements of the Olympus cameras made during the ship route include nine total tracklog routes in the selected research area, including series of consequent images, completely covering the area under the boat path. The received data contain information on seagrass presence within the study area, distribution of seagrass *P.oceanica* meadows and nature of the seafloor cover types: rocks, sandy, mixed (Fig. A.11, Fig.A.10, Fig.A.8). Seagrass species on the Ligaria and Agia Pelagia beach consist of P.oceanica. The types of sediment on the Ligaria vary from coarse sand, *P.oceanica* patches, sand, mud, rock gravel and fine sand (Fig.A.11).

3.3. Review of the collected data

The remote sensing imagery was collected for the Crete island area covering the research period and area, enabling the field data to be used for the calibration and validation. The available aerial and satellite imagery are commonly used for the mapping of seagrass landscapes and their application is proven by various research papers. The imagery includes satellite multi-spectral imagery (Landsat-TM, ETM+) and aerial imagery from the Google Earth. The overview of the collected data enables to summarize their following types:

- Optical spectra of *P.oceanica*, carbonate sand, seawater with sediments and seawater measured in aquarium tank, without sediments, at different environmental conditions (e.g., Fig.A.20)
- Aerial imagery from the Google Earth
- Satellite images from various open sources (e.g. Landsat, Tab A.19) (previews: Fig.A.43)
- Results of underwater videometric measurements of the Olympus cameras made during the ship route

The available satellite (Fig.A.344, Tab.A.31) and aerial images are read into the ArcGIS project. The available broadband and hyperspectral remote sensing data are used for the mapping of the seagrass in shelf areas no deeper than 4.0 meters (Fig.A.45, Fig.A.45, Fig.A.47, Fig.A.48), for the environmental monitoring in order to detect the spatial distribution of the seagrass along Crete during the past ten years using different satellite images for 2000-2010 (Fig.3.7).

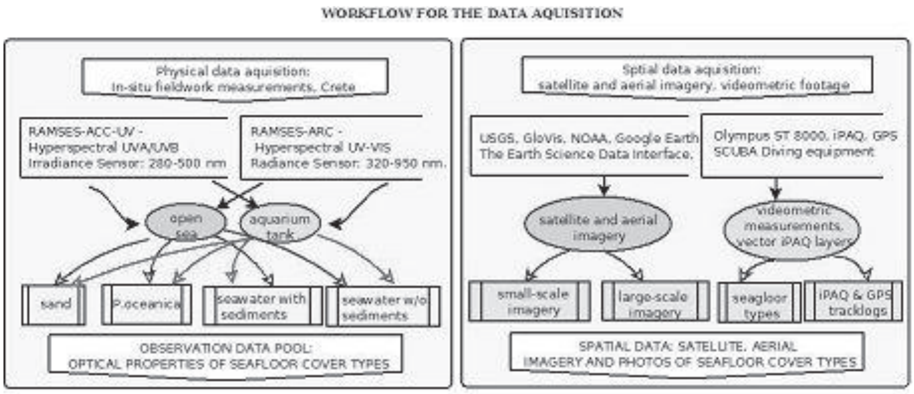

Figure 3.7: Work flow for the data acquisition, Dia display

The spatial resolution of Landsat ETM+ image is 30 m in the visible and near infrared bands (bands 1-5 and 7); the spatial resolution of ASTER 15 m for the

visible and near-infrared bands. IKONOS acquires data in 3 visible channels and NIR, with spatial resolution of 1-4 meters. ASTER and IKONOS images are suggested to be included as soon as available, in addition to the Landsat. The research includes fieldwork *in-situ* measurements of the seagrass distribution along the northern and south-eastern coasts of Crete in chosen locations. The optical measurements of the irradiance and radiance of the sea water and bottom cover types of the seafloor have been received by the means of the optical sensors Trios-RAMSES Hyperspectral UVA/UVB Irradiance Sensor and RAMSES-ARC Hyperspectral UV-VIS Radiance Sensor (Fig. 2.1), both adjusted for the measurements of the irradiance and radiance (see appendices: Tab. A.1, Tab. A.2).
These products have been used for the radiance and irradiance measurements in at the Hellenic Centre for Marine Research (HCMR) at the Institute of Aquaculture, Crete Island, 2009 by Ms Sylvia Noralez using following workflow. The spectrometer was adjusted for automatic measurements mode, with measurements taken as fast as possible. The spectrometer head was held submerged, and the sampling was controlled by an operator (Ms S.Noralez) on the surface boat. The head of the sensor was pointed downward at an angle of 0 (nadir) in order to capture the spatial discernibility in the radiance for the benthic cover types. The frame was held at 45 degree angle in order to keep sensor looking down at 0 degree (nadir view). A waterproof camera was attached to the platform to assist with the identification of the target object being measured (Noralez, 2010).
The highest measured values are located in the diapason of 410-730 nm for the water irradiance (Fig. A.19), and 430-650 nm for the water radiance (Fig.A.16). Afterwards, the measured values of the radiance and irradiance, respectively, have been used for the computation of the spectral reflectance properties of the sea water and bottom cover types (Fig.A.30). The spectral range of radiance cover diapason of 320-950 nm, and irradiance measurements are covered in the interval of 280-500 nm, which is suitable for characteristics of seagrass reflectance. Different curves on the reflectance, radiance and irradiance graphs for example, on Fig.A.27, or Fig.A.29, enlarged) represent several series of the measurements. The values of the spectral reflectance are received from the computations of these values using mathematical formulae. The graphs shown on Fig. 4.2, Fig.A.20, Fig. A.33, Fig. A.18 display values of the radiance and irradiance of the sea water in Agia Pelagia, with and without sediments and suspended particles, respectively. Graph on Fig. A.28 displays statistical analysis of the measured sets of observations, i.e. shows the midspread of the statistical quartiles (Q1-Q3), mean and extreme values.

3.4. Data pre-processing

3.4.1. Auxiliary data: spectral dataset

A collection of visible spectra of two seafloor cover types - *P.oceanica* and carbonate sand - consist of multiple measurement sets of *P.oceanica* made by means of RAMSES hyperspectral radiometer: 1-350 for 15th October (fragment on Tab. A.11), 1-445 for 14th October 2009 for P.oceanica; 1-106 for water without sediments, measured in aquarium tank, 1-27 for seawater with sediments measured in aquarium tank; 1-75 for carbonate sand (Tab. A.17). Measurements of 2009 has been used for the database and statistical analysis, because 2010 data pool was not available. All these data have been analysed and statistically tested. We measured mean, extreme values (min-max), median and statistical quartiles, in order to visualise distribution of the values at various spectral wavelengths. Carbonate sand was measured at wavelengths 402-750 nm, while *P.oceanica* - at the interval 318-951 nm. We visualised the behaviour of different spectra on relevant graphs (Fig. 4.3, A.39, A.37). The available collected data were tested for the spectral variability and separability under varying conditions of different environmental constituents (e.g. depth, water content, sun angle), in order to determine the potential that it may have on the approaches for further images processing and classification. Behaviour of the spectra of *P.oceanica* have been tested using datasets for various depths: 0.5, 1.5 and 2.5 meters (Tab. A.9, Tab. A.710). The raw initial data of measurements of the spectral reflectance have been pre-processed and statistically analysed thereafter with graphs visualising mean spectra and Q1-Q3 interval, instead of the series of single observations which is illustrated, for example, on Figures A.17, 4.6, 4.1). These data have been measured using different step of the wavebands: some measurements were made with 3 nm interval, while others – using 4 and 1 nm step. Therefore, these data had to be interpolated (Fig.A.15) and standardized to one format, which is values of spectral reflectance with one nm step. For the interpolation we used script written on Python programming language that allowed receiving more detailed data by interpolating them from 3 and 4 nm step up to 2 nm (Fig.A.13). The interpolated data contained spectral measurements of the seagrass *P.oceanica* (measured at Agia Pelagia beach, Crete), sand (measured at Agia Pelagia beach, Crete), silt and default artificial spectrum of constant albedo at WASI (Fig.A.14).

3.4.2. Modelling method: WASI water colour simulator

To estimate and further analyze particularities of the *P.oceanica* remote sensing reflectance spectra over regions with different bathymetry (0.5, 1.5 and 2.5 meters column depth) we used WASI RTM software, which incorporates measurements of the seafloor reflectance and water column optical properties. We have chosen WASI RTM software among other aquatic RTM (2.3. Radiative Transfer Models....) due to its effective cognitive approach and because it is specifically adjusted and developed for the purpose of aquatic optical modelling. Consistency of simple and logical GUI (Fig.5.1) let the researcher to easily define model parameters, which can be changed directly in the main window tools menu, and to choose between forward or inverse calculations. Besides other important advantages of WASU we would mention its learnability: available documentation, supporting materials, learning curve with hints and tips, as well as its user-friendly GUI, enabling to learn this product in a most effective and prompt way in a tight schedule of MSc studies. Technically, WASI need for system memory is minimised and the installation is simple and easy.

To create sensor-specific reflectance spectra using WASI, spectral responses of MERIS, MODIS, CZCS and SeaWiFS sensors were applied for simulation of seagrass spectral signatures in full-resolution spectra.

We also included measurements of other seagrass species - *Thalassia* seagrass (measured at Southern Chinese Sea by C.Yang and D.Yang) in order to compare spectral reflectance of different seagrasses under various environmental conditions. The most suitable wavebands for the seagrass monitoring usually lay between 400 and 700 nm, which can be concluded by the visual examination, comparison and analysis of the different spectra of the seagrasses. Therefore, we have chosen the spectra 400-750 as the most appropriate range for further research experiment. The results of the linear interpolation (Fig.A.39) demonstrate values of the sand spectral reflectance with 1 nm interval covering the wavelength diapason of 400-750 nm.

3.4.3. Implementation of statistical analysis

The initial measured data were stored in raw-oriented format, so that re-formatting them into the column-based layout was done using "transpose" command in Open Office or Excel (Fig. A26). The next step included calculation of the median, mean, quartiles and other statistical values at every data set (see appendices, Fig.A.35, Tab. A.17). After the preliminary analysis, the measured data were visualised using Gnuplot program, which enables fine plotting of various datasets together: Fig 4.3, Fig.A.17, Fig.4.51. The most acceptable method of interpolation was Bézier curve (Fig. A.19, Fig. A.16), as it has trend-friendly graph better showing the general behaviour of the curves at different wavebands comparing to splines (see appendices for more results). Therefore, after several experiments with various interpolation techniques (Fig.A.30, Fig.A.20), we have chosen Bézier curves interpolation (Fig.A.19) which contains convex hulls made on its control points, and therefore is best suitable for our case: analysis of optical properties of seawater.

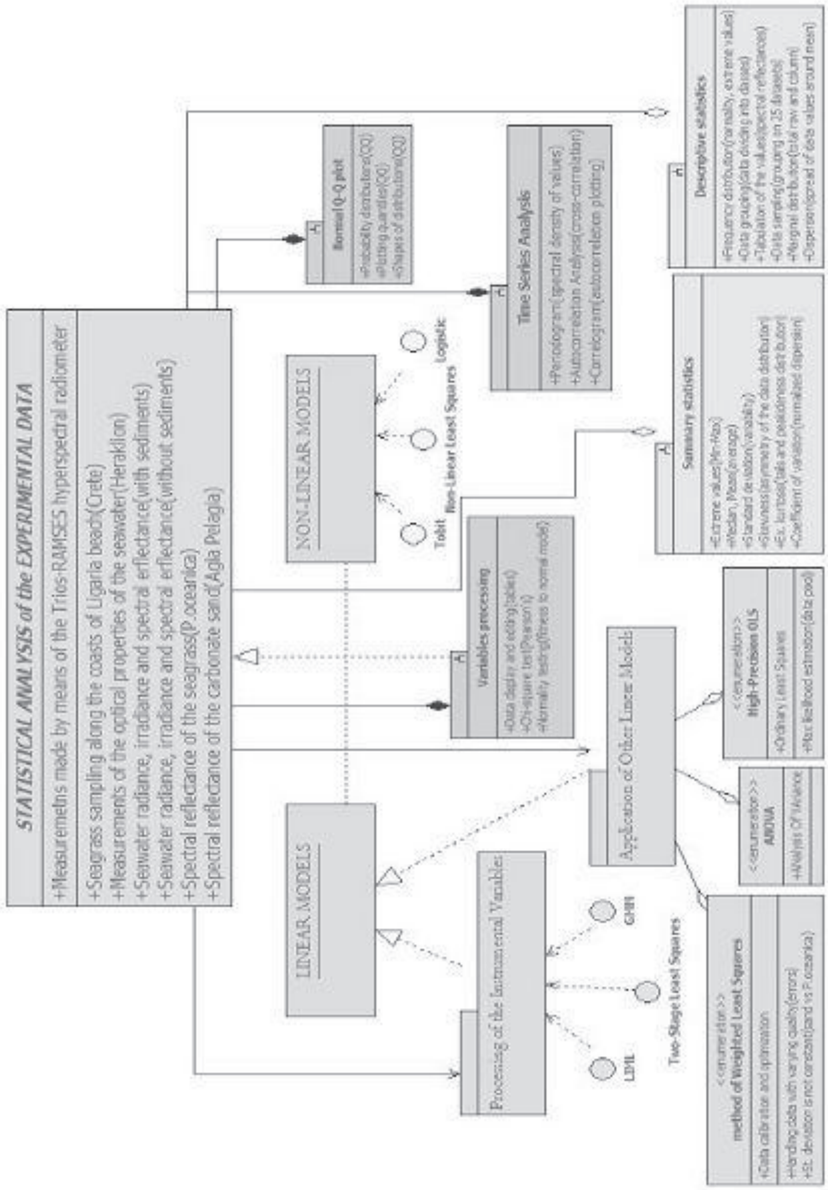

Figure 3.8: Work Flowchart Diagram illustrating algorithm of the Statistical Analysis applied towards the observation dataset (StarUML)

To analyse average values of spectral reflectance of *P.oceanica* by means of the measured sets we calculated mean values for the total set of measurements 1 – 350 (15th October): mean of min and max values, mean of average for each waveband,

mean for statistical quartiles for each wavelength and mean for median, respectively. The adjusted averages evaluate mean values, needed for statistical analysis of the datasets (Fig.A.21). The outcome of this calculations is shown in the Tab.A.6 and Tab.A.47 (appendices). As a result, we received mean values of spectral reflectance of *P.oceanica* for extreme, average (Fig.A.23, A.22), median and both quartiles, independent of the individual sets 1-350.
We used several statistical methods (Fig.3.8) to asses data received as a result of measurements. The Student-t test, one of the most commonly used techniques for testing a hypothesis on the basis of a difference between sample means, is used for the data analysis. In our case the Student t-test demonstrates, if the variation between two analysed groups – values of spectral reflectance of seagrass *P.oceanica* and sand - is significant. Therefore, we use Student t-test to compare two sets of quantitative data of spectral reflectance of *P.oceanica* and sand, respectively, with samples collected independently of one another. The Student-t test can be performed knowing just the means, standard deviation, and number of data points. Therefore, we used the data (appendices) of means of spectral reflectance of the both cover types within data sets, their standard deviation, and the number of data points.

3.5. Spectral simulation of aquatic objects

The main aim of this part of research is to clarify if the bottom reflectance of the different seafloor types including patches of the seagrass *P.oceanica* meadows, silt and carbonate sand differ and can be clearly discriminated while mapping. A study is based on three seafloor types containing silt, carbonate sand and seagrass, as well as mixed types, where the spectral signatures were examined. WASI software (Fig.5.1) is used to simulate spectral reflectance and colour discrimination of water, affected by presence of *P.oceanica* and other factors, under various environmental conditions which influence its colour.

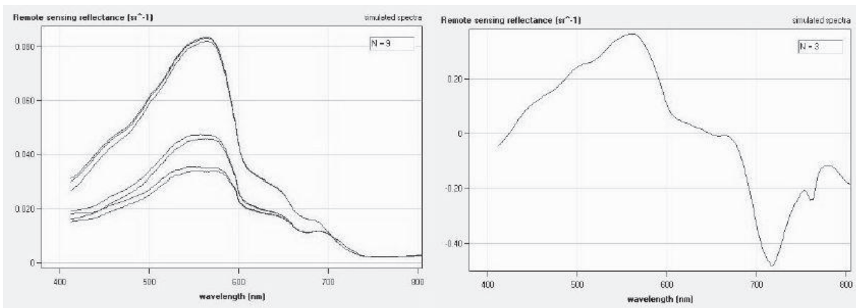

(a) Concentration of Gelbstoff at depths 0.5 8.0 m

(b) Bottom reflectance at depth 0.5-4.0 meters

Figure 3.9: Sea water physical properties, modelled by WASI

The data provided with the model was determined at freshwater of the Boddensee [44], yet the model was adjusted for the marine environment, so that its parameters (concentration of chlorophyll, concentration of small particles, yellow substance, etc) now perfectly simulate the Mediterranean water conditions. The remote sensing reflectance has been compared under the conditions of different water depths and cover fraction of the seafloor, in order to assess spectral signatures of the seagrass and carbonate sand as major seafloor types. WASI enables to use forward or inverse calculation for the spectrum types at a diapason of 350-800 nm with a 1nm spectral resolution. For the spectral analysis we applied forward calculations, i.e. a computing and plotting of series of spectra according to specified parameter settings, with exactly defined depths and cover fraction.

The specific parameters have been chosen for the simulation of the environmental conditions where seagrass grow. The adaptations to life in salt sea water requires various physical and chemical parameters which include salinity, temperature of 17-25°C, light requirements with 10-20 % on average, ranging from 4.4% minimal up to 29 % [91], so that the zenith angle is taken as 35- 45° and reflection factor 0.0201. P.oceanica. These values, simulating the environment of the Mediterranean Sea, are fixed (Tab.3.1) among WASI user-defined parameters. The calculations are done for the spectrum 350-800 nm, covering the most important part of the RS spectrum: 1) Blue-green 0.45 - 0.5 μm; 2) Green 0.5 - 0.6 μm; 3) Red 0.6 - 0.7 μm; 4) Red-NIR 0.7 - 0.8 μm (Fig.3.9).

3.5.1. Model parameters: depth and bottom cover fraction

Although seagrass *P.oceanica* can be found until depth limits down to 40 m depth [52], the most preferable limits of its distribution in the Mediterranean Sea are shallow waters until 4 meters of depth.

The increase of depths (zB) influences weakening of light and thus directly affects production of chlorophyll, because when light passes through the water and suspended particles, it is being largely modified through the absorption and scattering before it finally reaches plant canopy of the seagrass. Therefore, the most healthy and suitable areas for the seagrass grow are located at depths lesser than 4 meters (Fig.4.5).

3.6. Google Earth aerial imagery for the seagrass mapping

Apart from the satellite imagery, the aerial photographs from the Google Earth provide a powerful tool for seagrass mapping, because they are important, reliable, detailed and up-to-date source of imagery. Perhaps, the clearest advantage of the Google Earth imagery is its high resolution (15 m in land areas and lower in the oceans). Obtained from the airborne platforms, Google Earth images have general spatial resolution of several meters (though varying in different areas), which allows very detailed habitat and seafloor types discrimination, comparing with images acquired from the space-borne satellite platforms.

Parameter, WASI	Name and description	Values
C-L	Concentration of large suspended particles	8
C(i), i=0..5	Concentration of Phytoplankton	0.035 -0.089 ug -l
bbS	Specific backscattering for small particles	0.005 m2g-1
T-W	Temperature of water	17-25 C
n	Exponent of Backscattering by small particles	0.005 m2g-1
Q	Anisotropy factor of upwelling radiation ("Q-factor")	5.00
sigma-L	Reflection factor of sky radiance	0.0201
b1	Backscattering coefficient of saline waters	0.00144 m-1
0	Reference Wavelength for Gelbstoff absorption	440
sun	Sun zenith angle	45.0
zB	Bottom depth	4.00
f(i), i=0...5	Areal fraction of bottom surface type number n	01/10/10
K0	Coefficient of Attentuation	1.0546
view	Viewing angle (0 = nadir)	0
C-X	Concentration of non-chlorophyllous particles (absorption at 0)	0
S	Reference wavelength for scattering of small particles	500
C-S	Concentration of small suspended particles	0
S	Exponent of Gelbstoff absorption	0.0140
C-Y	Concentration of Gelbstoff (absorption at 0)	0.400
Bn	BDRF of bottom reflectance (sand)	0.318 sr -1

Table 3.1: Model-specific parameters of water WASI adjusted to simulate environment of the Mediterranean Sea along Crete

The spatial coverage of the Google imagery is lesser comparing to space-borne images, but this can be solved as well: while in general providing smaller area coverage than satellites images, the Google Earth images can be stitched to the composite maps of the acceptable spatial extent, using script written on Python (Fig.A.1) and Geospatial Data Abstraction Library (GDAL) technologies (Fig.A.2) for the Google grabbing process (Fig.A.52) which allows multiple overlapping of single images over the flight paths, and generates mosaics.

3.7. Image processing using Erdas Imagine

The analysis of the imagery of Cretan coasts is based on the images classification and is aimed to investigate the distribution of the seagrass *P.oceanica* within the research area. In the image processing part of the research supervised classification has been applied to the aerial and satellite images. Seagrass meadows and other seafloor cover types were evaluated through a detailed examination of the imagery. Seagrass beds are clearly visible in color aerial Google Earth photographs (Fig.A.42, Fig.A.43), contrasting against slightly-yellow and brownish sand bottom. The seagrass areas are detected using different bands combinations, masked and studied for the estimation of the changes in the areas. The classification is based on the properties of the *P.oceanica*, such as brightness, colour, texture and structure of the seagrass mattes (Fig.3.10a). The raster-based mapping includes supervised classification with training sites of seagrasses (10-15 set areas) in different bands for each photograph by classification a series of polygons characteristic of each of the sea floor bottom types: sandy surface, seagrass bed for each species including *P.oceanica* (meadows), patchy seagrass bed and algae on rock, rocks, muddy surface, etc (Fig.3.10b).

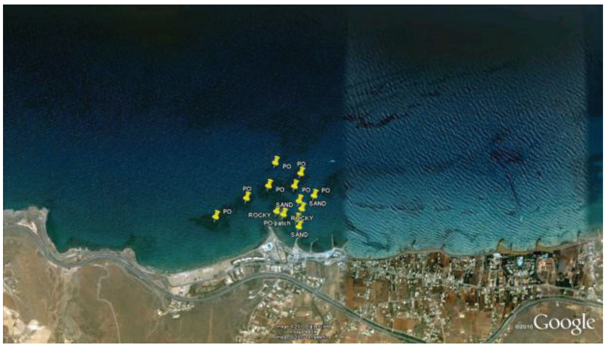

small-scaled (1:54,000)

enlarged (1:10,000)

Figure 3.10: Seafloor types of the Arina beach: P.oceanica, sand, rocks. Google Earth images

On the basis of the image processing and classification, applied to the northern coats of Crete, the marine bottom types between 10 m depth has been mapped, including the limit depths of the of the seagrass meadows provided on the basis of the available and collected field data. The classification has been completed using ENVI and Erdas Imagine software.

4 Results

4.1. Analysis of spectral signatures

The distinguishing spectral signatures for various seafloor types (e.g. seagrass species, coral reefs, various types of sand, mud, other sediments, (Fig.4.3) exist in well-defined and narrow (10–20 nm) wavelength ranges.

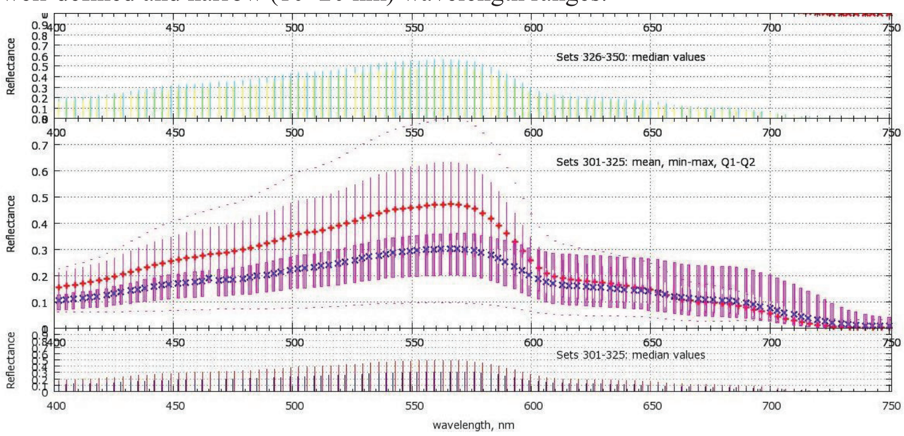

Figure 4.1: Statistical comparison of spectral reflectance of P.oceanica and carbonate sand. Selected measurements sets. Gnuplot graph

The values of their spectral reflectance are accepted as constant. The results of spectral measurements enable to analyse, whether *P.Oceanica* is spectrally distinct from other sea floor types with changing environmental conditions, using the differences in their spectral signatures on the graphs in a WASI, the Water Colour Simulator software. The Water Colour Simulator WASI, a software tool for analysing and simulating the most common types of spectra [44], is highly suitable for the seagrass spectral analysis. There are several environmental characteristics, included in WASI interface (Fig.5.1), which influence the results of water spectral reflectance, e.g. different bottom depths, concentration of suspended particles in water column, water temperature, sun angle, concentration of Gelbstoff (coloured dissolved organic matter), concentration of phytoplankton, aerosol scattering, exponent of backscattering by small particle [43]. The backward-scattering coefficient (bb), also included in WASI, is a fundamental optical property which plays a central role in the ocean-colour remote sensing, providing the remotely sensed optical signal, as well as suspended particle distributions, water clarity, and underwater visibility [79]. WASI enables simulation of backscattering of pure water, large and small particles. The values of all these parameters can be redacted and changed manually. However, the most important, major factors affecting the *in-situ* conditions are water depth (Fig.4.5) and cover fraction of the seafloor types: *P.oceanica* and carbonate sand.

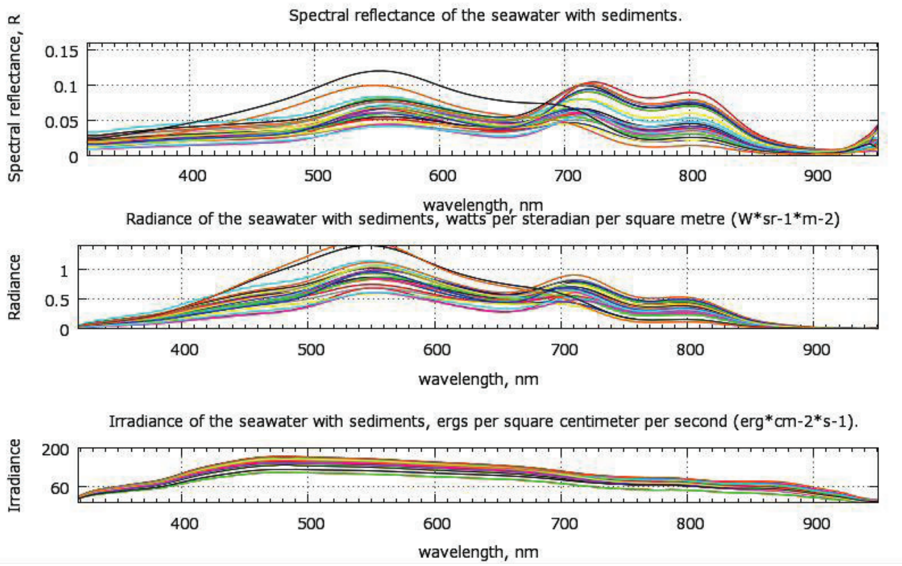

Figure 4.2: Optical properties of the sea water with sediments, measured in aquarium tank. Agia Pelagia district, Crete. Gnuplot

Seagrass *P.oceanica* can be mapped using remotely acquired spectral imagery, if it has distinctive reflectance signatures at different depths. Therefore, the depths of the shelf area are the first variable condition for this research question. The depths values chosen for the current research are lesser than 3.5 meters, covering shelf zone, and providing the best environmental conditions for the seagrass P.oceanica: 0.5, 2.0 and 3.5 meters with an interval of 1.5 meters.

The 3.5 m depth limit was chosen based on the analysis of the separability of seagrass reflectance signatures, received by the means of previous *in-situ* measurements (year 2009) of the radiance and irradiance of water in Agia Pelagia bay, which indicated that *P.oceanica* seagrass could be only well separated within depths of 3.5 m. A statistical analysis of WASI-simulated spectral reflectance has been used in order to answer the first research question: whether the *P.oceanica* spectra is spectrally distinct at varying environmental *in-situ* conditions, and if *P.oceanica* remains spectrally distinct with the increasing water column depth. To answer this research question, different seafloor cover types are discriminated using data of the broadband remote sensing.

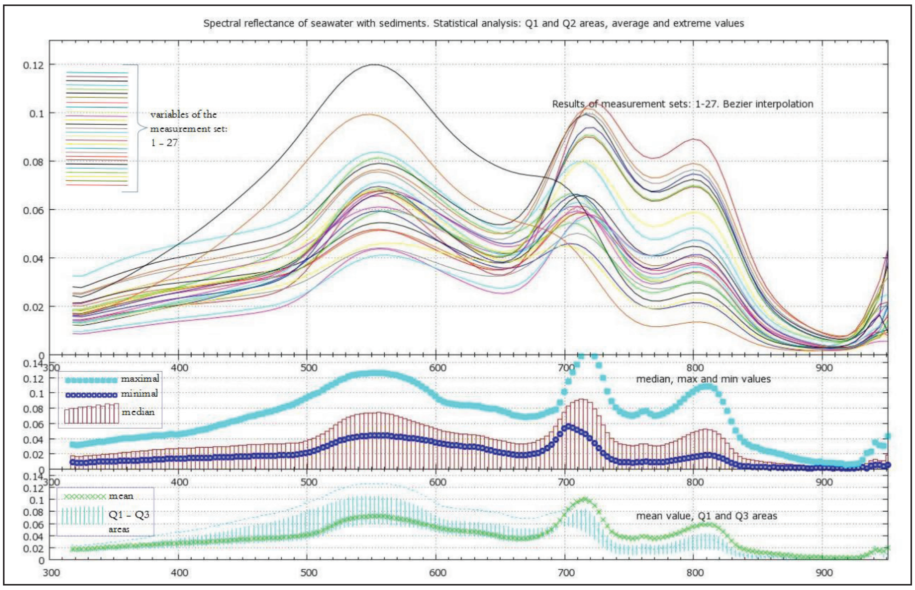

Figure 4.3: Multiplot showing spectral reflectance of the seawater with sediments, measured in aquarium tank, Agia Pelagia district, Crete. Gnuplot.
Two complimentary graphs below show the results of the statistical analysis.

The results enable to study reflectance properties of the seagrass and other seafloor types. Application of the optical radiative transfer model WASI is suggested to simulate remote sensing sensors (MODIS, ASTER, MERIS and SeaWiFS), (Fig.4.4, Fig.A.34). In order to focus on the factors of primary importance, other and less influencing factors are excluded, i.e. sun angle, concentration of the suspected particles in the water column, content of Gelbstoff, etc. For these factors default values of WASI are accepted. Under normal conditions by independent water colour sampling, values of the remote-sensing reflectance can vary by 12–24 per cent [133], and these variations in the radiometric determinations are mainly caused by the variety of the environmental factors.

Different factors influence colour and spectral reflectance of water, among which different bottom depths, concentration of suspended particles in water column, water temperature, sun angle, concentration of Gelbstoff (coloured dissolved organic matter), concentration of phytoplankton, aerosol scattering, exponent of backscattering by small particles, cloudiness, viewing geometry and wind speed (which is, however, not the major source of uncertainty). All these environmental components increase the absorption and scattering of light which, in its turn, results in a complex relationship between their concentrations and the radiance of water that finally influence its spectral reflectance.

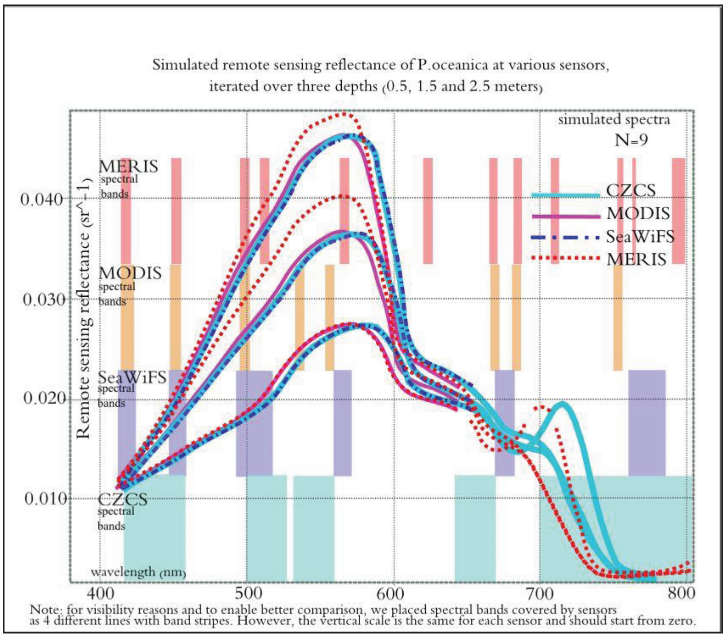

Figure 4.4: Simulated remote sensing reflectance of P.oceanica at various sensors, iterated over three depths: 0.5, 1.5 and 2.5 meters

4.2. Spectral discrimination of *P.oceanica*

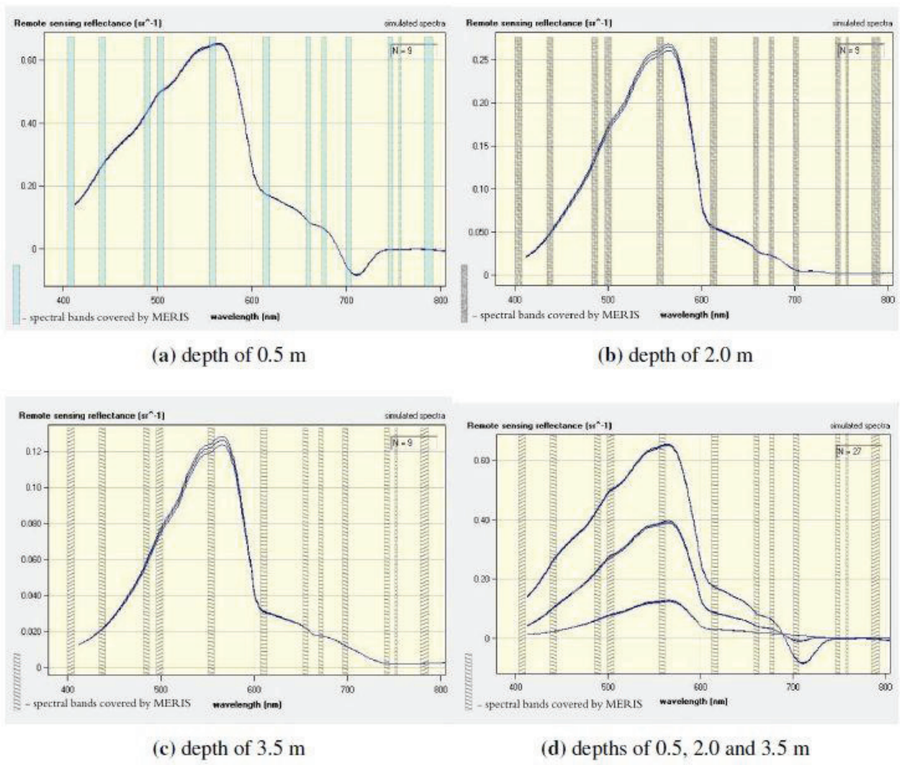

(a) depth of 0.5 m

(b) depth of 2.0 m

(c) depth of 3.5 m

(d) depths of 0.5, 2.0 and 3.5 m

Figure 4.5: Remote sensing reflectance of P.oceanica at various depths simulated for broadband sensors.

An analysis of the spectral reflectance of *P.oceanica* is done using the WASI simulations in order to determine, which wavebands can be still used to identify *P.oceanica*. The analysis of spectra shows that the appropriate wavebands for seagrass mapping lay between 500 and 600 nm and has also peaks at around 700 nm, ca between 680 and 710 nm (Fig.4.6). The highest values of the bottom reflectance are at spectra of 500-600 nm. The most appropriate depths at which the spectral signatures of the seagrass could still be discriminated are lesser than 2.5 meters.

The patches of white sandy bottoms of the seafloor, studied in the fieldwork in Ligaria beach, are much brighter than mattes of *P.oceanica* (Fig.A.11, A.10): seafloor types in Ligaria), which can be clearly seen at the graph comparing values of the spectral reflectance of the carbonate sand (Fig.A.39) and that of *P.oceanica* (Fig.A.37). The graph is received in excel spreadsheet using mean values of spectral reflectance of sand (Fig.4.10) and seagrass (Fig.A.39), respectively, which have been calculated from measurements of radiance and irradiance received in Agia Pelagia bay.

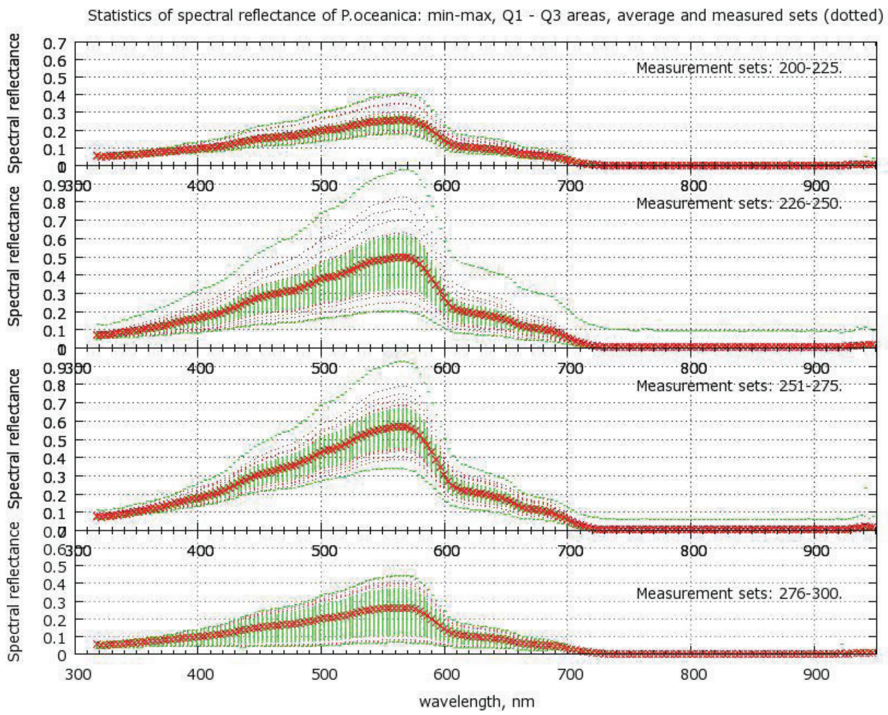

Figure 4.6: Statistical analysis of the spectral reflectance of P.oceanica: min-max, average values (red bold points), Q1-Q3 areas (green vertical dashed) and measured values (dotted): multiplot of measurement sets 200-300. <u>*Gnuplot*</u>

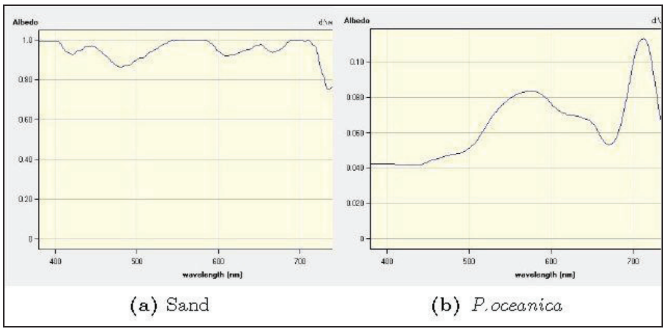

Figure 4.7: Bottom albedo of carbonate sand and P.oceanica, Agia Pelagia

4.2.1. Statistical analysis of the observational data and hypothesis testing

The total amount of measured data was large and included following datasets made using hyperspectral radiometer Ramses: 350 measurement sets of *P.oceanica* reflectance for 14th Oct (Tab.A.28), 400 sets of *P.oceanica* reflectance for 15th Oct (Tab.A.11), 84 datasets for seawater reflectance with sediments, 105 datasets for seawater reflectance without sediments, 87 sets for spectral reflectance of carbonate sand. A statistical approach is evidently necessary for the proper processing of such amounts of data. The schematic view of the statistical approach used for the data processing can be seen on Fig.3.8. Statistical pre-processing of large sets of serial data enables to generalize data by using the most typical and predicted values of spectral reflectance for further calculations, and to get rid of the extreme values, noise and errors. The statistical calculators were mainly made by means of Gretle and SPSS. The Open Office was used for preliminary data view and pre-processing, and included following computations at each data set (for example, Fig.A.26) with summary outcome of mean, median, Q1 and Q3, standard deviation, min and max values (Tab.4.1, Tab.A.11). The statistical pre-processing and analysis were made to display the mean values of spectral reflectance, which were used for comparison with reflectance data of various seafloor cover types as well as seawater with and without sediment (e.g. Fig..A.16). In the statistical analysis of the raw observed data pool of the values of spectral reflectance (about 400 single measurements for P.oceanica, e.g. Tab.A.11), we summarize their complexity by concentrating on some simple numerical characteristics that they possess, i.e. parameters. Examples are the mean and variance of a probability distribution of measurements dataset (for example, Tab.A.5). We divided the total data pool into datasets of 25 measurements for more probability distribution of spectral reflectance describes the average value of the random variable over all of its possible realizations (appendices). Conceptually, there are an infinite number of such realizations, therefore parameters are not known to us. However, in the statistical analysis of the observed data our goal is to estimate these parameters using a finite amount of information available to us: fieldwork observations. Thus, we collected a number of realizations (a sample of 25 measurements for both sand and P.oceanica) and then estimate the statistical parameters (appendices).

Finally we analysed about 400 datasets totally (example of carbonate sand on Fig.4.9, *P.oceanica* - on Fig.4.8) made during different days. Since the actual values that measured variables of spectral reflectance take on are not actually known before we observed them, they are random. Thus, we analysed the statistical distribution of the spectral reflectance values of seafloor cover types using common mathematical formulae, implemented in Gretl software (Tab.A.3). Their probability expresses uncertainty about the possible values of the spectral reflectance of *P.oceanica* and sand, respectively. There is a distinction to be made between variables whose values are not yet observed (random variables) and those whose values have been observed (observations). Each time we observe the outcome of a random variable of spectral reflectance, we obtain an observation, which is hence no longer random. We applied various methods of statistical analysis towards data pool (some examples of the selected tables are in the appendices: Tab.A.18, Tab.A.25, Tab.A.23, Tab.A.24, Tab.A.29), in order to analyse the distribution of values of spectral reflectance of P.oceanica. A probability distribution, a mathematical statement about the possible values that the random observations of spectral reflectance can take on, displays the relative frequency with which each possible value of spectral reflectance is observed. The least absolute deviations (LAD), a popular optimization technique, were used to show the main trend of the distribution of spectral reflectance values along the spectra (Tab.A.4). Non-linear logistic analysis is applied to specify and estimate a model of spectral distribution, in which the dependent variable (i.e. the value of spectral reflectance for each single observation) is not continuous, but discrete and independent for each case (Tab.A..12).

As the observations were made in a repeated way, we also analysed the data pool using autocorrelation as well: Tab.A.19 and Tab.A.14 for *P.oceanica* and Tab.A.27 for carbonate sand. The autocorrelation, a cross-correlation of an observed value with itself, made on two different days (14th and 15th October), shows the similarity between observations as a function of the time separation between them, as can be seen on Fig.A.32, Fig.A.31 and Fig.A.41, it is a useful tool for finding repeating patterns for a single value of observations, such as the presence of a periodic signal which has been buried under noise. The autocorrelation analysis has been performed using both SPSS and Gretl software (Fig.A.27). The method of least squares minimizes the sum of the squares of the errors made in solving every single observation made. We tried different approaches of the least squares methods: Tab.A.15, Tab.A.18, WLS: Tab.A.26, OLS: Fig.A.15.

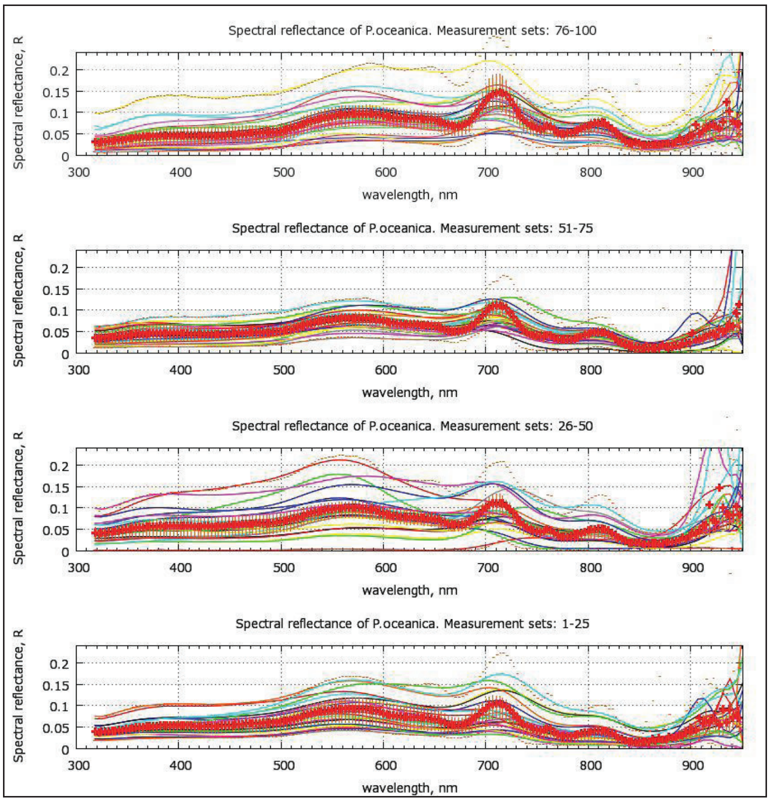

Figure 4.8: Multiplot display of spectral reflectance of P.oceanica. Series 1-100. Shown midspread of the statistical quartiles Q1 and Q3 (vertical dashes) and mean value within the range (red bold dots).

To focus on the relationship between a dependent variable (each single observation of the spectral reflectance) and independent variables (three various depths: 0.5, 1.5 and 2.5 meters) we used the regression analysis, which enables modelling and analyzing values of the spectral reflectance at several depths: Tab.A.6, Tab.A.47, Tab.A.8. The summary of the values of spectral reflectance properties on various depths is presented on the Tab.A.10. The k-means cluster analysis has been used for partitioning observation sets into k clusters (Tab.A.19, Tab.A.20, Tab.A.21, Tab.A.212) in which each observation belongs to the cluster with the nearest mean. It enables to highlight the main areas of the location of values of spectral reflectance along the spectra. To estimate spectral density of optical measurements we used periodogram function (Tab.A.30), which corresponds to the general spectrum of the observations with representation of a variable quantity. Thus, the periodogram

(Fig.A.40) of the series of observation highlights so-called “dead spots” of low power between the frequencies we wish to exclude (can be seen clearly at the end of the graphs, e.g. Fig.A.27) and the frequencies we want to retain (the general profile that lies in the 450-850 nm, Fig.A.29, enlarged part of 500-660nm). The visualization of the data plotting was made by means of Gnuplot software, which enables fine drawing and advanced displaying of large amounts of serial data, ultimate control over graph properties, the simplicity of plotting and the ease of scripting (see Fig.4.8, appendices).

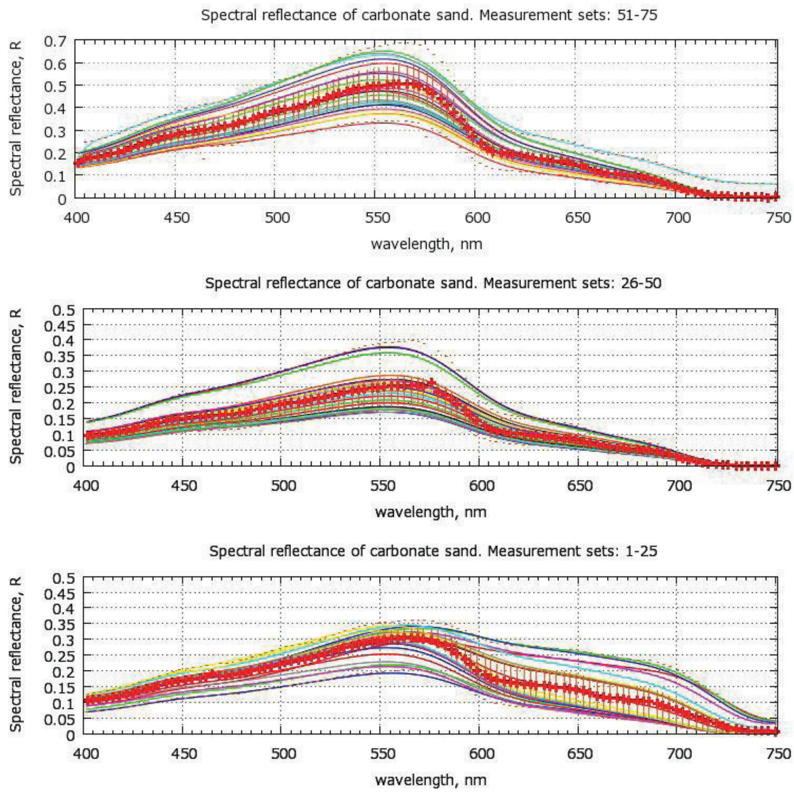

Figure 4.9: Multiplot of spectral reflectance of carbonate sand. Series 1-75. Shown mid spread of the statistical quartiles Q1 and Q3 (vertical dashes) and mean value within the range (red bold dots).

The graphs illustrating spectral signatures of various seafloor cover types display the mean values and areas of quartiles (Q1, Q3, Fig.A.38, and shaded areas on graph, Fig. 4.6, Fig.4.9), which cover most probable data distribution (spectral reflectance) for each spectral band. In x-axis displayed are the areas of 400 – 950 nm in spectra, where the measurements were done; the y-axis was adjusted for the better visualisation of the *P.oceanica* spectra: as its spectral values are mostly located in the lower part of the spectra (usually no more than 0.20 nm, except for borders), we did not extend the y-scale up to 100 percent, in order to focus on the most necessary area of spectral values (Fig.4.9, Fig.4.3 and appendices). The mean values are highlighted using bold red points, as we used these values for plotting the final graph of *P.oceanica* spectra in Ligaria beach, Agia Pelagia.

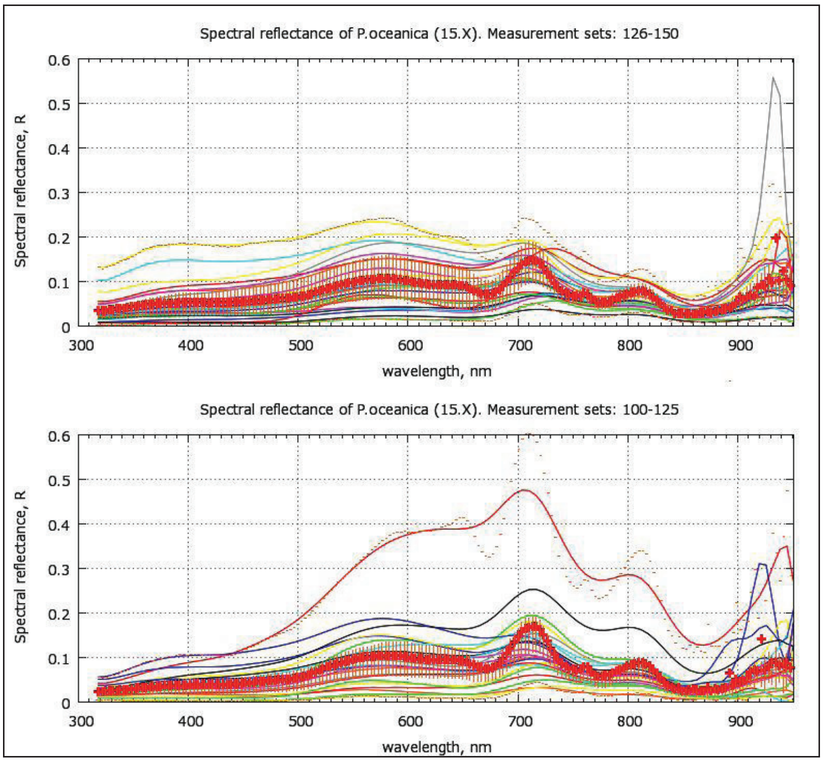

Figure 4.10: Multiplot display of spectral reflectance of P.oceanica. Measurement sets 126-150, 15th October. Bold red dots show the mean values within each dataset; vertical areas: quartiles Q1-Q2.

A statistical hypothesis test has been applied for the making decision and controlling the wealth of the observational data of the hyperspectral measurements of the water reflectance. The received results are statistically significant if they are unlikely to have occurred by chance alone, according to a pre-determined threshold probability, the significance level. Therefore, we applied critical tests of significance to analyse the measured data according to their significant value.

Answering the first research question, we suggest the following statement. If the *Hypothesis Ho* is true, then the spectral distinguishability of the seagrass *P.oceanica* from other seafloor types (carbonate sand) is not changing with varying *in-situ* conditions, *Ho*: $\mu1 = \mu2 = \mu3 = ... = \mu n$. The alternative *Hypothesis Ha* claims the opposite statement: “the spectral discernibility of the seagrass *P.oceanica* is distinctly changing with varying *in-situ* conditions, i.e. increasing depth, Ho: $\mu \neq \mu 2 \neq \mu 3 \neq \ldots \neq \mu n$“. Two statistical approaches have been used for confirmatory data analysis and hypothesis testing.

ANOVA-testing

We applied ANOVA (ANalysis Of Variance) testing for the analysis of the probability of the spectral reflectance of *P.oceanica* to be more or less spectrally distinct from other seafloor cover types with changing depth. W are checking the statement Hypothesis Ho, is true, which is “the spectral distinguishability of the seagrass *P.oceanica* from other seafloor types is not changing with varying *in-situ* conditions, Ho: $\mu 1 = \mu 2 = \mu 3 = \ldots = \mu n$.” which gives the following outcome. P(reject H0|H0 is valid)= P(X>c|p=)=.05 where c comes for critical values and p=probability. The result P=.05 is (Tab.A.9), hence, very small, which makes the statement of Hypothesis Ho highly unlikely (less than 1 in a 10 chance). The one-way ANOVA highlighted a significant difference between data of spectral reflectance of *P.oceanica* and carbonate sand at different depths, and proved spectral discernibility of seagrass *P.oceanica* from carbonate sand (Fig.5.1), i.e. true is the opposite statement: *Hypothesis Ha*=“the spectral discernibility of the seagrass *P.oceanica* is distinctly changing, and seagrass can be spectrally discriminated from carbonate sand with varying *in-situ* conditions, i.e. increasing depth, Ho: $\mu \neq \mu 2 \neq \mu 3 \neq \ldots \neq \mu n$“.

As a result of the statistical testing, we came to the following conclusion. The Hypothesis Ha is true, which claims that the spectral discernibility of the seagrass *P.oceanica* is distinctly changing and can be discriminated from other seafloor cover types (carbonate sand) with varying *in-situ* conditions, i.e. increasing depth, Ho: $\mu 1 \neq \mu 2 \neq \mu 3 \neq \ldots \neq \mu n$, which positively answers first research question. Statistical results are illustrated with Error bars made using Excel’s vertical box and Whisker Charts (Box Plots). The graphs were plotted on the basis of the following statistical data calculated from the sampling measurements data: Tab.A.11, Tab.A.28 , Tab.A.5

Statistical values	318.19	418.3448	518.8361	619.3662
Mean	0.034521	0.049235	0.076088	0.085287
St Dev	0.019849	0.030338	0.042587	0.046569
Median	0.033035	0.046197	0.07704	0.080277
Q1	0.019293	0.023706	0.045606	0.049468
Q3	0.042477	0.057934	0.092289	0.114191
Minimum	0.007898	0.010087	0.021373	0.022691
Maximum	0.076835	0.110906	0.18938	0.216231
25th Pct	0.019293	0.023706	0.045606	0.049468
50th Pct	0.013743	0.022491	0.031435	0.030808
75th Pct	0.009441	-0.01174	-0.01525	-0.03391
Min	0.011395	0.013618	0.024232	0.026777
Max	0.034358	0.052972	0.097091	0.1

Table 4.1: Statistical analysis of the measurements of spectral reflectance of P.oceanica (fragment)

The abbreviations stand for the following values: Mean: Average of the data to be plotted, AVERAGE data St Dev: Standard deviation, STDEVdata Median: Median of the data, MEDIANdata Calculating interquartile ranges: Q1=First quartile, PERCENTILE(data*0.25) and Q3=Third quartile, PERCENTILE(data*0.75) Minimum: Minimum value, MINdata Maximum: Maximum value, MAXdata 25th Pct: Plotting value of first quartile = Q1 50th Pct: Plotting value of median = Median-Q1 75th Pct: Plotting value of third quartile = Median-Q3 Min: Lower error bar length=Q1 - Minimum Max: Upper error bar length=Maximum - Q3 The statistical analysis is displayed on the Graph 1.1 which compares the spread in sets of measurement data of spectral reflectances of under various environmental conditions (depth).

4.2.2 Remote sensing application

The *in situ* spectral reflectance data of *P.oceanica* and sand were used to model these seafloor cover types as the different sensors would percept them: MODIS, ASTER, MERIS, SeaWiFS and CZCS. These sensors vary in technical characteristics and therefore, have different spectral sensitivity, which we briefly illustrated in a small summary table (Tab.2.1) These models simulate spectral views of the chosen sensors, how these sensors will "see" seagrass (Fig.4.51) and sand as pixels, with accepted default atmosphere and water column effects (given by WASI software). In such a way we defined an empirical upper limit to the discriminative potential of these sensors. The analysis of the remote sensing reflectance simulated by these sensors shows that the measured spectra of seagrass P.oceanica (Fig.4.8, Fig.4.10) were statistically different at most of the spectral bands (Fig.A.35, Fig.A.36,), with a 95% confidence level (p value < 0. 05). The F values of the test (F=8.477 as on Tab.A.7) are greater than F critical value, which is 2.64 at 0.05

confidence level. This proves that broadband and hyperspectral sensors enable spectral discrimination of seagrass. Therefore, we answer the second research question positively, i.e. broadband and hyperspectral sensors (Fig.4.4 and Fig.A.34) provide enough radiometric information for spectral discrimination of seagrass and can therefore be used for P.oceanica mapping.

4.3. GIS mapping of seagrass

4.3.1. Data integration

The integrated approach used in this research work has high potential as a means to monitor changes in seagrass landscape occurring in shallow waters over Crete area. It encompasses the integration of high resolution aerial color Google Earth photography, spaceborne satellite imagery, assessment of spectral signatures using WASI software, image processing by means of Erdas Imagine (Fig:A.50, Fig.A.49) and ArcGIS based mapping. The use of GIS for data incorporation (Fig.4.11), storage, analyses, visualizing and mapping enables to analyze environmental changes within seagrass landscapes based on data from various sources: aerial and satellite images, geographically referenced maps of Crete Island and results of images classification showing areas of seagrass distribution. The final mapping has been supported in ArcGIS through the data exporting, conversion and integration of various data in one GIS-project (Fig.4.11). Data collected during the fieldwork, imagery of the seagrass distribution are added into a GIS dataset for the assessment and spatial analysis.

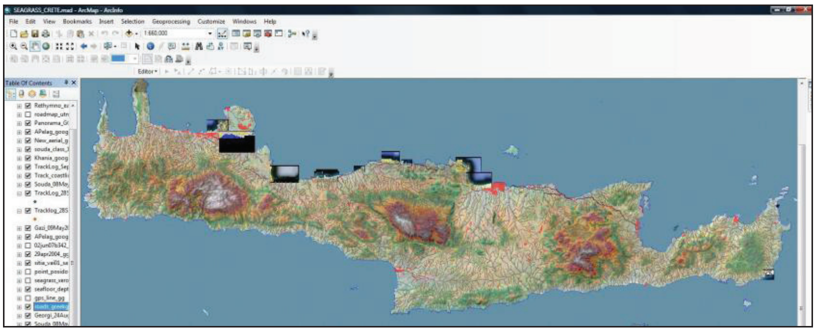

Figure 4.11: Google aerial images incorporated into the GIS project: fragment of ArcGIS layout

4.3.2. Accuracy assessment

We prepared the error confusion matrices (Fig.A.32 and Fig.A.33) using kappa statistics to assess and evaluate accuracy of the classification. The accuracy assessment has been done using Erdas Imaging function *Classifier/Accuracy Assessment*. In the Accuracy Assessment viewer we have chosen utility *Edit* in order to generate random points throughout the classified image, and then chosen the *Create or add random points* dialog. After the points were generated, we entered the class values for the reference points from the supervised classification. In order to perform a proper accuracy assessment we needed about 300 points so that we defined the number of points for the selection. From the option parameters for points distribution we have chosen "*stratified random*" as better representing the variables. Then we evaluated the location of the points and determined their class value, which was done with ground truth points from Google Earth aerial photos for various data and seafloor imagery and with reference to the signature file, to find the numeric value that has been assigned to each class previously. Finally, to print the errors matrix, we selected *Accuracy Assessment* viewer again and chosen there *Report/ Options* with turned on *Error Matrix, Kappa Statistics* and *Accuracy Total*. The error matrix is just comparing reference points of various seafloor cover types to the classified points (i.e. seagrass, carbonate sand, various land cover types on the coast). The Kappa coefficient takes into account chance agreement and thus, shows the reduction in errors generated by a classification process compared with the errors which could be received by a completely random classification – in other words, it evaluates quality of the classification. The overall map accuracy by supervised classification is 72% (Fig.A.33), which means that 72% of the pixels are classified to the correctly chosen seafloor cover type in case, and in case of unsupervised classification we received result of 64% (Fig.A.32) which proves that supervised classification is preferable method for seagrass mapping.

5 Discussion

5.1. Remote sensing for seagrass mapping

An approach of the seagrass spectral analysis, monitoring and mapping has been taken in this work, which integrates various research techniques and tools, combining remote sensing methods of spectral analysis of the seafloor cover types, and knowledge of the ecology of *P.oceanica*, with the aim to develop a method of seagrass spectral optical discrimination for the seagrass mapping based on the aerial imagery classification.

In *Chapter 1* we discussed main objective of this MSc thesis, which was to study possibilities of seagrass mapping, based on the application of the remote sensing measurement of the seawater optical properties using hyperspectral radiometers.

The relationship between the optical properties (spectral reflectance) of the seafloor cover types and hydrological parameters of the environment has been studied in order to analyse limitations and capabilities of broadband and narrowband sensors under the conditions of altering environmental parameters. For the retrieval of hydrological parameters - seawater radiance, irradiance and spectral reflectance of various seafloor cover types, - spectral optical field measurements were carried out in 2009 at the testing sites in Agia Pelagia, Heraklion and Ligaria beach, Crete Island using Trios-RAMSES spectroradiometers.

Further in *Chapter 1, 1.8 Research assumptions*, we assume the constant values of the optical properties of the seawater, phytoplankton, total amount of suspended particles and solids, atmospheric conditions, as well as coloured dissolved organic matter (CDOM), which have been set up in modelling part of this work, during WASI simulations of various remote sensors.

The second *Chapter: Seagrass monitoring: overview of literature and research resources* starts from the review of the available research resources and then discusses various RTM and reported experience of the remote sensing application towards seagrass mapping. In section *2.2 of Chapter 2, Measuring water optical properties: hyperspectral radiometers,* the RAMSES-ACC-UV and RAMSES-ARC spectroradiometers of Trios-RAMSES Hyperspectral Sensor series are described.

The instruments Trios-RAMSES have been used during the fieldwork measurements-2009 for the collection of the reflectance spectra. The RAMSES-ACC-UV measures spectra in the wavelength domain between 280 nm and 500nm, the RAMSES-ARC, suitable for UV and visible spectra, covers diapason of 320-950 nm with spectral accuracy of 0.3nm (better than 6%), typical saturation (at 200nm) of *1Wm-2nm-1sr-1* in 256 channels with a sampling interval of 3.3 nm/pixel and a field of view is 7 degrees. The spectral reflectance of the seawater with and without sediments was calculated by the ratio of the radiance and irradiance values.

The reflectance spectra of *P.oceanica* show (Fig.4.6, A.27, A.28, A.35, A.36) a values maximum between 450 nm and 600 nm, first, because of the chlorophyll absorption peak at 465 and 665nm (Fig.A.4), secondly, because of the weakening of CDOM (or Gelbstoff) in the blue part of the VIS spectrum, as it most strongly absorbs short wavelength light in blue to ultraviolet range, and finally, because the absorption of the seawater increases in the red part of the VIS spectra. The decrease in spectral reflectance values of *P.oceanica* after 660 nm (Fig.A.28) is caused by the second absorption peak of phytoplankton. The magnitude of the reflectance maximum slightly varies at single variables between about 8 % and 12 % (as on Fig.A.27) and is probably related to the individual pigmentation and colour composition of single leaves, their structure and geometric orientation, which naturally causes variations in radiance values.

Figure 4.7: WASI water color spectral simulation modeller: Spectral reflectance of P.oceanica and silt at 0.5-4.0m

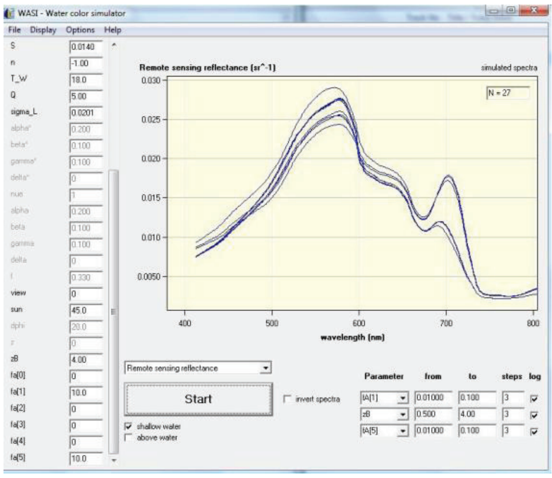

The ecological variables, specific to the field environmental conditions, were factored into the WASI-based simulation models. Through the WASI simulation process, imitating spectral properties of *P.oceanica* and carbonate sand for various broadband and narrowband sensors, models were created that accounted for not only atmospheric conditions (i.e. sun zenith angle), but also height of water column, thus approaching it to the Mediterranean conditions, and chemical content of the seawater (i.e. amount of suspended particles, Gelbstoff, etc), which results in models of optical properties of "seawater with sediments" and "seawater without sediments".

The *in-situ* field large-scale matte-level level of seafloor monitoring was then upscaled to airborne Google Earth aerial imagery interpretation, to provide a meadow-level view of seagrass landscapes. An attempt of the small-scale mapping is designed on an example of Landsat satellite imagery. However, in upscaling to this third, small-scale mapping level further environmental variables need to be considered: health conditions of the seagrass, presence of other underwater vegetation (e.g. other seagrass species), hydrological specifications (e.g. direction and speed of currents, amplitude of tidal waves, etc), season, date and times of the image taken. Therefore, we focused on the first two levels in the current work. These different levels have been individually considered in terms of the seagrass spectral discernibility for monitoring and mapping, from which the first two levels have been brought together, to provide a roundup of the achieved results and an overview of what still has to be done in *P.oceanica* seagrass mapping by future researchers (see Recommendations).

In *Chapter 3: Materials and Methods*, describing data collection, a videographic approach tested in previous works, has been applied during the summer fieldwork, when we captured imagery and video footage of the seafloor on several routes of the boat in the Ligaria beach.

The finding of *Chapter 4: Results* showed that the relationship between the spectral reflectance of various seafloor cover types was tied to depth, i.e. water column height. Thus, the results of the *in-situ* fieldwork measurements revealed that spectral reflectance of *P.oceanica* undergo alterations at depths of 0.5, 2.0 and 3.5m (Fig.4.5). The analysis of the spectral signatures of the seagrass *P.oceanica* and sand clearly shows (Fig.A.17) that seagrass has spectral reflectance much lesser than that of a carbonate sand, in general not increasing values of 10% reflectance in spectra of 500-600 nm, while sand has spectral reflectance approaching 33% in its highest values. These results indicate that seagrass P.oceanica can in general be detected and discriminated from other seafloor cover types with varying environmental conditions, i.e. water column height, by hyperspectral spectroradiometers (Trios-RAMSES), which positively answers the **first research question** of this thesis ("Is *P.oceanica* spectrally distinct from carbonate sand with varying *in-situ* conditions ?"). Further in *Chapter 4: Results*, studies of the broadband and narrowband sensors demonstrate that simulated spectra of the seagrass, made using WASI modeller, have the best results at CZCS scanner, especially devoted to the measurement of ocean color. The spectrum of *P.oceanica* reflectance, simulated for CZCS, covers the wavelength interval of 400-800 nm, and is distinctive for various depths. Other remote sensors (MODIS, SeaWiFS) may also be used for the seagrass mapping, because their technical characteristics enable to spectrally discriminate *P.oceanica* seagrass from other seafloor cover types (Fig.4.4), particularly carbonate sand as tested in the current work. Therefore, the **second research question** of this MSc thesis ("Do broadband and hyperspectral sensors provide enough radiometric information for spectral discrimination of seagrass, and therefore, can be used for mapping of P.oceanica ?") is answered with "yes" and the most suitable sensor is the Coastal Zone Color Scanner CZCS. The graphs showing optical properties of seawater with and without sediments (Fig.4.3, A.17, 4.2) focused on spectral variability of the water with changed physical and chemical content. The alterations in the individual spectral signatures of single measurements (e.g. on Fig.4.8, Fig.A.35, Fig.4.10, Fig.A.37) reflect individual health properties of leaves: different nitrogen and chlorophyll content causing diverse colour pigmentation and light absorption, water content in leaves and plant physiological conditions, which vary across seagrass meadow, shoot morphology, etc. The differences in spectral reflectance values of the measurements taken on various days might have been caused by the impact of atmospheric conditions, such as solar radiation and sun illumination by different zenith angle.

For further development of the remote sensing based monitoring and mapping of the seagrass and other seafloor cover types it is desirable to consider upscale mapping with concern to bathymetry. Studies of the substratum and underwater relief in a more detailed way, i.e. bathymetric properties of the testing sizes, gives information about seagrass landscape distribution, because changes in relief directly cause and reinforce the colonisation process of *P.oceanica* meadows. Thus, the depression and valleys in relief in general stimulate increase of the sedimentation process. In turn, it enables accumulation of necessary nutrient for seagrass plant growth, increases resource allocation to the seagrass roots for better exploitation of pore-water nutrients by the *P.oceanica* shoots. While studying size of patterns and patchiness in seagrass landscapes, we would stress that anthropogenic caused disturbances (e.g. ocean trawling) should be considered as a main source *P.oceanica* landscapes fragmentation.

5.2 Upscale mapping of the seagrass landscapes

Although ocean pelagic landscapes have a high degree of spatial variance and less structurally complex, comparing to the terrestrial ones, the landscape-level phenomena have similar features, and there are accepted definitions of landscapes elements within the seagrass meadows [124]. In general, the structure of seagrass landscape is simpler than that of the terrestrial ecosystems in biodiversity and complexity; however, seagrass landscapes show variation in spatial patterns over different special scales (Fig.5.2). The complexity of the landscape of seagrass meadow is shown by the measure of patches in size and shape, expressed in ratio of patch perimeter to area. The fragmentation of the seagrass landscapes is expressed in contiguity displaying patch aggregation within meadows.
The general principles of the hierarchy within the seagrass landscapes are based upon the quantitative analysis of the spatial patterns, consisted by components and separate elements. Thus, bunches of individual shoots construct patches, the first hierarchical level. Patches are arranged into discrete clumps of mattes (at a scale of centimetres to meters) which, in turn, make up beds with l-100m in diameter. Finally, seagrass beds are arranged into meadows that may extend over kilometre-wide areas, historically defined as landscapes [124].

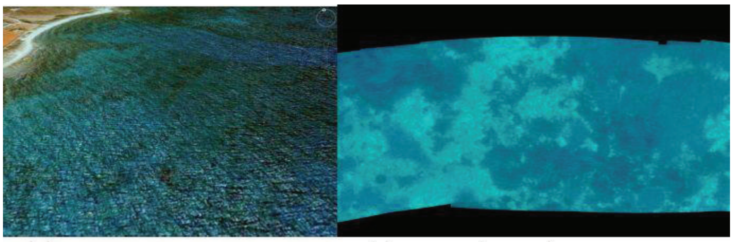

(a) Meadows of the seagrass. Source: Google Earth

(b) Patches (mattes) of the seagrass. Source: in-situ videometric measurements

Figure 4.18: Variations in spatial structure of the seagrass landscapes

Besides spatial structure of the seagrass meadows, there are strong and complex patterns of depth zoning, specific to individual seagrass species, but such detailed

classification goes beyond the scope of the current study. Unique feature of seagrass meadows, most characteristic for shallow areas, is dynamics of their landscapes. Homogeneous, continuous seagrass meadows can reach in size up to 40 m2 (Fig.3.10a), however they are often interrupted by gaps and channels of open spaces generated by the complex, disturbing sedimentation processes, turbulence and turbidity regime of waters and landscape dynamics, which form gaps and channels within meadows, making them "patchy-looking", i.e. diversified by separate mattes (Fig.3.10 b). The traditional definition for gap in vegetation cover is "disturbance generated openings in either floral or faunal cover" [24].
Formation and increase of these gaps within the mosaic of seagrass meadows is caused by different reasons. The most probable drivers for the process of gaps formation within seagrass meadows are removal of interior vegetation, differential growth of seagrass meadows and increased sedimentation. Thus, storms lead to severe deposition of sediments, burying parts of seagrass meadow, the same effect has movements and deposition of sediments during and after floods[9]. Increased nutrient sedimentation, especially phosphorus, were explored [63] as a potential mechanism for increasing patch dynamics and morphological plasticity within seagrass meadows. Finally, increasing the degree of fragmentation of the landscapes of *P.oceanica* meadows can be caused by the invasion of alien species, such as *Cymodocea nodosa, Caulerpa prolifera, Caulerpa taxifolia*. Invaders are in general strong colonizers comparing to native P.oceanica: they occupy much greater habitat space within the regressed meadows of stressed native seagrass [97]. However, on the northern coasts of Crete the only dominating seagrass species is P.oceanica. Morphological differences in scale of seagrass landscape formations, discussed above, cause need for the different-scale mapping. Therefore, the investigation of the seagrass meadows at different levels is performed using underwater videometric measurements, aerial and satellite imagery.

6. Conclusion

The goal of this MSc research was to explore the perspectives, advantages and limitations of the narrow-band and broadband sensors for the environmental mapping and monitoring of *P.oceanica* seagrass along the coasts of Crete Island. The research outcome demonstrated that the application of the remote sensing data from the broadband sensors is highly advantageous for the seagrass mapping, the spectral discrimination of *P.oceanica* from other seafloor cover types is possible at diverse and changing environmental conditions, and that *P.oceanica* is spectrally distinct from other seagrass species (*Thalassia testudinum*), Fig.2.6.

The RTM software is a powerful means for analyzing spectral signatures of various seafloor types and enabling simulations of data received from broadband and narrowband remote sensors. The example of application of WASI RTM, given in this work, is an achievement of the research insight towards the spectral properties of *P.oceanica* and other bottom cover types, enabling to discriminate them from each other with changing environmental conditions. The research shows that spectral signatures of *P.oceanica* are distinct at various depths.

The methodology of the spectral discrimination of seafloor cover types is designed in the frame of this research and is based on the application of the remote sensing RTM techniques, data from broadband sensors, hyperspectral radiometers for measurements of optical properties of the seawater, categorical and continuous statistical analysis for the data processing and GIS raster based software for images visualization, classification and analysis. Technically, we used different software, adjusted for diverse research purposes, to manage, integrate and process data from various origin and resources, and finally to receive accurate research results.

The marine coastal ecosystems are complex, constantly changing and developing. Using flexibility of GIS combined with RS methods and application of data from broadband sensors is therefore advantageous for the monitoring of coastal areas. Besides Mediterranean area, the methodology of the seagrass environmental studies can be applied towards other shelf areas with dominating seagrass landscapes.

More than 50 % of the world population lives within one km of the coast, which results in continued anthropogenic pressure on the coastal regions. Therefore, management of coastal resources and shelf zone protection become increasingly important nowadays, and require large-scale monitoring and mapping of the shelf areas as a vital instrument for the environmental assessment.

This research is a contribution to the development of the methodology of seagrass mapping with aim of the environmental monitoring, and a case study of *P.oceanica* seagrass, dominating in underwater ecosystems along the coasts of Crete Island.

6. Recommendations

To make further studies of *P.oceanica* more effective we would suggest the following recommendations to be considered by the future researchers:

1. To extend the research area towards the eastern part of the Crete Island, in order to received more regular observations of the seagrass locations.
2. To use different sources of imagery and thus, to increase the total collection of scenes covering the research area.
3. To extend the temporal period of the imagery coverage, once the data are available. The current work only includes images covering short temporal period

(ca 10-year); further estimation of the dynamics of *P.oceanica* along the coasts of Crete would increase our understanding of the long-scale temporal variations of the seagrass distribution.

4. To apply various classifications methods for the available imagery in order to compare the results received by means of various techniques
5. To simulate various environmental conditions while modelling optical properties of different seafloor cover types. Not only the depths and the chemical content of the seawater should be considered, but also other factors determining the effect of the ecology and health of *P. oceanica*.
6. To consider seafloor geomorphology among other factors determining seagrass distribution. If possible, to find out bathymetric data for the research area, and to overlay them with existing images and maps, in order to analyse correlation between spatial distribution of seagrass *P. oceanica* and underwater relief along Cretan coasts.
7. In upscaling to the small-scale mapping level further environmental variables need to be considered: health conditions of the seagrass (usually, indicated by the number of leaves per shoot), presence of other underwater vegetation, hydrology (e.g. direction and speed of currents, amplitude of tides and waves), season, date and times of the image taken.
8. Other RTM software may be tested and the modelling outcomes compared.
9. Application of various open source GIS (ILWIS, GRASS) could be very useful for the validation of the cartographic results, assessment of accuracy and comparison of various classification methods.
10. The analysis of the health indicators of the seagrass (such as number of leaves per shoot, biomass estimation within the single shot, etc) was not considered in the current work, as it would go beyond the scope of the MSc thesis. However, ecological investigations could be used for the assessment of the vulnerability of the seagrass meadows in various locations on Crete.
11. A flexible combination of the multi-scale mapping and results of the fieldwork measurements with GPS-referenced underwater footage would enable more profound analysis of the coastal environment on Crete.

Appendices

A.1 Capturing aerial imagery from the Google Earth: grabbing process

gripper.py - C:\Users\Polina\Documents\MSc_GEM\Google grabbing\gripper.py

File Edit Format Run Options Windows Help

```
        # step size in x direction, depends on latitude!
        dx = EFFAREA * (East - West)

        i = 0
        while lonGE + i*dx < LRlonGE:
            x = lonGE + (i + 0.5) * dx

            print "Grabbing:", y, x
            jumpTo(ge, y, x, focusDistance)
            im = ImageGrab.grab()
            im = im.crop((le, to, ri, bo))
            saveIm(name, im, j, i, getBB(ge))

            i = i + 1
        j = j + 1

    print "Grabbing finished"
    # fly away to original view to show that we're finished
    jumpTo(ge, camLat, camLon, camRange, 0.5)

def findTop(im):
    mid = im.size[0] / 3
    i = 0
    while im.getpixel((mid, i)) == im.getpixel((mid+10, i)):
        i = i + 1
    return i

#################### Main #####################

# "Height" is screen size dependent!
# screen size: 1600x1200 (Willem's laptop screen)
# screen size: 1680x1050 (Polina's laptop screen)
#               Height 1400 - 1.02 m pixelsize
#               Height 2800 - 2.1 m
#               Height 7000 ~ 5 m
#focusDistance = 1400.0 # 1400== 1.02 meter on Willem's laptop screen
focusDistance = 1228.0  # 1228== 0.85 meter on Polina's laptop screen

# basename of the image
name = 'APelagia_KMS_Etimanet_2007-2009'

doGrab(name, focusDistance)

# running external command for merging images

command = r"python.exe gdal_merge.py -o %s.tif -srsWGS84 --optfile %s.opt" % (name, name)

print "Merging images:"
print command

if subprocess.call(command)==0:
    print "Success!"
```

Ln: 26 Col: 68

Figure A.1: Capturing aerial imagery from the Google Earth: grabbing process

```
cd C:\Program Files\FWTools\bin
gdal_translate    -of    ECW    -co    "TARGET=0"    -co    "DATUM=WGS84"
        "C:\Users\Polina\Documents\MSc_GEM\Google
        grabbing\APelagia_WMS_Ktimanet_2007-  2009.tif"
        "C:\Users\Polina\Documents\MSc_GEM\Google grabbing\APelagia_WMS_Ktimanet_2007-
        2009.ecw"
C:\Program  Files\FWTools2.4.7\bin>gdal_translate  -of  GTiff  -co  "DATUM=WGS84"  "C:
        \Users\Polina\Documents\MSc_GEM\HOLLAND\DISSER_MSc\Crete\ArcPad_crete\APela
        gia_google_15jun2002.ecw"
        "C:\Users\Polina\Documents\MSc_GEM\HOLLAND\DISSER_MSc\Crete\ArcPad_crete\A
        Pelagia_google_15juin2002.tif
```

Figure A.2: Script command of FWTools2.4.7 enabling to reduce the size of the aerial images, from .tif to .ecw format.

A.2 Illustrations of some concepts and principles of the remote sensing, relevant for this work

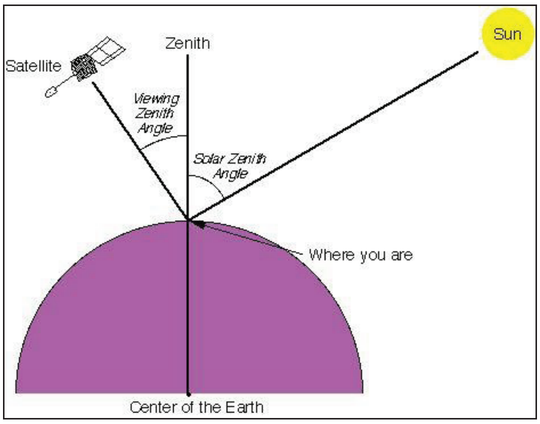

Fig. A.3. Schematic illustration of the solar zenith angle and viewing zenith angle for observations from satellite-based instrument. Source: http://sacs.aeronomie.be/

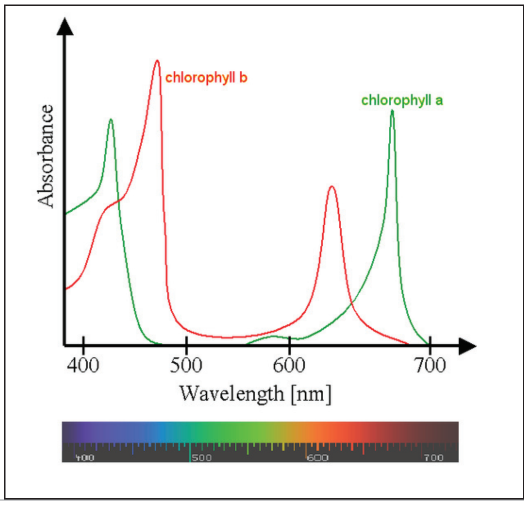

Figure A.4. Absorbance spectra of free chlorophyll a (green) and b (red) in a solvent. The spectra of chlorophyll molecules are slightly modified in vivo depending on specific pigment-protein interactions. Source: Wikipedia.org.

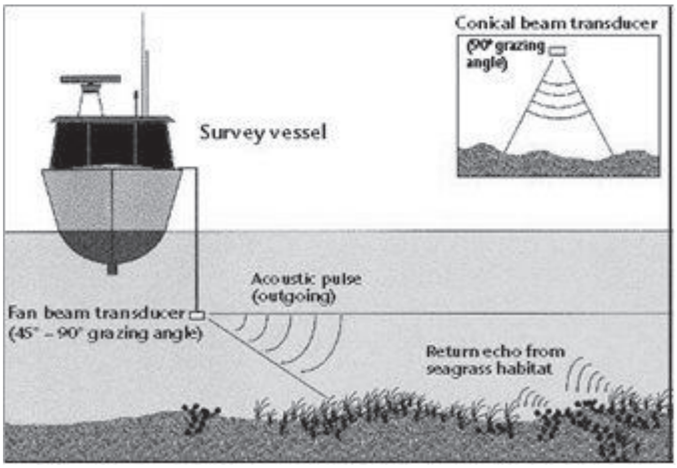

Figure A.5: Example of sonar beam acoustic systems used for mapping seagrasses habitat boundaries. Source: Reef Research.

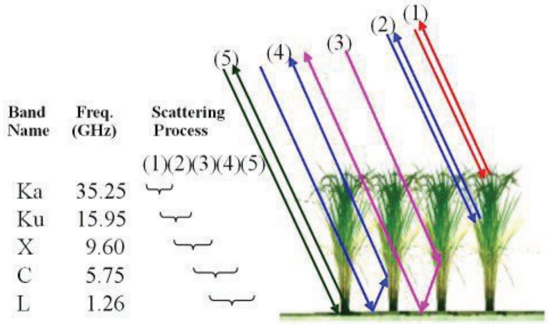

Figure A.6: Example of wave backscattering from the vegetation. Source: Yoshio Inoue, http://cse.niaes.affrc.go.jp/miwa/esid/highlight/microwave-backscatter.html

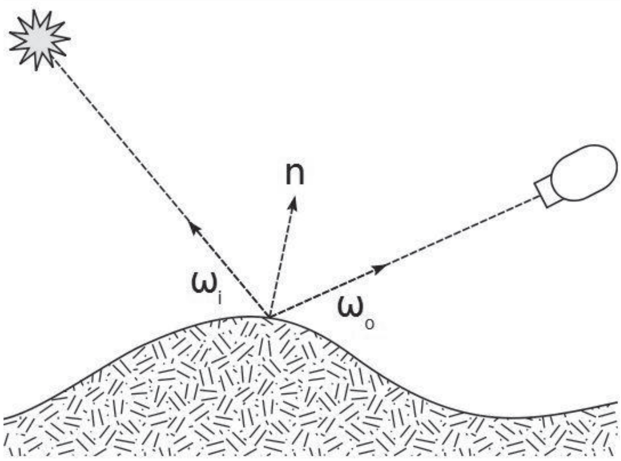

Figure A.7: BRDF is a ratio of reflected radiance along ωo to the irradiance from direction ωi, all parameterized by azimuth angle φ and zenith angle θ.
Source: Wikipedia.org

A.3. Instrumental adjustment and tuning (Trios-RAMSES setup)

Parameters	15 October, set 1	14 October, set 4
Version	1	1
IDData	78B1-2009-10-15-08-56-22-280-272	78B1-2009-10-14-15-15-59-342-726
IDDevice	SAM-820C	SAM-8204
IDDataType	SPECTRUM	SPECTRUM
IDDataTypeSub1	CALIBRATED	CALIBRATED
DateTime	2009-10-15 08:56:22	10/14/2009, 15:15:59
PositionLatitude	35.2451=3514'29.435	35.24752 = 35 14' 51.072"
PositionLongitude	25.01269=250'45.683	25.0098 = 250'35.2794"
Comment	P.oceanica	P.oceanica
CommentSub1	0.5m depth	2.5m depth
CommentSub2	diffuse	diffuse
CommentSub3	Agia Pelagia	Agia Pelagia site 2, close to rocks
IDMethodType	SAM Control	SAM Control
MethodName	SAM-820C	SAM-8204
Mission	No Mission	No Mission
MissionSub	1	1
RecordType	0	0
CalFactor	1	1
IDDataBack	DLAB-2008-02-06-14-13-18-865-675	DLAB-2008-01-25-20-42-29-607-062
IDDataCal	DLAB-2008-02-06-14-23-00-187-767	DLAB-2008-01-28-08-40-24-220-395
IntegrationTime	512	1024
P31	-1	-1
P31e	0	0
PathLength	+INF	+INF
RAWDynamic	65535	65535
Temperature	+NAN	+NAN
Unit1	0101 Wavelength nm	1 1 Wavelength nm
Unit2	03-06 Intensity mW/(m2nm)	03 03 Intensity mW/(m2 nm Sr)
Unit3	f0-06 Error mW/(m2 nm)	3-3 Error mW/(m2 nm Sr)
Unit4	f1-00 Status	f1-00 Status

Table A.1: Attributes of the Trios-RAMSES hyperspectral radiometer during measurement sets. Selected examples (14. X, set 1 and 15.X, set 4).

Parameters	14 October, set 1	15 October, set 4
Version	1	1
IDData	78B1-2009-10-14-15-32-02-078-323	78B1-2009-10-15-10-36-02-217-136
IDDevice	SAM-820C	SAM-8204
IDDataType	SPECTRUM	SPECTRUM
IDDataTypeSub1	CALIBRATED	CALIBRATED
DateTime	2009-10-14 15:32:02	2009-10-15 10:36:02
PositionLatitude	35.24752= 3514'51.072"	35.245071=3514'42.2556"
PositionLongitude	25.0098= 250'35.2794"	25.012661=250'45.5796"
Comment	P.oceanica	P.oceanica
CommentSub1	3.5m depth	1.5m depth
CommentSub2	diffuse	diffuse
CommentSub3	Agia Pelagia	Agia Pelagia site 1, close to rocks
IDMethodType	SAM Control	SAM Control
MethodName	SAM-820C	SAM-8204
Mission	No Mission	No Mission
MissionSub	1	1
RecordType	0	0
CalFactor	1	1
IDDataBack	DLAB-2008-02-06-14-13-18-865-675	DLAB-2008-01-25-20-42-29-607-062
IDDataCal	DLAB-2008-02-06-14-23-00-187-767	DLAB-2008-01-28-08-40-24-220-395
IntegrationTime	64	32
P31	-1	-1
P31e	0	0
PathLength	+INF	+INF
RAWDynamic	65535	65535
Temperature	+NAN	+NAN
Unit1	01-01 Wavelength nm	01-01 Wavelength nm
Unit2	03-06 Intensity mW/(m2nm)	03 03 Intensity mW/(m2 nm Sr)
Unit3	f0-06 Error mW/(m2 nm)	f0-03 Error mW/(m2 nm Sr)
Unit4	f1-00 Status	f1-00 Status

Table A.2: Attributes of the Trios-RAMSES hyperspectral radiometer during measurement sets. Selected examples (15. X, set 1 and 14.X, set 4).

A.4. Types of seagrass structural patterns, Ligaria beach, Crete

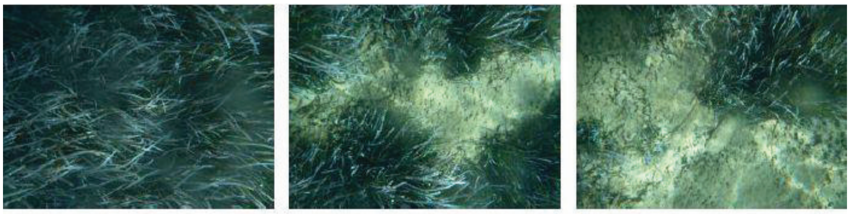

(a) Fragment of meadow

(b) Aggregated seagrass patch

(c) Isolated patch of seagrass

Figure A.8: Types of seagrass structural patterns, Ligaria beach, Crete

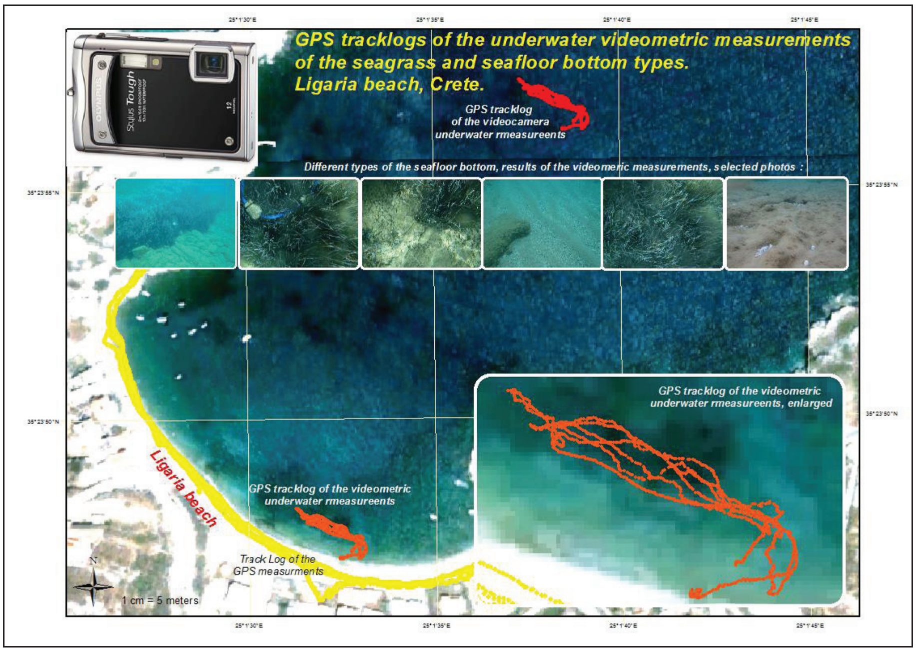

Figure A.9: Locations of the video measurements and GPS tracklogs, Ligaria

A.5. Results of videographic measurements: seafloor types on Crete Island

Figure A.10: Ligaria beach, Crete: seafloor types

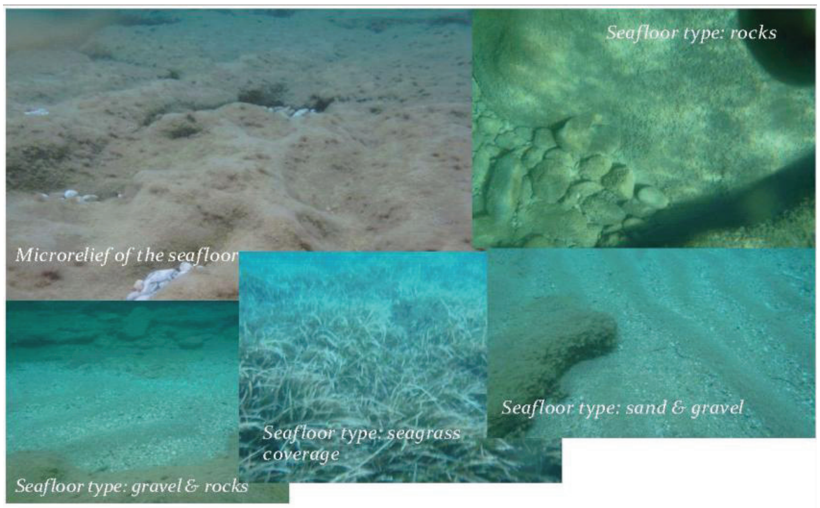

Figure A.11: Various seafloor types; Ligaria beach, Crete

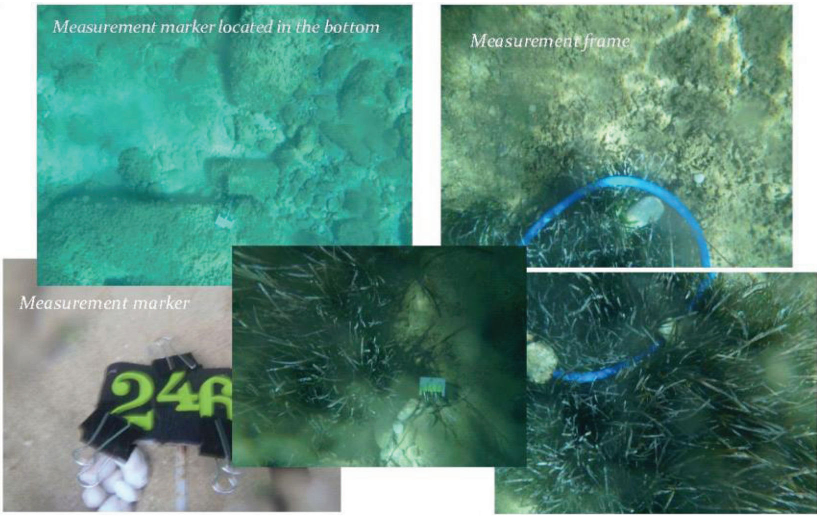

Figure A.12: Measurement underwater equipment

A.6. Data pre-processing

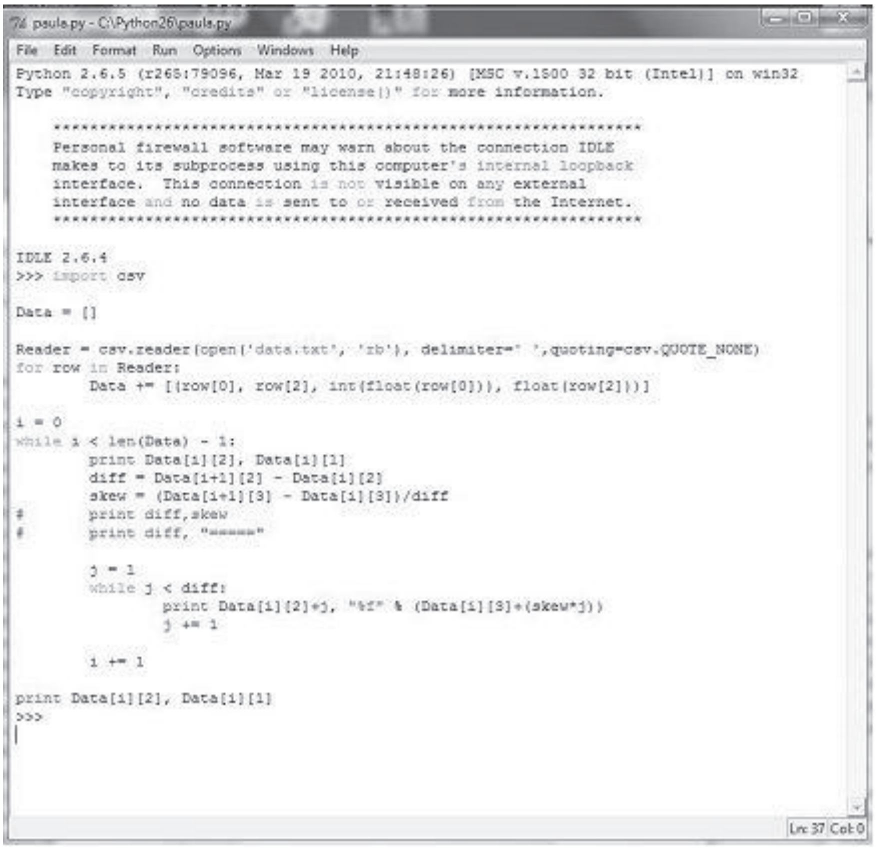
paula.py - C:\Python26\paula.py

File Edit Format Run Options Windows Help

```
Python 2.6.5 (r265:79096, Mar 19 2010, 21:48:26) [MSC v.1500 32 bit (Intel)] on win32
Type "copyright", "credits" or "license()" for more information.

    ****************************************************************
    Personal firewall software may warn about the connection IDLE
    makes to its subprocess using this computer's internal loopback
    interface.  This connection is not visible on any external
    interface and no data is sent to or received from the Internet.
    ****************************************************************

IDLE 2.6.4
>>> import csv

Data = []

Reader = csv.reader(open('data.txt', 'rb'), delimiter=' ',quoting=csv.QUOTE_NONE)
for row in Reader:
        Data += [(row[0], row[2], int(float(row[0])), float(row[2]))]

i = 0
while i < len(Data) - 1:
        print Data[i][2], Data[i][1]
        diff = Data[i+1][2] - Data[i][2]
        skew = (Data[i+1][3] - Data[i][3])/diff
#       print diff,skew
#       print diff, "====="

        j = 1
        while j < diff:
                print Data[i][2]+j, "%f" % (Data[i][3]+(skew*j))
                j += 1

        i += 1

print Data[i][2], Data[i][1]
>>>
```

Ln: 37 Col: 0

Figure A.13: Script written on Python, for the interpolation raw data of the Trios-RAMSES measurements

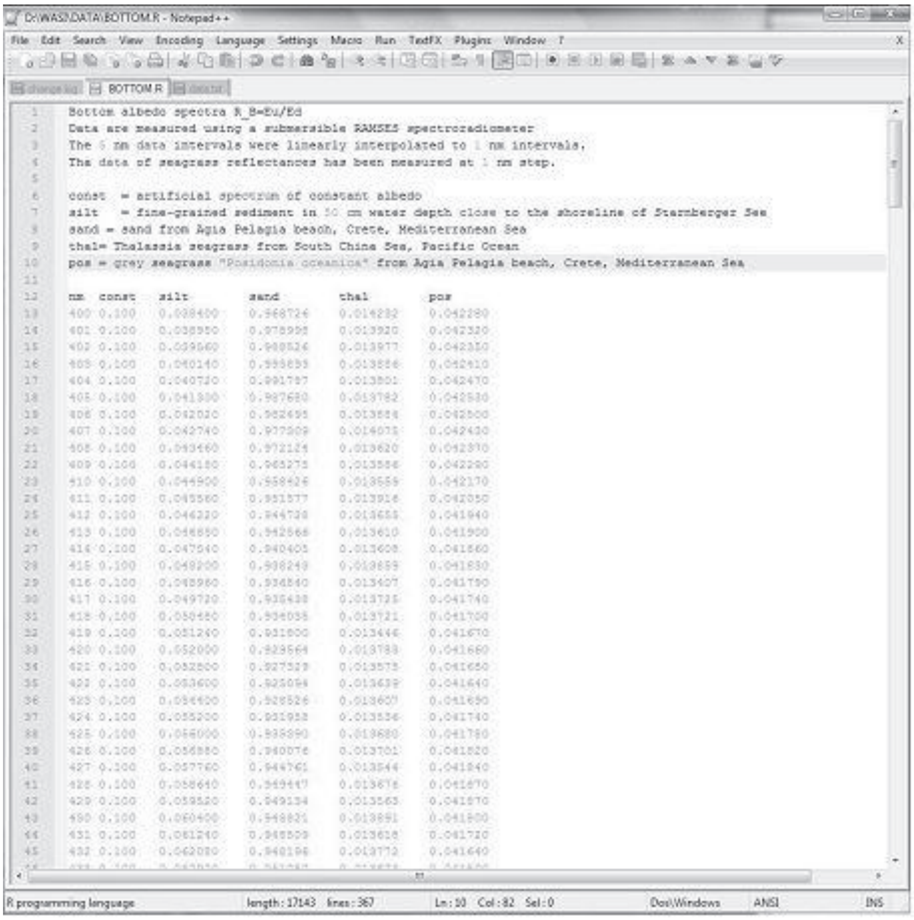


```
Bottom albedo spectra R_B=Eu/Ed
Data are measured using a submersible RAMSES spectroradiometer
The 5 nm data intervals were linearly interpolated to 1 nm intervals.
The data of seagrass reflectances has been measured at 1 nm step.

const  = artificial spectrum of constant albedo
silt   = fine-grained sediment in 50 cm water depth close to the shoreline of Starnberger See
sand = sand from Agia Pelagia beach, Crete, Mediterranean Sea
thal= Thalassia seagrass from South China Sea, Pacific Ocean
pos = grey seagrass "Posidonia oceanica" from Agia Pelagia beach, Crete, Mediterranean Sea

nm  const   silt       sand       thal       pos
400 0.100   0.038400   0.968724   0.014232   0.042280
401 0.100   0.038950   0.978995   0.013920   0.042320
402 0.100   0.039560   0.988526   0.013977   0.042350
403 0.100   0.040140   0.995655   0.013856   0.042410
404 0.100   0.040720   0.991787   0.013801   0.042470
405 0.100   0.041300   0.987680   0.013782   0.042530
406 0.100   0.042020   0.982495   0.013884   0.042500
407 0.100   0.042740   0.977309   0.014075   0.042430
408 0.100   0.043460   0.972124   0.013620   0.042370
409 0.100   0.044180   0.965275   0.013586   0.042290
410 0.100   0.044900   0.958426   0.013659   0.042170
411 0.100   0.045560   0.951577   0.013916   0.042050
412 0.100   0.046220   0.944728   0.013655   0.041940
413 0.100   0.046880   0.942566   0.013610   0.041900
414 0.100   0.047540   0.940405   0.013608   0.041860
415 0.100   0.048200   0.938243   0.013659   0.041830
416 0.100   0.048960   0.936840   0.013407   0.041790
417 0.100   0.049720   0.935438   0.013725   0.041740
418 0.100   0.050480   0.934035   0.013721   0.041700
419 0.100   0.051240   0.931800   0.013446   0.041670
420 0.100   0.052000   0.929564   0.013788   0.041660
421 0.100   0.052800   0.927329   0.013575   0.041650
422 0.100   0.053600   0.925094   0.013639   0.041640
423 0.100   0.054400   0.928526   0.013607   0.041690
424 0.100   0.055200   0.931958   0.013536   0.041740
425 0.100   0.056000   0.935390   0.013680   0.041780
426 0.100   0.056880   0.940076   0.013701   0.041820
427 0.100   0.057760   0.944761   0.013544   0.041840
428 0.100   0.058640   0.949447   0.013678   0.041870
429 0.100   0.059520   0.949134   0.013563   0.041870
430 0.100   0.060400   0.948821   0.013891   0.041800
431 0.100   0.061240   0.945509   0.013618   0.041720
432 0.100   0.062080   0.940196   0.013772   0.041640
```

Figure A.14: Fragment of Bottom.R file: values of spectral measurements of the seagrasses (various species), sand, silt and artificial spectrum of constant albedo

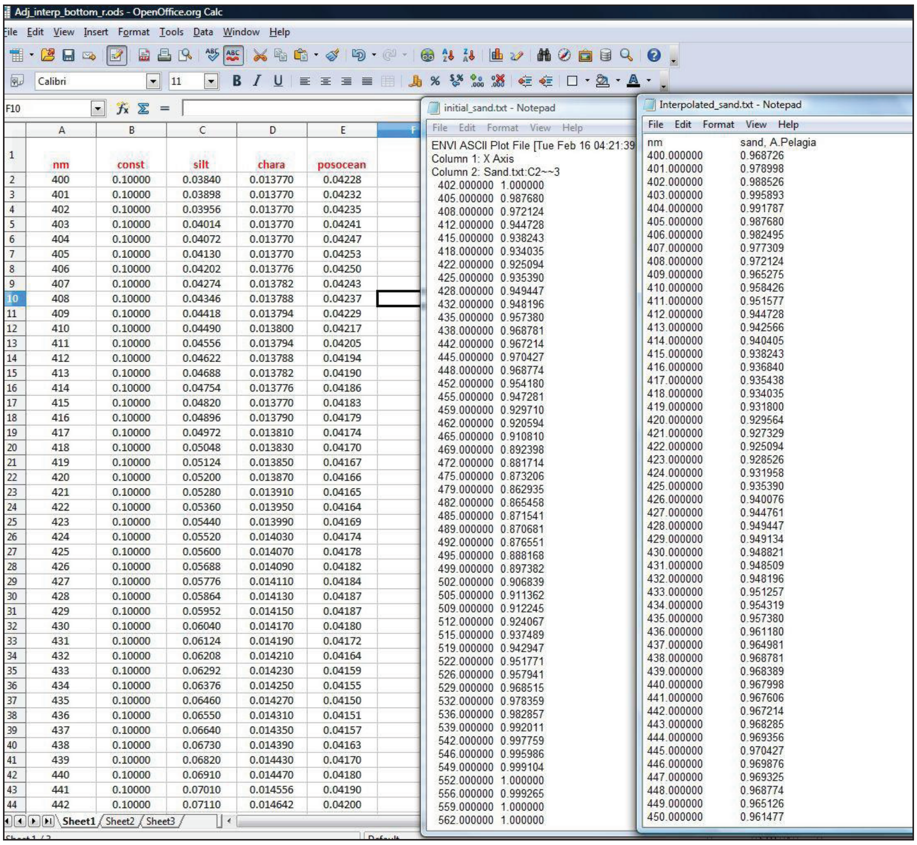

Figure A.15: Interpolation of the spectral measurements by means of Open Office

A.7. Data processing and statistical evaluation: measurements of the seafloor optical properties.

Table A.3: Basic mathematical formulae used for statistical analysis of the measurement set of the spectral reflectance.

Basic Statistics	Math Formulae
Mean	$\Sigma(x_i/n = \bar{x})$
Variance	$\frac{1}{n-1}\,\Sigma(x_i - \bar{x}) = s_x^2$
Standard Deviation	$s = s^2$
Coefficient of Variation	$s/\bar{x}$
Skewness	$\frac{1}{n-1}\,\Sigma(x_i - \bar{x})/s^3$
Excess Kurtosis	$\frac{1}{n-1}\,\Sigma(x_i - \bar{x})/s^4 - 3$

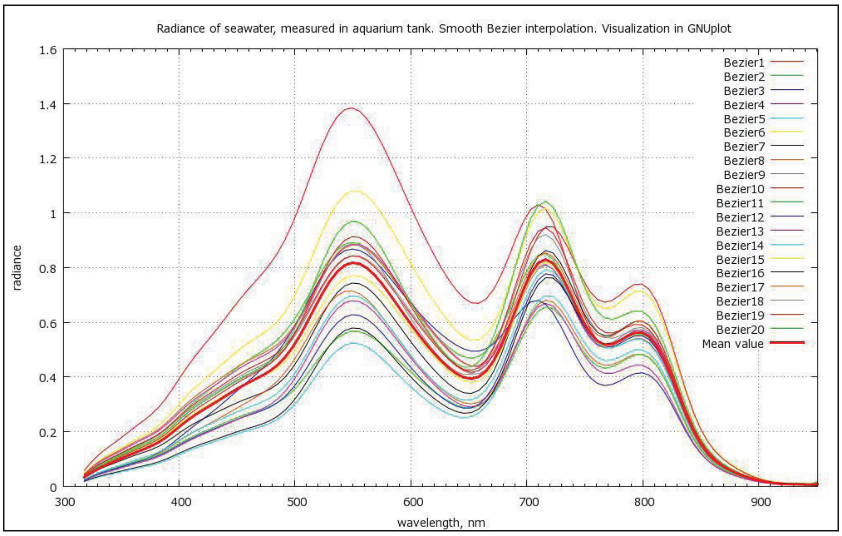

Figure A.16: Radiance of the seawater with sediments. Measured in aquarium tank. Bezier Interpolation. Gnuplot

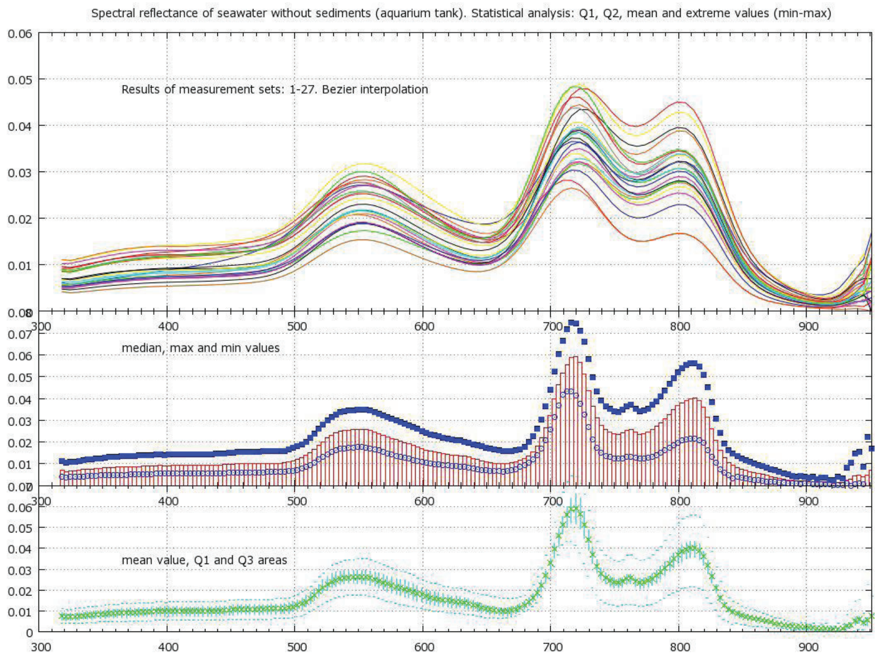

Figure A.17. Multiplot graph showing spectral reflectance of the seawater without sediments, measured in aquarium tank, Agia Pelagia district, Crete. Gnuplot. Two complimentary graphs below show the results of the statistical analysis

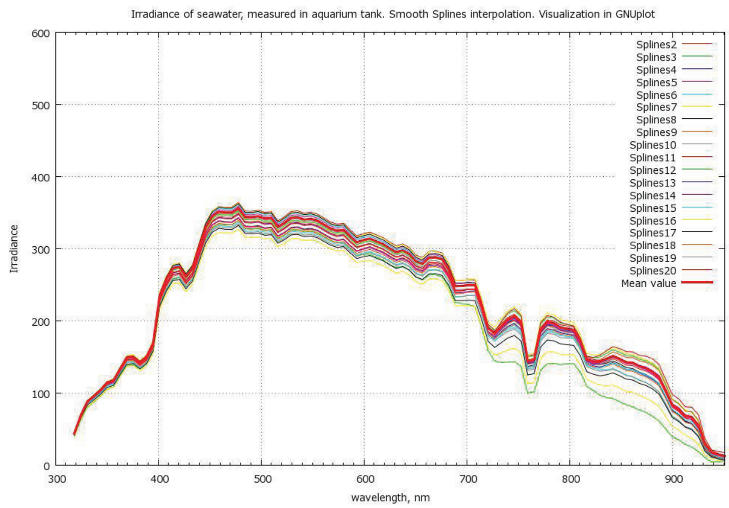

Figure A.18: Irradiance of the seawater, measured in aquarium tank. Smooth Splines interpolation. Visualization in Gnuplot

Table A.4: Robust estimation of the seawater radiance (measured in aquarium tank, Heraklion): results of the least absolute deviation (LAD), Series:V16. Gretl

Model 6: LAD, using observations 1:01–8:23 (T = 191). Dependent variable: v16

	Coefficient	Std. Error	t-ratio	p-value
[1ex] const	0.738911	0.0862011	8.5719	0.0000
v1	-0.000775186	0.000114010	-6.7993	0.0000

Median depend. var	0.227857	S.D. dependent var	0.205031
Sum absolute resid	30.22342	Sum squared resid	8.059632
Log-likelihood	28.74727	Akaike criterion	-53.49454
Schwarz criterion	-46.99000	Hannan–Quinn	-50.85990

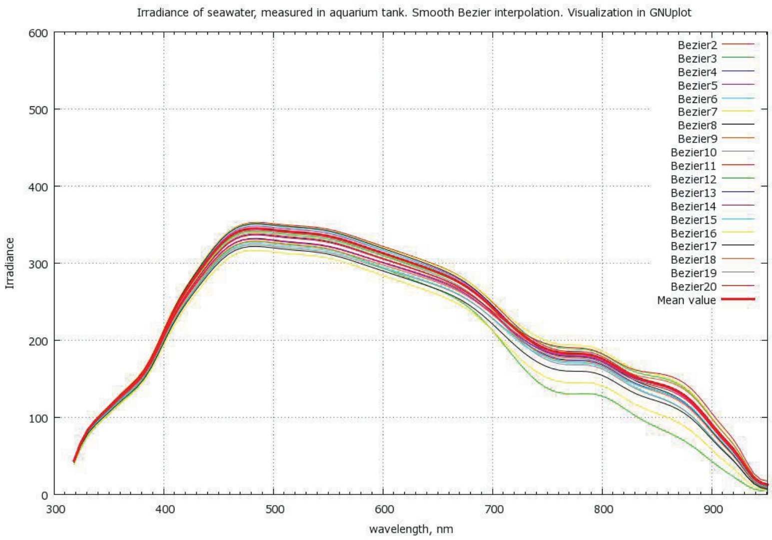

Figure A.19: Irradiance of the seawater, measured in aquarium tank. Smooth Bezier interpolation. Visualization in Gnuplot

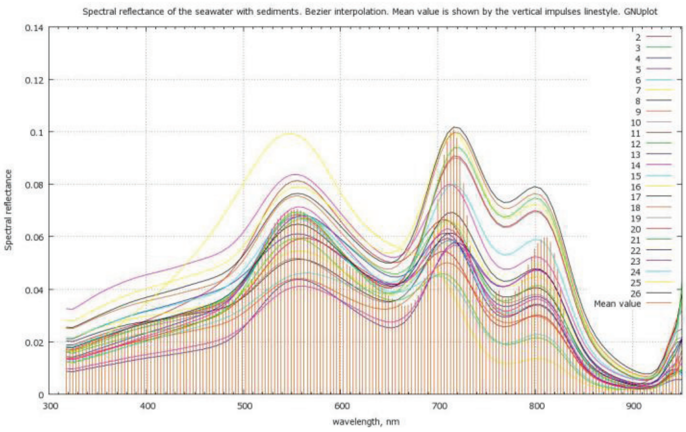

Figure A.20: Spectral reflectance of the seawater with sediments. Bezier interpolation. Mean value is shown by the vertical impulses linestyle. Gnuplot

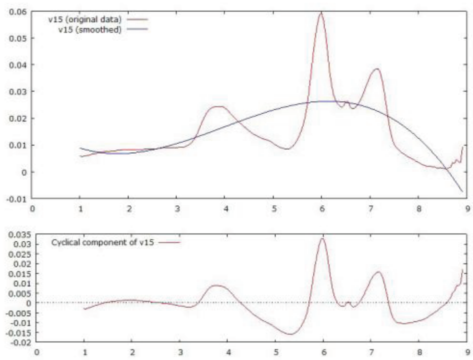

Figure A.21: Plot illustrating polynomial trend for spectral reflectance of seawater without sediments (Ligaria Beach), variable V15. Gretl modelling visualization

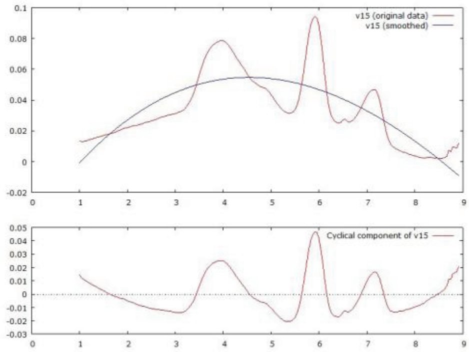

Figure A.22: Plot illustrating polynomial trend for spectral reflectance of seawater with sediments (Ligaria Beach), variable V15. Gretl modelling visualization

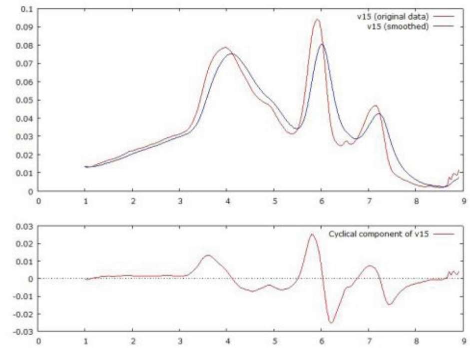

Figure A.23: Exponential moving average of spectral reflectance of seawater with sediments (Ligaria Beach), variable V15. Gretl modelling visualization

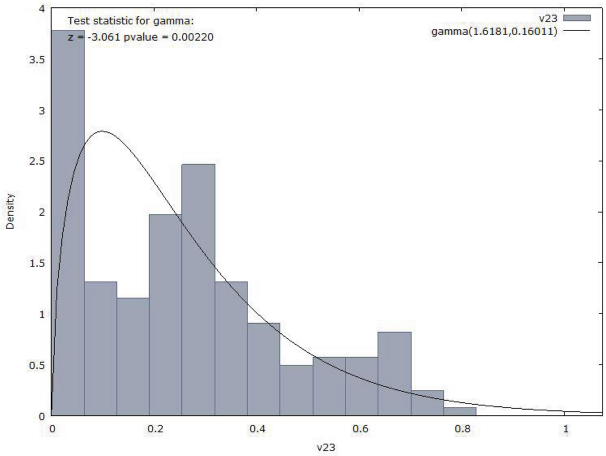

Figure A.24: Frequency normality test against gamma distribution: radiance of the seawater, measured in aquarium tank. Visualization in Gretl

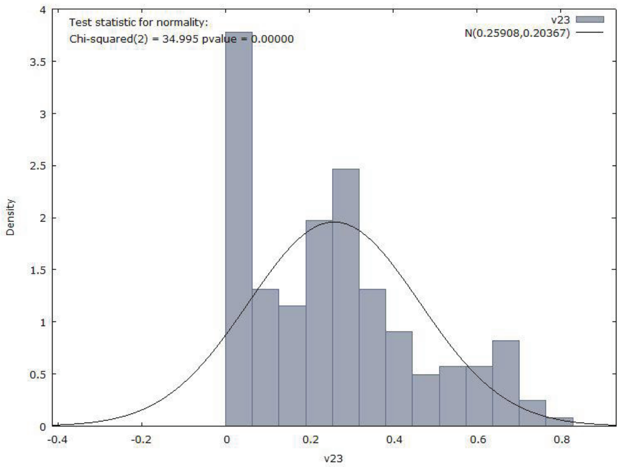

Figure A.25. Frequency normality test against normal distribution: radiance of the seawater, measured in aquarium tank. Visualization in Gretl

A.7.1 Data processing and statistical evaluation: *P.oceanica*

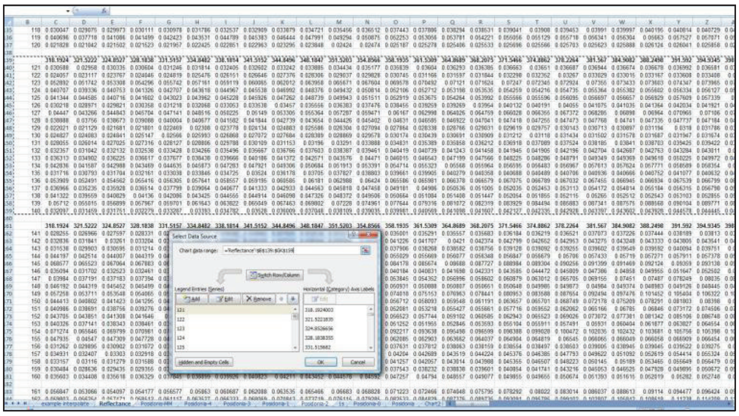

Figure A.26: Values of spectral reflectance of seagrass *P.oceanica* (fragment)

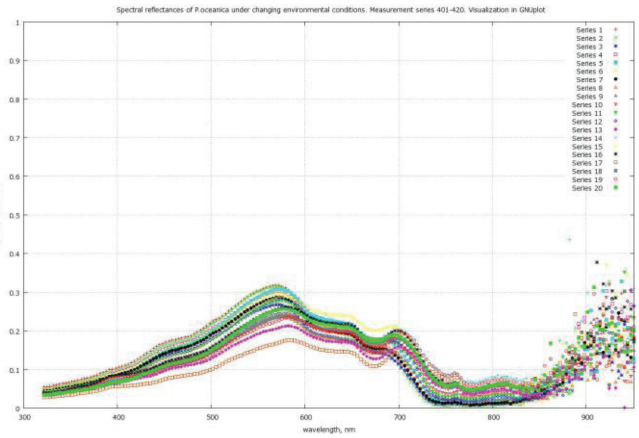

Figure A.27: Spectral reflectance of *P.oceanica*.
Measurement series 401-420. Gnuplot

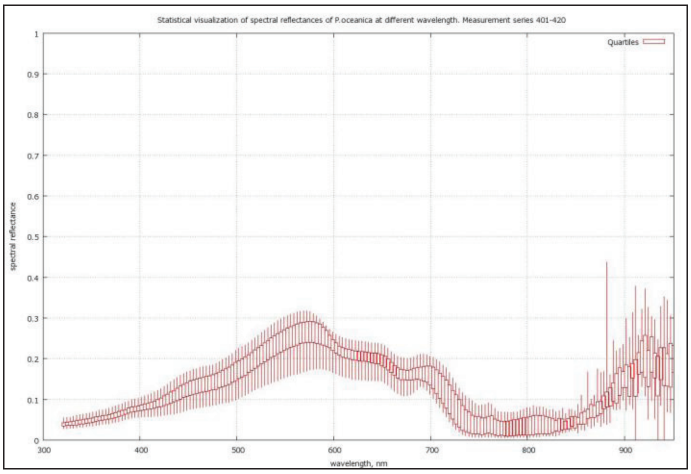

Figure A.28: Statistical analysis of the measurement data: spectral reflectance of the P.oceanica. Visualisation of the interquartile ranging. Example of data set 401-420. Shown midspread of statistical quartiles Q1 and Q3, min and max values within the range. Gnuplot

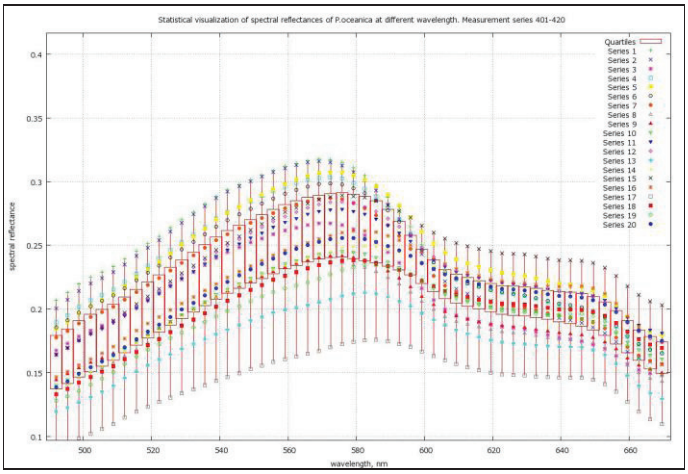

Figure A.29: Enlarged fragment of the statistical analysis of the measurement data. Example of data set 401-420. Visualisation of the inter-quartile ranging and plotted together with measurement data. Gnuplot

Wavelength, nm	mean	Q1	min	Q3	max	median
318.23354	0.030467	0.038907	0.029764	0.069762	0.116100	0.048984
338.29900	0.033560	0.043030	0.032847	0.076252	0.128290	0.054334
358.37932	0.039897	0.051320	0.039131	0.091143	0.154409	0.066354
378.47247	0.045786	0.058849	0.045039	0.105993	0.177150	0.078339
398.57640	0.052346	0.066859	0.051625	0.122328	0.201038	0.091905
418.68905	0.058942	0.074842	0.058240	0.138984	0.226028	0.106207
438.80838	0.070690	0.089761	0.069999	0.167825	0.267712	0.130580
458.93235	0.080107	0.102089	0.079392	0.191424	0.304933	0.149762
479.05891	0.086278	0.110348	0.085546	0.207940	0.332934	0.162881
499.18600	0.098498	0.126592	0.097689	0.239161	0.380603	0.188192
519.31159	0.110222	0.143976	0.109022	0.265948	0.421370	0.210237
539.43363	0.125694	0.166156	0.124310	0.302678	0.475842	0.240492
559.55006	0.131844	0.175865	0.130257	0.319385	0.503907	0.253726
579.65885	0.121915	0.166084	0.120186	0.302078	0.485661	0.237873
599.75794	0.077236	0.111113	0.075669	0.200557	0.343876	0.154016
619.84529	0.057038	0.085386	0.055588	0.154781	0.281737	0.117003
639.91885	0.050841	0.077438	0.049432	0.141810	0.265181	0.106188
659.97657	0.038118	0.059971	0.036997	0.110774	0.223366	0.082411
680.01641	0.032892	0.052265	0.032012	0.095789	0.198389	0.071686
700.03633	0.034756	0.058426	0.033643	0.101504	0.215413	0.075789
720.03426	0.026287	0.047084	0.025162	0.082940	0.193535	0.061184
740.00817	0.009740	0.022355	0.010145	0.042861	0.132244	0.029414
759.95601	0.008651	0.020234	0.009191	0.039371	0.128165	0.026558
779.87573	0.006019	0.014157	0.006397	0.028320	0.100314	0.019322
799.76528	0.008607	0.020030	0.009050	0.037323	0.118123	0.026535
819.62263	0.008777	0.020295	0.009288	0.037598	0.118055	0.026799
839.44571	0.002562	0.008010	0.002864	0.017472	0.076515	0.011432
859.23249	0.002653	0.006921	0.002897	0.016121	0.070377	0.009889
878.98091	0.002327	0.008080	0.002821	0.018625	0.082462	0.011617
898.68893	0.004077	0.013098	0.004709	0.031217	0.101146	0.019767
918.35451	0.006215	0.020162	0.007229	0.045213	0.199711	0.029950
937.97559	0.005783	0.026132	0.007307	0.065475	0.195072	0.040848
951.03058	0.002296	0.026581	0.002380	0.067924	0.265845	0.041463

Table A.5. Results of the statistical analysis of spectral reflectance of P.oceanica, with average values (for sets 1 - 350). Generalisation up to step 20 nm

Table A.6: Model summary of the regression analysis: curve estimation and ANOVA table tested for single observations within one measurement set: spectral reflectance of P.oceanica. SPSS

R	R square	Adjusted R square	Std. Error of the Estimate
.277 1	.077	.068126692	.462

The independent variable is wavelength.

Table A.7: ANOVA table: exponential curve estimation in the regression analysis, tested for single observations within one measurement set: spectral reflectance of P.oceanica. SPSS

	Sum of squares	df	Mean Square	F	Sig.
Regression	1.810	1	1.810	8.477	.004
Residual	21.781	102	.214		
Total	23.592	103			

The independent variable is wavelength.

Table A.8: Coefficients of the regression analysis (exponential curve estimation) of the spectral reflectance of P.oceanica. SPSS

	Unstandardized Coefficients				
	B	Std.Error	Stand. Coef. Beta	t	Sig.
wavelength	-.001	.000	-.277	-2.912	.004
constant	.464	.121		3.821	.000

The underlying process assumed is independence (white noise). Based on the asymptotic chi-square approximation.

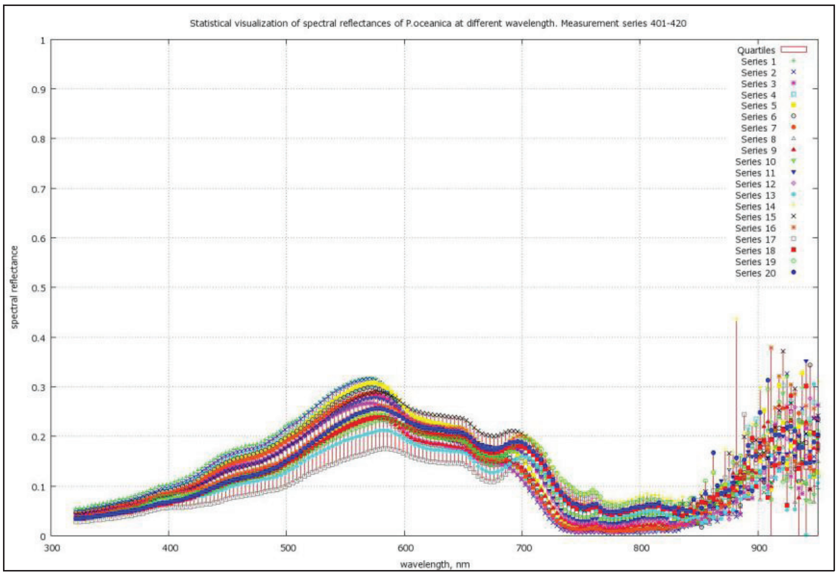

Figure A.30: Fragment of the statistical analysis of the P.oceanica reflectance. Example of data set 401-420. Visualisation of the measured data together with statistical values: inter-quartile ranging, medians, means. Gnuplot

Source of Variation	SS	df	MS	F	P value	F crit
Between Groups	373841.7048	2	186920.8524	407.85359	1.11677	3.01153
Within Groups	261233.1668	570	458.3038014			
Total	635074.8716	572				

Table A.9: Results of the ANOVA one-way analysis: results of the single factor (depth) testing of the radiance of P.oceanica at various depths: 0.5, 1.5 and 2.5 meters. SPSS

P more than .05, which means that there is a significant difference in radiance of *P.oceanica* at three different depth (0.5, 1.5 and 2.5).

Groups	Count	Sum	Average	Variance
Column 1	191	760.126692	3.9797209	18.6948046
Column 2	191	4527.214218	23.7026922	251.4863978
Column 3	191	12465.19972	65.2628257	1104.7302015

Table A.10. Summary of the ANOVA one-way analysis: results of the single factor (depth) testing of the radiance of P.oceanica at various depths: 0.5, 1.5 and 2.5 meters. SPSS

P>0.05, which means that there is a significant difference in radiance of *P.oceanica* at three different depth (0.5, 1.5 and 2.5).

Table A.11: Results of the statistical analysis of spectral reflectance of P.oceanica, sets 1-350). Wavelength step: 3 nm. Measured on Agia Pelagia beach, 15th October

wl	mean	Q1	min	Q3	max	median
318.23354	0.030467	0.038907	0.029764	0.069762	0.116100	0.048984
321.57666	0.028129	0.037310	0.027965	0.066572	0.110918	0.046450
324.92025	0.030163	0.038570	0.029502	0.068216	0.114120	0.047710
328.26428	0.030457	0.038936	0.029789	0.069098	0.116080	0.048574
331.60876	0.031407	0.040192	0.030731	0.071247	0.119681	0.050299
334.95367	0.032480	0.041545	0.031781	0.073494	0.123651	0.051941
338.29900	0.033560	0.043030	0.032847	0.076252	0.128290	0.054334
341.64474	0.034067	0.043938	0.033356	0.077587	0.131152	0.055506
344.99089	0.035346	0.045272	0.034616	0.080212	0.135395	0.057653
348.33743	0.036199	0.046719	0.035465	0.082716	0.139829	0.059655
351.68436	0.037336	0.048027	0.036587	0.085062	0.144101	0.061509
355.03166	0.038611	0.049598	0.037852	0.087963	0.149193	0.063835
358.37932	0.039897	0.051320	0.039131	0.091143	0.154409	0.066354
361.72735	0.040712	0.052408	0.039951	0.093252	0.157952	0.068034
365.07572	0.041541	0.053517	0.040782	0.095491	0.161650	0.069682
368.42442	0.042378	0.054625	0.041622	0.097634	0.164944	0.071524
371.77346	0.043682	0.056205	0.042926	0.100782	0.169458	0.074006
375.12281	0.044525	0.057191	0.043779	0.102916	0.172533	0.075888

wl	mean	Q1	min	Q3	max	median
378.47247	0.045786	0.058849	0.045039	0.105993	0.177150	0.078339
381.82243	0.047361	0.060698	0.046615	0.109681	0.182421	0.081219
385.17269	0.048457	0.062067	0.047717	0.112447	0.186097	0.083586
388.52322	0.049503	0.063533	0.048767	0.115361	0.190440	0.086143
391.87402	0.051271	0.065536	0.050529	0.119310	0.196618	0.089165
395.22508	0.052033	0.066436	0.051298	0.121231	0.199547	0.090884
398.57640	0.052346	0.066859	0.051625	0.122328	0.201038	0.091905
401.92796	0.053246	0.067963	0.052517	0.124750	0.204926	0.093940
405.27975	0.054472	0.069505	0.053749	0.127847	0.209718	0.096463
408.63176	0.055492	0.070692	0.054773	0.130382	0.213406	0.098620
411.98399	0.056331	0.071703	0.055621	0.132628	0.216692	0.100545
415.33642	0.057682	0.073235	0.056976	0.135758	0.221309	0.103354
418.68905	0.058942	0.074842	0.058240	0.138984	0.226028	0.106207
422.04186	0.060504	0.076815	0.059805	0.142833	0.231707	0.109487
425.39485	0.062547	0.079376	0.061847	0.147773	0.238892	0.113584
428.74801	0.064817	0.082141	0.064115	0.153137	0.246681	0.118126
432.10132	0.066664	0.084493	0.065967	0.157743	0.253230	0.122093
435.45478	0.068616	0.086926	0.067925	0.162414	0.259765	0.126092
438.80838	0.070690	0.089761	0.069999	0.167825	0.267712	0.130580
442.16211	0.072701	0.092360	0.072010	0.172808	0.275027	0.134721
445.51596	0.074550	0.094801	0.073855	0.177420	0.282203	0.138517
448.86992	0.076196	0.096995	0.075496	0.181512	0.288621	0.141853
452.22397	0.077581	0.098795	0.076876	0.184975	0.294309	0.144634
455.57812	0.079009	0.100624	0.078296	0.188516	0.300251	0.147486
458.93235	0.080107	0.102089	0.079392	0.191424	0.304933	0.149762
462.28665	0.081264	0.103609	0.080545	0.194453	0.309937	0.152238
465.64102	0.082366	0.105087	0.081658	0.197331	0.314862	0.154601
468.99543	0.083316	0.106273	0.082589	0.199757	0.319033	0.156521
472.34990	0.084192	0.107427	0.083464	0.202075	0.323294	0.158350
475.70439	0.085122	0.108714	0.084392	0.204674	0.327802	0.160310
479.05891	0.086278	0.110348	0.085546	0.207940	0.332934	0.162881
482.41344	0.088011	0.112712	0.087275	0.212533	0.340090	0.166595
485.76798	0.090064	0.115295	0.089321	0.217585	0.348041	0.170644
489.12252	0.091822	0.117678	0.091073	0.222210	0.355070	0.174440
492.47704	0.093593	0.120058	0.092835	0.226915	0.361882	0.178261
495.83154	0.095851	0.123152	0.095072	0.232757	0.370879	0.182979
499.18600	0.098498	0.126592	0.097689	0.239161	0.380603	0.188192
502.54043	0.100497	0.129243	0.099648	0.243918	0.387852	0.192036
505.89480	0.101834	0.131069	0.100939	0.246962	0.392456	0.194588
509.24911	0.103094	0.133022	0.102139	0.249966	0.397001	0.196947
512.60336	0.104998	0.136069	0.103967	0.254523	0.404017	0.200556
515.95752	0.107481	0.139807	0.106364	0.259986	0.412790	0.205238
519.31159	0.110222	0.143976	0.109022	0.265948	0.421370	0.210237
522.66557	0.112891	0.148090	0.111650	0.272217	0.430485	0.215339
526.01943	0.115799	0.152266	0.114534	0.278942	0.440382	0.220946
529.37318	0.118594	0.156156	0.117302	0.285384	0.450045	0.226407

wl	mean	Q1	min	Q3	max	median
532.72680	0.121111	0.159690	0.119794	0.291491	0.458964	0.231403
536.08029	0.123519	0.163063	0.122169	0.297338	0.467779	0.236144
539.43363	0.125694	0.166156	0.124310	0.302678	0.475842	0.240492
542.78681	0.127313	0.168524	0.125897	0.306828	0.482311	0.243819
546.13983	0.128393	0.170255	0.126944	0.309747	0.487098	0.246131
549.49267	0.129369	0.171844	0.127887	0.312256	0.491208	0.248155
552.84533	0.130192	0.173167	0.128678	0.314539	0.495323	0.249936
556.19780	0.131149	0.174662	0.129597	0.317126	0.499790	0.251984
559.55006	0.131844	0.175865	0.130257	0.319385	0.503907	0.253726
562.90211	0.132098	0.176510	0.130479	0.320731	0.506658	0.254511
566.25394	0.131944	0.176786	0.130273	0.321450	0.508802	0.254761
569.60554	0.131139	0.176171	0.129456	0.320617	0.508657	0.253650
572.95690	0.129337	0.174497	0.127627	0.317523	0.505482	0.250781
576.30800	0.126457	0.171261	0.124730	0.311678	0.498350	0.245834
579.65885	0.121915	0.166084	0.120186	0.302078	0.485661	0.237873
583.00943	0.116464	0.159695	0.114741	0.289985	0.469210	0.227889
586.35972	0.110124	0.152038	0.108417	0.275585	0.449536	0.216026
589.70973	0.102719	0.142758	0.101038	0.258779	0.425248	0.201868
593.05945	0.094713	0.132871	0.093063	0.240383	0.399506	0.186687
596.40885	0.086028	0.121987	0.084416	0.220594	0.372134	0.170438
599.75794	0.077236	0.111113	0.075669	0.200557	0.343876	0.154016
603.10670	0.070071	0.102079	0.068539	0.183962	0.320865	0.140543
606.45513	0.064972	0.095380	0.063465	0.172189	0.304973	0.131080
609.80321	0.061747	0.091191	0.060257	0.164863	0.295132	0.125235
613.15094	0.059707	0.088656	0.058235	0.160355	0.289194	0.121614
616.49830	0.058283	0.086915	0.056821	0.157314	0.285336	0.119161
619.84529	0.057038	0.085386	0.055588	0.154781	0.281737	0.117003
623.19189	0.055996	0.084129	0.054556	0.152697	0.278854	0.115243
626.53811	0.055200	0.083282	0.053763	0.151068	0.277016	0.113879
629.88392	0.054368	0.082234	0.052931	0.149414	0.275056	0.112433
633.22932	0.053299	0.080860	0.051869	0.147176	0.271850	0.110512
636.57430	0.052033	0.079147	0.050611	0.144415	0.268135	0.108222
639.91885	0.050841	0.077438	0.049432	0.141810	0.265181	0.106188
643.26296	0.049737	0.075977	0.048336	0.139466	0.263239	0.104485
646.60662	0.048467	0.074330	0.047076	0.136488	0.260596	0.102251
649.94982	0.046762	0.072058	0.045397	0.132376	0.255761	0.099096
653.29255	0.044482	0.068866	0.043159	0.126637	0.248247	0.094730
656.63481	0.041366	0.064447	0.040108	0.118961	0.236639	0.088686
659.97657	0.038118	0.059971	0.036997	0.110774	0.223366	0.082411
663.31784	0.035847	0.056353	0.034750	0.104541	0.212843	0.077616
666.65861	0.034385	0.054006	0.033356	0.100476	0.205602	0.074622
669.99886	0.033576	0.052732	0.032604	0.098106	0.201320	0.072881
673.33858	0.033122	0.052033	0.032194	0.096638	0.198744	0.072021
676.67777	0.032897	0.051894	0.032003	0.095851	0.197694	0.071600
680.01641	0.032892	0.052265	0.032012	0.095789	0.198389	0.071686
683.35451	0.033331	0.053301	0.032432	0.097053	0.201578	0.072478

wl	mean	Q1	min	Q3	max	median
686.69203	0.033823	0.054940	0.032870	0.098577	0.206179	0.073481
690.02899	0.034458	0.056468	0.033426	0.099736	0.209895	0.074120
693.36536	0.034436	0.056844	0.033329	0.100112	0.211708	0.074967
696.70114	0.034695	0.057874	0.033554	0.100594	0.213198	0.075367
700.03633	0.034756	0.058426	0.033643	0.101504	0.215413	0.075789
703.37090	0.034209	0.058339	0.033206	0.101601	0.215696	0.075467
706.70485	0.033056	0.057120	0.031999	0.100262	0.213853	0.073792
710.03817	0.031680	0.055368	0.030599	0.097286	0.209716	0.071411
713.37085	0.030077	0.053314	0.028958	0.093925	0.206402	0.068982
716.70288	0.028935	0.050808	0.027789	0.089359	0.202502	0.066018
720.03426	0.026287	0.047084	0.025162	0.082940	0.193535	0.061184
723.36497	0.023116	0.041962	0.022192	0.075244	0.182863	0.055350
726.69500	0.019755	0.037276	0.019223	0.067583	0.171617	0.049522
730.02435	0.016355	0.032668	0.016168	0.059609	0.159449	0.042677
733.35299	0.013247	0.028377	0.013325	0.052370	0.147592	0.036934
736.68094	0.010923	0.024633	0.011200	0.046727	0.138634	0.032350
740.00817	0.009740	0.022355	0.010145	0.042861	0.132244	0.029414
743.33467	0.008848	0.020756	0.009299	0.040084	0.127367	0.027450
746.66045	0.008789	0.019615	0.009272	0.038166	0.123288	0.025956
749.98548	0.007817	0.018631	0.008305	0.036577	0.119290	0.024701
753.30975	0.007533	0.017951	0.008013	0.035542	0.116242	0.023967
756.63327	0.007777	0.018797	0.008273	0.036601	0.119191	0.024621
759.95601	0.008651	0.020234	0.009191	0.039371	0.128165	0.026558
763.27797	0.008355	0.020033	0.008883	0.038779	0.126589	0.026439
766.59914	0.007232	0.017224	0.007708	0.033862	0.113056	0.022658
769.91951	0.005575	0.015235	0.005970	0.029884	0.103584	0.020196
773.23907	0.006016	0.014264	0.006407	0.028277	0.100504	0.019270
776.55781	0.005801	0.013966	0.006189	0.027876	0.099265	0.019096
779.87573	0.006019	0.014157	0.006397	0.028320	0.100314	0.019322
783.19280	0.006136	0.014643	0.006524	0.028946	0.101978	0.019978
786.50903	0.006559	0.015475	0.006967	0.030261	0.104960	0.021034
789.82440	0.007038	0.016900	0.007440	0.031880	0.107764	0.022351
793.13891	0.007598	0.017699	0.008021	0.033662	0.111651	0.023996
796.45254	0.008137	0.018912	0.008556	0.035621	0.114760	0.025299
799.76528	0.008607	0.020030	0.009050	0.037323	0.118123	0.026535
803.07713	0.009078	0.020935	0.009544	0.038749	0.120699	0.027598
806.38808	0.009299	0.021600	0.009772	0.039865	0.122278	0.028669
809.69811	0.009526	0.022082	0.009994	0.040470	0.124400	0.029071
813.00722	0.009575	0.022239	0.010086	0.040394	0.124681	0.029112
816.31539	0.010059	0.021517	0.010572	0.039929	0.124390	0.028547
819.62263	0.008777	0.020295	0.009288	0.037598	0.118055	0.026799
822.92891	0.007647	0.017661	0.008133	0.034147	0.112749	0.024239
826.23423	0.006897	0.015734	0.007343	0.030561	0.104462	0.021328
829.53858	0.005932	0.013286	0.006340	0.026347	0.095980	0.018276
832.84195	0.004547	0.010824	0.005261	0.022895	0.087424	0.015291
836.14433	0.003285	0.009222	0.003567	0.019407	0.080997	0.013090

wl	mean	Q1	min	Q3	max	median
839.44571	0.002562	0.008010	0.002864	0.017472	0.076515	0.011432
842.74608	0.002580	0.007522	0.002094	0.016318	0.073901	0.010511
846.04544	0.003121	0.007283	0.003442	0.015689	0.080570	0.010195
849.34376	0.002719	0.006935	0.002961	0.016016	0.076860	0.009926
852.64105	0.002742	0.006733	0.002994	0.015949	0.070643	0.009824
855.93730	0.002840	0.007120	0.003106	0.015919	0.074262	0.010103
859.23249	0.002653	0.006921	0.002897	0.016121	0.070377	0.009889
862.52661	0.002825	0.006846	0.003153	0.016677	0.078344	0.009943
865.81966	0.002508	0.007308	0.002710	0.016406	0.073265	0.010239
869.11162	0.002322	0.007310	0.002532	0.017118	0.081434	0.010382
872.40249	0.001873	0.007289	0.002542	0.017948	0.086487	0.010688
875.69226	0.001769	0.007640	0.001769	0.017981	0.074717	0.010912
878.98091	0.002327	0.008080	0.002821	0.018625	0.082462	0.011617
882.26844	0.001661	0.008815	0.002284	0.019452	0.079564	0.011996
885.55484	0.002940	0.008588	0.003400	0.021344	0.080998	0.012489
888.84010	0.002827	0.009126	0.003467	0.022626	0.089420	0.013547
892.12421	0.002523	0.010281	0.002997	0.023568	0.129197	0.015324
895.40716	0.001578	0.010879	0.001578	0.025648	0.091357	0.016328
898.68893	0.004077	0.013098	0.004709	0.031217	0.101146	0.019767
901.96953	0.004560	0.014295	0.005228	0.032824	0.141000	0.020699
905.24894	0.004167	0.014798	0.004249	0.034899	0.135645	0.022265
908.52716	0.003891	0.015616	0.002986	0.037403	0.150828	0.024065
911.80416	0.003641	0.018706	0.004306	0.043272	0.115375	0.027328
915.07995	0.003120	0.018093	0.003995	0.045688	0.135804	0.027234
918.35451	0.006215	0.020162	0.007229	0.045213	0.199711	0.029950
921.62783	0.004669	0.021630	0.005940	0.047785	0.245588	0.032131
924.89991	0.003051	0.019678	0.003957	0.051741	0.127093	0.032278
928.17074	0.002955	0.021413	0.004277	0.053042	0.266342	0.035277
931.44030	0.002679	0.023349	0.004029	0.057574	0.225003	0.036074
934.70859	0.003446	0.023229	0.004285	0.059098	0.549439	0.037722
937.97559	0.005783	0.026132	0.007307	0.065475	0.195072	0.040848
941.24130	0.005209	0.024892	0.006147	0.058814	0.281685	0.039602
944.50571	0.003354	0.025994	0.004299	0.064521	0.232462	0.041118
947.76881	0.003156	0.023476	0.003813	0.059536	0.246006	0.037035
951.03058	0.002296	0.026581	0.002380	0.067924	0.265845	0.041463

Table A.12: Nonlinear model: results of the logistic analysis of the seawater radiance with sediments (15.X.), Series:V16. Gretl

Model 2: Logistic, using observations 1:01–8:23 (T = 191)

Dependent variable: v16, $\hat{y} = 1/(1+e^{-X})$

	Coefficient	Std. Error	t-ratio	p-value
[1ex] const	1.58324	0.407258	3.8876	0.0001
v1	-0.00512630	0.000615503	-8.3286	0.0000

Statistics based on the transformed data:

Sum squared resid	462.8481	S.E. of regression	1.564906
R^2	0.268481	Adjusted R^2	0.264610
F(1,189)	69.36634	P-value(F)	1.63e–14
Log-likelihood	-355.5467	Akaike criterion	715.0935
Schwarz criterion	721.5980	Hannan–Quinn	717.7281
	0.980662	Durbin–Watson	0.020351

Statistics based on the original data:

Mean dependent var	0.262542	S.D. dependent var	0.205031
Sum squared resid	10.80565	S.E. of regression	0.239108

Lag	Partial Autocorrelation	Std error
1	.844	.072
1	.358	.072
3	.217	.072
4	.125	.072
5	-.093	.072
6	.003	.072
7	.310	.072
8	-.403	.072
9	-.117	.072
10	.033	.072
11	-.104	.072
12	.023	.072
13	.246	.072
14	-.164	.072
15	.084	.072
16	.152	.072

Table A.13: Results of the partial autocorrelation analysis of the measurement set 1-16 of the spectral reflectance of P.oceanica (15.X.), Series:V3. SPSS

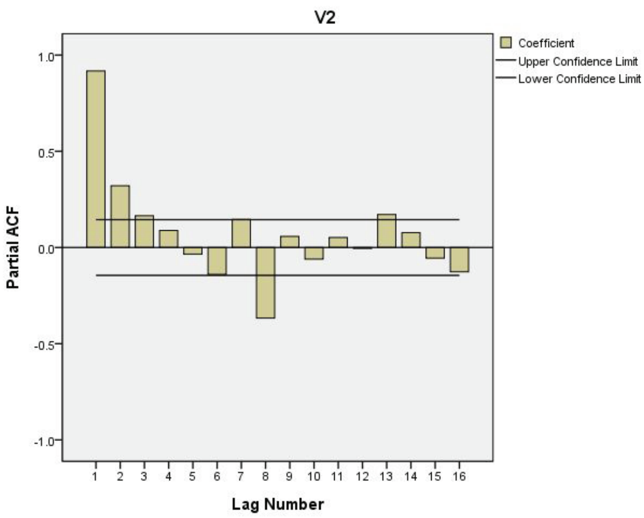

Figure A.31: Partial correlation analysis of the measurement set 1-16 of the spectral reflectance of P.oceanica (15.X.). Visualization in SPSS

Lag	Autocorrelation	Std error(a)	Box-Ljung Statistic Value	df	Sig (b)
1	.844	.071	141.324	1	.000
2	.816	.071	273.208	2	.000
3	.799	.071	400.323	3	.000
4	.780	.071	522.217	4	.000
5	.723	.070	627.372	5	.000
6	.700	.070	726.581	6	.000
7	.745	.070	839.623	7	.000
8	.624	.070	919.336	8	.000
9	.584	.070	989.540	9	.000
10	.562	.069	1054.920	10	.000
11	.522	.069	1111.681	11	.000
12	.464	.069	1156.693	12	.000
13	.475	.069	1204.314	13	.000
14	.463	.069	1249.726	14	.000
15	.401	.069	1283.916	15	.000
16	.389	.068	1316.427	16	.000

Table A.14: Results of the autocorrelation analysis of the measurement set 1-16 of the spectral reflectance of P.oceanica (15.X.), Series: V3. SPSS.
The underlying process assumed is independence (white noise).
Based on the asymptotic chi-square approximation.

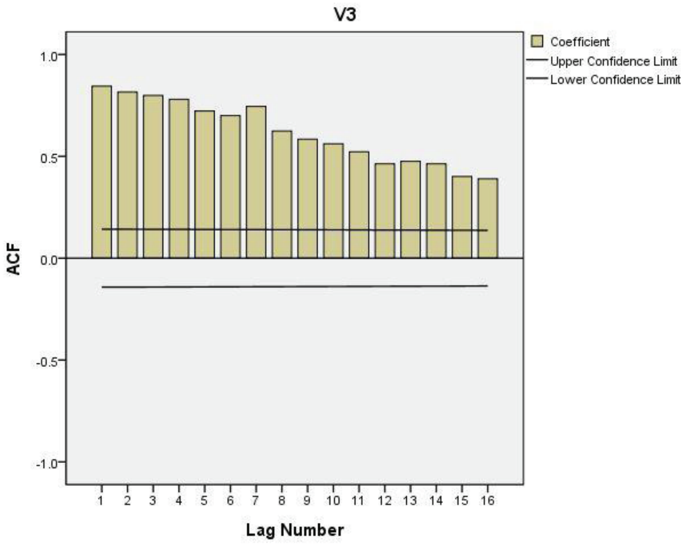

Figure A.32: Autocorrelation analysis of the measurement set 1-16 of the spectral reflectance of P.oceanica (15.X.). Visualization in SPSS

Table A.15: Ordinary Least Squares: results of the OLS analysis of the measurement set 326-350 of the spectral reflectance of P.oceanica (15.X.). Gretl. Model 2: OLS, using observations 326–350. Dependent variable: v20

	Coefficient	Std. Error	t-ratio	p-value
[1ex] const	0.414957	0.0299342	13.8623	0.0000
v1	-0.000441803	4.52185e–005	-9.7704	0.0000

Mean dependent var	0.134005	S.D. dependent var	0.140653
Sum squared resid	2.497416	S.E. of regression	0.114951
R^2	0.335585	Adjusted R^2	0.332070
F(1,189)	95.46076	P-value(F)	1.65e–18
Log-likelihood	143.1678	Akaike criterion	-282.3357
Schwarz criterion	-275.8311	Hannan–Quinn	-279.7010

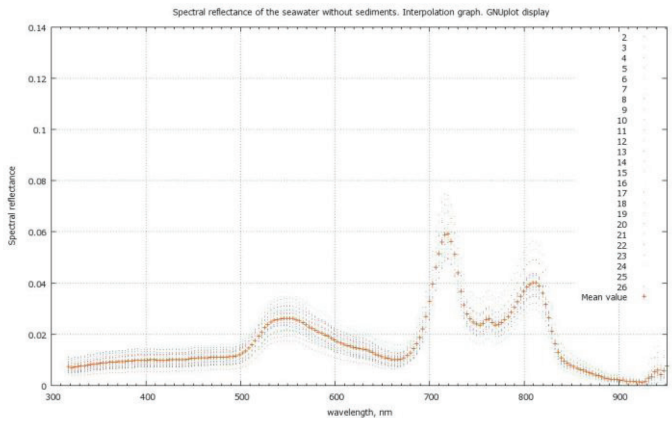

Figure A.33: Spectral reflectance of the seawater without sediments. Interpolation graph. Gnuplot display

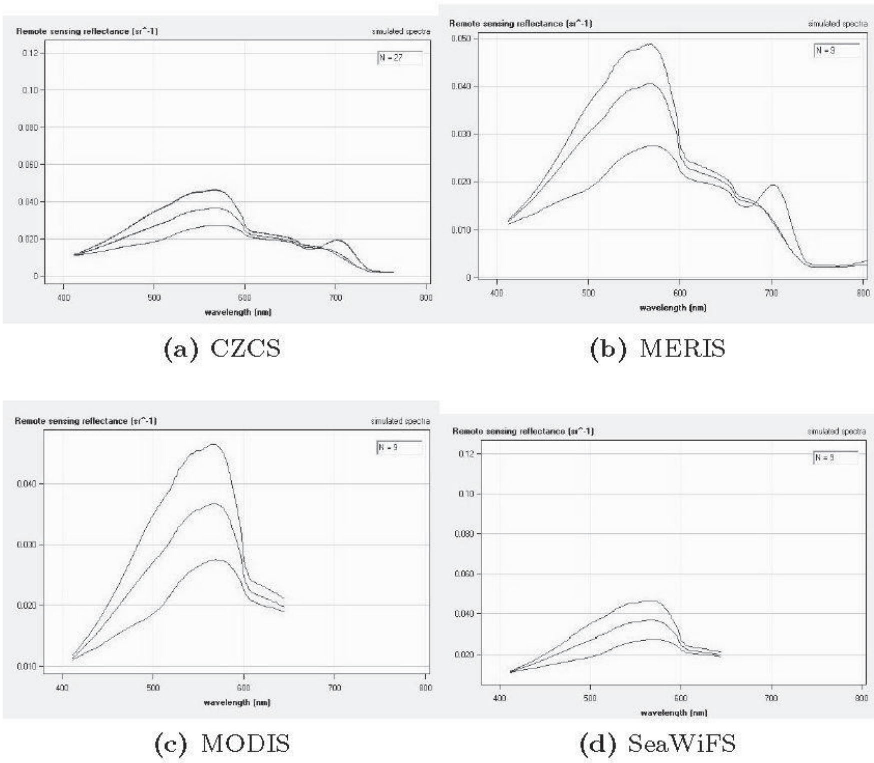

Figure A.34: WASI-simulated remote sensing reflectance of P.oceanica at various sensors

Table A.16: Summary statistics of measurements set: 301-325. Example of selected variables 12-22. Gretl. Summary Statistics, using the observations 301–325

Variable	Mean	Median	Minimum	Maximum
[1ex] v12	0.221475	0.139032	0.00101700	0.780730
v13	0.217074	0.139285	0.00108700	0.754430
v14	0.167442	0.110878	0.000348000	0.575242
v15	0.155908	0.111737	0.0125650	0.483602
v16	0.158329	0.111647	0.0101590	0.498096
v17	0.167575	0.111349	0.000836000	0.579004
v18	0.125868	0.0863670	0.000662000	0.417701
v19	0.179261	0.117898	0.000935000	0.612021
v20	0.141302	0.0932400	0.000714000	0.478343
v21	0.228822	0.143105	0.00149500	0.800529
v22	0.174892	0.114994	0.000343000	0.592146

Variable	Std. Dev.	Coef.Var.	Skewness	Ex. kurtosis
[1ex] v12	0.246134	1.11134	0.930598	-0.393370
v13	0.239324	1.10250	0.910879	-0.440017
v14	0.181797	1.08573	0.884089	-0.466508
v15	0.151811	0.973718	0.796534	-0.646866
v16	0.155834	0.984241	0.832126	-0.587890
v17	0.182383	1.08837	0.901570	-0.435120
v18	0.134253	1.06662	0.820573	-0.603688
v19	0.195217	1.08901	0.873615	-0.515800
v20	0.152787	1.08128	0.863700	-0.525357
v21	0.252696	1.10434	0.924172	-0.408867
v22	0.189797	1.08523	0.858809	-0.546215

wl	X0.5m	X1.5m	X2.5m
Min. :318.2	Min. :0.00000	Min. : 0.7792	Min. :0.005096
1st Qu.:476.9	1st Qu.:0.03398	1st Qu.:14.4084	1st Qu.:0.091878
Median :636.1	Median :0.10955	Median :22.4621	Median :0.269328
Mean :635.6	Mean :0.11392	Mean :19.6899	Mean :0.301121
3rd Qu.:794.5	3rd Qu.:0.17198	3rd Qu.:25.8785	3rd Qu.:0.431055
Max. :950.9	Max. :0.32937	Max. :30.9573	Max. :0.981314

Table A.17: Summary of the table with values of the spectral reflectance of P.oceanica measured on three different depths, R.

From: DepthData <- read.table(file="Three-Depths.dat", sep="", header=T); summary(DepthData).

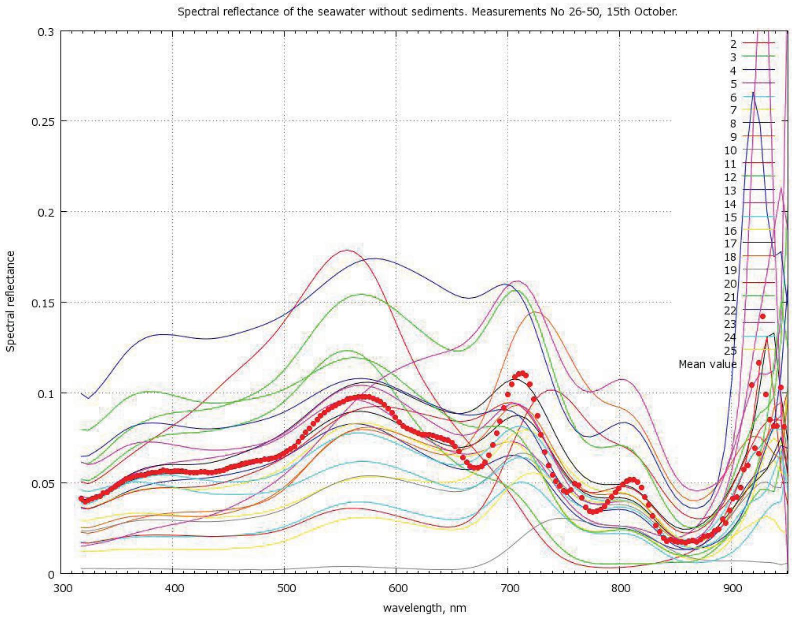

Figure A.35: Spectral reflectance of P.oceanica. Measurement series 25-50. Gnuplot display

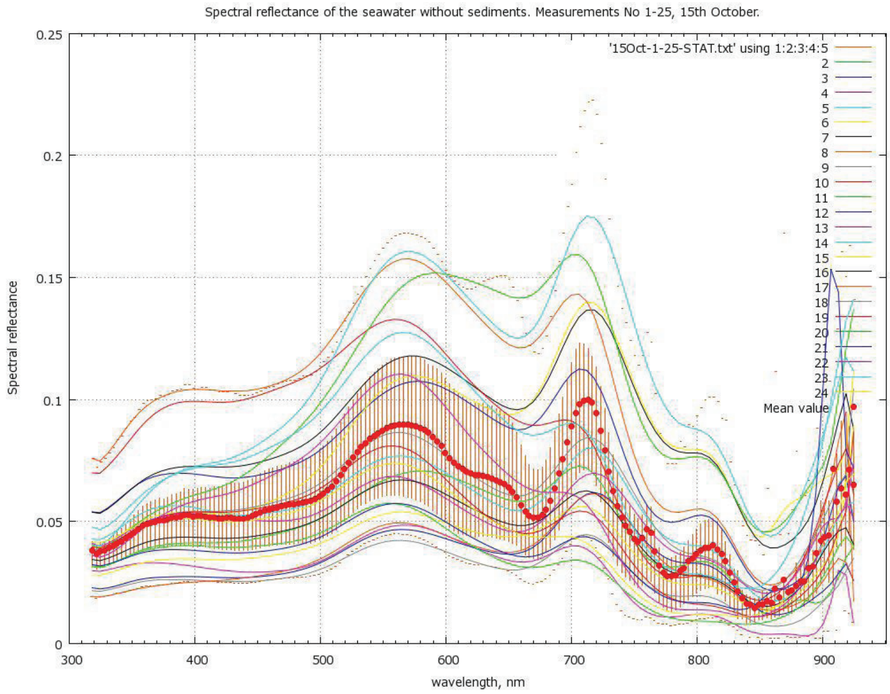

Figure A.36: Remote sensing reflectance of P.oceanica. Series 1-25.
Shown midspread of the statistical quartiles Q1 and Q3 (vertical dashes) and mean value within the range. Gnuplot

Table A.18: Two-Stage Least Squares: results of the TSLS analysis of the measurement set 1-191 of the spectral reflectance of P.oceanica (15.X.). Gretl
Model 1: TSLS, using observations 1–191.
Dependent variable: const Instrumented: v17 Instruments: v12

	Coefficient	Std. Error	z	p-value
[1ex] v17	6.88502	0.527503	13.0521	0.0000

Mean dependent var	1.000000	S.D. dependent var	0.000000
Sum squared resid	97.51535	S.E. of regression	0.716407
Log-likelihood	-237.5799	Akaike criterion	477.1598
Schwarz criterion	480.4121	Hannan–Quinn	478.4771

Hausman test – Null hypothesis: OLS estimates are consistent

Asymptotic test statistic: $\chi^2(1) = 13.2834$ with p-value = 0.000267768
Weak instrument test – First-stage F(1,190) = 16670.2

Table A.19: Initial Cluster Centers: results of the K-means analysis of the measurement set 201-236 of the spectral reflectance of P.oceanica (15.X.). SPSS

	Cluster			Cluster	
	1	2		1	2
V2	.353010	.000644	V16	.240091	.000374
V3	.271519	.000394	V17	.270306	.000435
V4	.273594	.000644	V18	.196188	.000211
V5	.406525	.000527	V19	.301486	.000370
V6	.344973	.000509	V20	.178575	.000328
V7	.395117	.000646	V21	.231708	.000440
V8	.254642	.000352	V22	.186493	.000365
V9	.288881	.000267	V23	.261761	.000418
V10	.191850	.000255	V24	.282032	.000264
V11	.249462	.000323	V25	.190709	.000375
V12	.209622	.000414	V26	.177432	.000206
V13	.218312	.000206	V27	.195104	.000268
V14	.177432	.000268	V28	.256630	.000386
V15	.184836	.000223	V29	.283744	.000436
			V30	.406525	.000646

Table A.20: Iteration History(a): results of the K-means analysis of the measurement set 201-236 of the spectral reflectance of P.oceanica (15.X.). SPSS

	Change in Cluster	
Iteration	1	2
1	.326	.206
2	.024	.010
3	.008	.003
4	.000	.000

Convergence achieved due to no or small change in cluster centres. The maximum absolute coordinate change for any centre is .000. The current iteration is 4. The minimum distance between initial centres is 1.435.

Table A.21: Number of Cases in each Cluster: results of the K-means analysis of the measurement set 201-236 of the spectral reflectance of P.oceanica (15.X.). SPSS

Cluster 1	55.000
Cluster 2	136.000
Valid	191.000
Missing	.000

Table A.22: Final Cluster Centers: results of the K-means analysis of the measurement set 201-236 of the spectral reflectance of *P.oceanica* (15.X.). SPSS

	Cluster			Cluster	
	1	2		1	2
V2	0.265141	0.046966	V16	0.181395	0.033191
V3	0.202643	0.036088	V17	0.202698	0.036614
V4	0.20699	0.037789	V18	0.149364	0.028217
V5	0.298975	0.052158	V19	0.225452	0.040193
V6	0.25915	0.045968	V20	0.135163	0.025506
V7	0.293508	0.049314	V21	0.175176	0.031866
V8	0.193292	0.036402	V22	0.142295	0.027148
V9	0.215848	0.038738	V23	0.19514	0.034553
V10	0.147798	0.027489	V24	0.214946	0.038321
V11	0.188955	0.034031	V25	0.14585	0.027665
V12	0.157947	0.029319	V26	0.134787	0.024912
V13	0.165877	0.029961	V27	0.149217	0.028326
V14	0.137149	0.02626	V28	0.193388	0.034999
V15	0.140563	0.026211	V29	0.214436	0.038433
			V30	0.299183	0.053451

Table A.23: Results of the tobit analysis with censored dependent variable (2) from the selected dataset Series 151-175 of the s. reflectance of P.oceanica. Gretl

Model 2: Tobit, using observations 1:01–8:23 (T = 191)
Dependent variable: v12

	Coefficient	Std. Error	z	p-value
[1ex] const	-0.00413795	0.0502867	-0.0823	0.9344
v2	0.890117	0.957730	0.9294	0.3527

Mean dependent var	0.035372	S.D. dependent var	0.053185
Censored obs	1	sigma	0.050920
Log-likelihood	295.1357	Akaike criterion	-584.2715
Schwarz criterion	-574.5147	Hannan–Quinn	-580.3195
	-0.032865	Durbin–Watson	2.065699

Test for normality of residual – Null hypothesis: error is normally distributed
Test statistic: $\chi^2(2)$ = 190.404 with p-value = 4.51226e-042

Table A.24: Results of the Prais-Winsten estimation applied towards variables 15 from the selected dataset 151-175 of the spectral reflectance of P.oceanica. Gretl

Model 3: Prais–Winsten, using observations 1:01–8:23 (T = 191) Dependent variable: v12 = -0.0343656

	Coefficient	Std. Error	t-ratio	p-value
[1ex] const	-0.00498439	0.00977709	-0.5098	0.6108
v2	0.912742	0.205904	4.4328	0.0000

Statistics based on the rho-differenced data:

Mean dependent var	0.035372	S.D. dependent var	0.053185
Sum squared resid	0.490951	S.E. of regression	0.050967
R^2	0.086511	Adjusted R^2	0.081678
F(1,189)	19.67163	P-value(F)	0.000016
	-0.001888	Durbin–Watson	2.003741

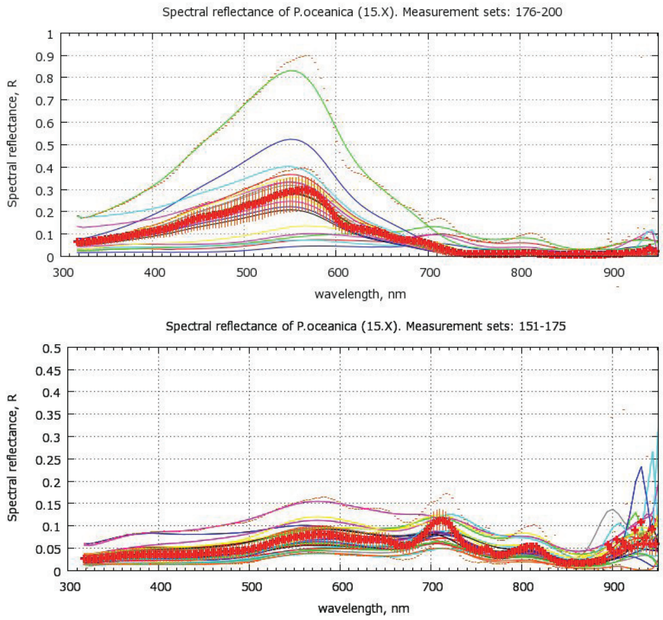

Figure A.37: Multiplot of spectral reflectance of P.oceanica. Series 151-200. Shown midspread of the statistical quartiles Q1 and Q3 (vertical dashes) and mean value within the range (red bold dots). Gnuplot visualization

Table A.25: Results of the Principal Components Analysis: measurement variables 1-7 from the selected dataset 301-325 of the spectral reflectance of P.oceanica (15.X.). Gretl

Eigenanalysis of the Correlation Matrix

Component	Eigenvalue	Proportion	Cumulative
1	6.4848	0.9264	0.9264
2	0.4949	0.0707	0.9971
3	0.0140	0.0020	0.9991
4	0.0052	0.0007	0.9998
5	0.0008	0.0001	1.0000
6	0.0002	0.0000	1.0000
7	0.0001	0.0000	1.0000

Eigenvectors (component loadings)

v1	-0.308	-0.880	0.334	-0.126	0.033	-0.042	0.006
v2	0.383	-0.295	-0.512	-0.230	-0.365	-0.370	-0.425
v3	0.383	-0.300	-0.465	-0.010	0.562	0.307	0.370
v4	0.390	-0.145	0.203	0.714	-0.129	-0.415	0.293
v5	0.392	-0.091	0.300	0.262	0.020	0.568	-0.597
v6	0.392	-0.011	0.259	-0.410	-0.543	0.299	0.476
v7	0.390	0.138	0.460	-0.429	0.488	-0.427	-0.113

Eigenvectors (component loadings)

Table A.26: Results of the Weighted Least Squares Analysis applied towards variables 12-20 from the selected dataset 301-325 of the spectral reflectance of P.oceanica. Gretl

Model 1: WLS, using observations 1–95. Dependent variable: v20

Variable used as weight: v12

	Coefficient	Std. Error	t-ratio	p-value
[1ex] const	0.239525	0.0771338	3.1053	0.0025
v1	0.000120809	0.000147131	0.8211	0.4137

Statistics based on the weighted data:

Sum squared resid	0.290924	S.E. of regression	0.055930
R^2	0.007197	Adjusted R^2	-0.003478
F(1,93)	0.674200	P-value(F)	0.413691
Log-likelihood	140.1579	Akaike criterion	-276.3158
Schwarz criterion	-271.2081	Hannan–Quinn	-274.2519

Statistics based on the original data:

Mean dependent var	0.136154	S.D. dependent var	0.149193
Sum squared resid	5.689669	S.E. of regression	0.247344

A.7.2 Data processing and statistical evaluation: carbonate sand

Table A.27: Results of the autocorrelation analysis of the measurement set 51-75 of the spectral reflectance of carbonate sand, Gretl

LAG	ACF		PACF		Q-stat	[p-value]
1	0.9851	***	0.9851	***	104.8293	[0.000]
2	0.9657	***	-0.1598	***	206.5423	[0.000]
3	0.9420	***	-0.1337	***	304.2787	[0.000]
4	0.9144	***	-0.1107	***	397.2949	[0.000]
5	0.8835	***	-0.0905	***	484.9833	[0.000]
6	0.8495	***	-0.0732	***	566.8791	[0.000]
7	0.8131	***	-0.0565	***	642.6707	[0.000]
8	0.7748	***	-0.0423	***	712.1933	[0.000]
9	0.7350	***	-0.0317	***	775.4114	[0.000]
10	0.6941	***	-0.0280	***	832.3807	[0.000]
11	0.6524	***	-0.0221	***	883.2508	[0.000]
12	0.6103	***	-0.0197	***	928.2405	[0.000]
13	0.5679	***	-0.0170	***	967.6289	[0.000]
14	0.5256	***	-0.0162	***	1001.7381	[0.000]
15	0.4835	***	-0.0154	***	1030.9237	[0.000]
16	0.4418	***	-0.0172	***	1055.5584	[0.000]
17	0.4v004	***	-0.0196	***	1076.0231	[0.000]
18	0.35v94	***	-0.0216	***	1092.7041	[0.000]
19	0.3189	***	-0.0224	***	1105.9911	[0.000]
20	0.2788	***	-0.0269	***	1116.2679	[0.000]

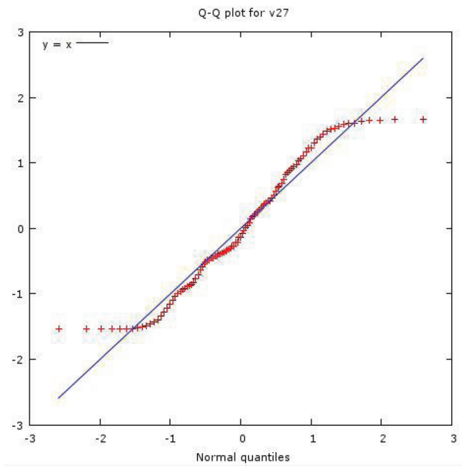

Figure A.38: Normal Q-Q plot: estimated versus observed values of the measurement of carbonate sand, variable 27. Series 51-75. Gretl modelling visualization

Table A.28: Results of the statistical analysis of spectral reflectance of carbonate sand, with average values (for sets 1-3). Wavelength step: 3 nm. Measured on Agia Pelagia beach, 14th October

wl	min	Q1	mean	Q3	max	median
402	0.091522	0.108252	0.119264	0.125199	0.156262	0.120855
405	0.094129	0.111507	0.126390	0.139560	0.174126	0.124623
408	0.096608	0.114474	0.129816	0.143488	0.178780	0.127983
412	0.098703	0.117396	0.133108	0.147164	0.183246	0.131282
415	0.101803	0.120880	0.137375	0.151792	0.189039	0.135571
418	0.105012	0.124746	0.141910	0.156937	0.195073	0.140136
422	0.108640	0.129140	0.147168	0.162721	0.202021	0.145337
425	0.113279	0.134815	0.153679	0.169999	0.210668	0.151906
428	0.118544	0.141149	0.160985	0.178059	0.220194	0.159402
432	0.122987	0.146844	0.167659	0.185518	0.228841	0.166154
435	0.127911	0.152289	0.174248	0.192960	0.237370	0.172836
438	0.132310	0.158310	0.181427	0.201169	0.246705	0.180044
442	0.136621	0.163674	0.187881	0.208310	0.255343	0.186472
445	0.140316	0.168266	0.193508	0.214558	0.262974	0.192106
448	0.143322	0.172017	0.198207	0.219703	0.269568	0.196709
452	0.145645	0.174991	0.201955	0.223770	0.274973	0.200367
455	0.148101	0.178031	0.205747	0.227926	0.280378	0.204052
459	0.149944	0.180646	0.208895	0.230917	0.284950	0.207175
462	0.151978	0.183204	0.212228	0.234461	0.289839	0.210556
465	0.136264	0.184985	0.214436	0.238727	0.294286	0.213490
469	0.155248	0.187804	0.217729	0.240237	0.298004	0.215926
472	0.156554	0.189708	0.220128	0.242769	0.301445	0.218291
475	0.158239	0.192110	0.223000	0.246279	0.305677	0.221116
479	0.160611	0.195242	0.226849	0.250810	0.310961	0.224984
482	0.164012	0.200152	0.232478	0.257229	0.318555	0.230599
485	0.168472	0.205823	0.238938	0.264573	0.327001	0.237010
489	0.172449	0.211132	0.245045	0.271446	0.334981	0.243087
492	0.176260	0.216078	0.250975	0.278269	0.342800	0.249133
495	0.180950	0.222148	0.258178	0.286469	0.352048	0.256243
499	0.186009	0.228774	0.265843	0.295200	0.361896	0.263884
502	0.189596	0.233599	0.271417	0.301563	0.368882	0.269139
505	0.191587	0.236300	0.274828	0.305379	0.372817	0.272281
509	0.193259	0.238538	0.277796	0.309446	0.376347	0.275357
512	0.196153	0.242620	0.282441	0.315177	0.381948	0.279890
515	0.200015	0.248183	0.288410	0.322126	0.389945	0.285937
519	0.204139	0.253981	0.294768	0.329524	0.398796	0.291707
522	0.208548	0.259760	0.301397	0.337066	0.407969	0.298231
526	0.213382	0.266241	0.308821	0.345426	0.418276	0.305397
529	0.218205	0.272715	0.316136	0.353749	0.428329	0.312514
532	0.222568	0.278565	0.322872	0.361518	0.437755	0.319122
536	0.226789	0.284495	0.329470	0.369010	0.446804	0.325558
539	0.230711	0.289790	0.335482	0.376082	0.455017	0.331317
542	0.233458	0.293802	0.340066	0.381589	0.461345	0.335918

wl	min	Q1	mean	Q3	max	median
546	0.235193	0.296532	0.343224	0.385560	0.465598	0.338854
549	0.236680	0.299381	0.345918	0.388909	0.469140	0.341256
552	0.237769	0.301722	0.348197	0.391858	0.472296	0.343234
556	0.239247	0.304604	0.350951	0.395307	0.476036	0.345633
559	0.240209	0.306984	0.353309	0.398254	0.479382	0.347674
562	0.240654	0.308165	0.354596	0.400054	0.481185	0.348907
566	0.240416	0.308874	0.355162	0.401224	0.481897	0.348929
569	0.238748	0.307064	0.353688	0.400427	0.480263	0.347042
572	0.235026	0.302640	0.349433	0.395980	0.475648	0.342958
576	0.212260	0.294628	0.340050	0.386378	0.466085	0.334751
579	0.219835	0.283193	0.329664	0.375185	0.450895	0.324215
583	0.208955	0.268530	0.314599	0.359047	0.432720	0.308769
586	0.196370	0.252380	0.296960	0.338330	0.411550	0.290283
589	0.181828	0.233326	0.276049	0.316609	0.386565	0.267500
593	0.166276	0.212916	0.253544	0.293790	0.359268	0.243094
596	0.149323	0.191055	0.229373	0.267668	0.331353	0.217166
599	0.132182	0.169324	0.205072	0.241088	0.303079	0.191137
603	0.117895	0.151271	0.185181	0.219420	0.280528	0.170074
606	0.107449	0.138360	0.171146	0.203897	0.264634	0.155317
609	0.101008	0.130206	0.162388	0.194168	0.254754	0.146269
613	0.097084	0.125265	0.157073	0.188174	0.248485	0.140671
616	0.094383	0.121987	0.153592	0.184349	0.244702	0.137070
619	0.092105	0.119159	0.150566	0.180848	0.241217	0.134371
623	0.090017	0.116792	0.147899	0.177856	0.238265	0.131097
626	0.088364	0.114636	0.145734	0.175448	0.236222	0.128638
629	0.086562	0.112565	0.143418	0.173135	0.233625	0.126183
633	0.084448	0.109785	0.140489	0.170056	0.230251	0.123296
636	0.082208	0.106766	0.137216	0.166497	0.226502	0.119990
639	0.079925	0.103852	0.134122	0.162951	0.222721	0.116886
643	0.077879	0.101395	0.131468	0.159978	0.219899	0.114099
646	0.075563	0.098621	0.128409	0.156518	0.216573	0.110812
649	0.072328	0.095004	0.124254	0.151735	0.212143	0.106456
653	0.068455	0.089876	0.118539	0.145085	0.205574	0.100544
656	0.063138	0.083138	0.110767	0.135900	0.196204	0.092816
660	0.057899	0.076562	0.102919	0.126826	0.186379	0.085030
663	0.054237	0.071651	0.097286	0.120346	0.179417	0.079514
666	0.051717	0.068781	0.093827	0.116423	0.175195	0.076101
670	0.050172	0.066690	0.091590	0.113854	0.172561	0.073923
673	0.048823	0.064991	0.089610	0.111550	0.170358	0.071985
676	0.047230	0.063165	0.087474	0.109078	0.167774	0.069807
680	0.045818	0.061108	0.085168	0.106421	0.165049	0.067486
683	0.044262	0.058946	0.082783	0.103630	0.162579	0.065041
686	0.041986	0.055955	0.079361	0.099441	0.158648	0.061599
690	0.040081	0.051396	0.074010	0.092741	0.152034	0.055896
693	0.034783	0.045555	0.067241	0.084820	0.143195	0.050116
696	0.030094	0.039507	0.060070	0.076166	0.133838	0.043600

Table A.29: Spectral reflectance of **carbonate sand** *(continued from previous page)*

wl	min	Q1	mean	Q3	max	median
700	0.025499	0.033281	0.052660	0.066929	0.124164	0.036937
703	0.020752	0.027050	0.045008	0.057197	0.113843	0.030173
706	0.016243	0.021080	0.037529	0.047681	0.103394	0.023549
710	0.012303	0.015914	0.030791	0.038860	0.093244	0.017834
713	0.007533	0.011641	0.025113	0.031338	0.084822	0.013233
716	0.006371	0.008236	0.020172	0.024328	0.077202	0.009214
720	0.004247	0.005386	0.015711	0.018057	0.069074	0.006121
723	0.002773	0.003524	0.012159	0.012999	0.061638	0.003836
726	0.001812	0.002194	0.009537	0.009237	0.055408	0.002543
730	0.001248	0.001453	0.007627	0.006800	0.049434	0.001739
733	0.000801	0.001018	0.006264	0.004722	0.044850	0.001208
736	0.000192	0.000855	0.005279	0.003743	0.042097	0.000954
740	0.000471	0.000718	0.004811	0.003055	0.039099	0.000816
743	0.000506	0.000644	0.004419	0.002901	0.037332	0.000740
746	0.000211	0.000582	0.004282	0.002898	0.036089	0.000715
750	0.000318	0.000557	0.003937	0.002175	0.033962	0.000667

Figure A.39: Spectral reflectance of carbonate sand on A.Pelagia beach. Results of single measurement set made by spectroradiometer Trios-RAMSES. Gnuplot

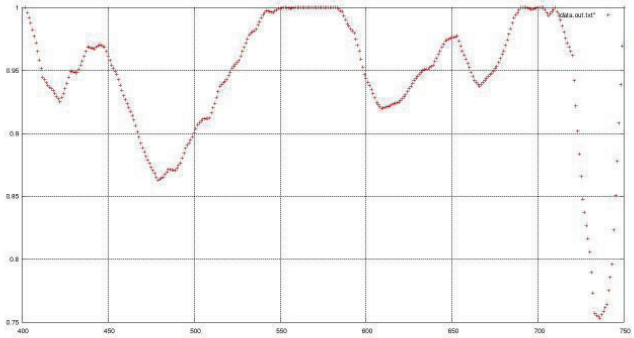

Table A.29: Results of the Quantile estimates: measurements 51-75 of the spectral reflectance of carbonate sand, Gretl

Model 2: Quantile estimates, using observations 1:01–5:09 (T = 105)

Dependent variable: v27 τ = 0.5 Asymptotic standard errors assuming IID errors

***	Coefficient	Std. Error	t-ratio	p-value
[1ex] const	0.837827	0.0386417	21.6820	0.0000
v1	-0.00111120	6.60949e–005	-16.8122	0.0000

Median depend. var	0.191024	S.D. dependent var	0.135439
Sum absolute resid	8.625039	Sum squared resid	1.370360

Log-likelihood	84.64508	Akaike criterion	-165.2902
Schwarz criterion	-159.9822	Hannan–Quinn	-163.1393

Table A.30: Results of the periodogram for v30 of the measurement set 51-75 of the spectral reflectance of carbonate sand, Gretl

omega	scaled frequency	periods	log spectral density	omega	scaled frequency	periods	log spectral density
0.05984	1	105.00	-1.2466	1.61568	27	3.89	-11.111
0.11968	2	52.50	-5.8761	1.67552	28	3.75	-11.170
0.17952	3	35.00	-4.0657	1.73536	29	3.62	-11.208
0.23936	4	26.25	-7.1031	1.79520	30	3.50	-11.461
0.29920	5	21.00	-6.1742	1.85504	31	3.39	-11.380
0.35904	6	17.50	-7.2772	1.91488	32	3.28	-11.686
0.41888	7	15.00	-8.7802	1.97472	33	3.18	-11.624
0.47872	8	13.13	-7.6806	2.03456	34	3.09	-11.724
0.53856	9	11.67	-8.4848	2.09440	35	3.00	-11.818
0.59840	10	10.50	-8.5764	2.15423	36	2.92	-11.805
0.65824	11	9.55	-9.4643	2.21407	37	2.84	-12.002
0.71808	12	8.75	-9.0868	2.27391	38	2.76	-11.930
0.77792	13	8.08	-9.3608	2.33375	39	2.69	-12.010
0.83776	14	7.50	-9.9332	2.39359	40	2.63	-12.124
0.89760	15	7.00	-9.6836	2.45343	41	2.56	-12.190
0.95744	16	6.56	-10.00	2.51327	42	2.50	-12.248
1.01728	17	6.18	-9.8994	2.57311	43	2.44	-12.306
1.07712	18	5.83	-10.188	2.63295	44	2.39	-12.323
1.13696	19	5.53	-10.197	2.69279	45	2.33	-12.353
1.19680	20	5.25	-10.467	2.75263	46	2.28	-12.420
1.25664	21	5.00	-10.505	2.81247	47	2.23	-12.382
1.31648	22	4.77	-10.641	2.87231	48	2.19	-12.487
1.37632	23	4.57	-10.906	2.93215	49	2.14	-12.433
1.43616	24	4.38	-10.957	2.99199	50	2.10	-12.609
1.49600	25	4.20	-10.785	3.05183	51	2.06	-12.410
3.11167	52	2.02	-12.477				

Number of observations = 105

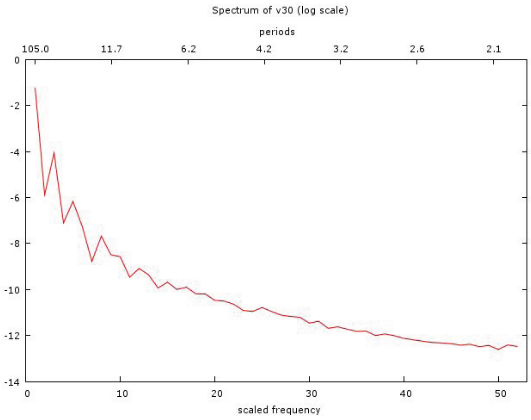

Figure A.40: Plot illustrating periodogram for v30 from measurements of carbonate sand, series 51-75. Gretl modelling visualization

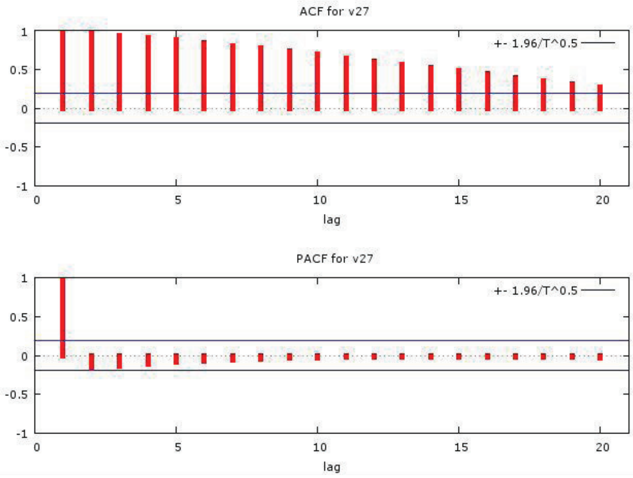

Figure A.41: Graph of the autocorrelation analysis of the measurements of carbonate sand. Series 51-75, variable 27. Gretl visualization

A.8. Satellite and aerial images covering research area of Crete island: selected examples

Figure A.42: Locations of selected measurements, visualization on Google Earth

Figure A.43: Random mosaic of selected aerial Google Earth images

No	Image cource	Data	Name
1	Landsat ETM+	2005/May/04	WRS2p181r035L71181035-035-20050504-ETM-GLS2005
2	Landsat TM	2006/Nov/07	WRS2p181r036L5181036-036-20061107-TM-GLS2005
3	Landsat ETM+	2005/Apr/25	WRS2p182r035L71182035-035-20050425-ETM-GLS2005
4	Landsat ETM+	2000/Jul/09	WRS2p181r036-7dx-20000709-ETM-GLS2000
5	Landsat TM	1987/Jun/10	LandsatWRS2p183r035p183r035-5dx-19870610-TM-GLS1990
6	Landsat ETM+/ Earth Sat	1999/Aug/08	071-261Mosaic-LandsatN-35N-35-35ETM-EarthSat-MrSID-19990808-20020624
7	Landsat ETM+/ Earth Sat	1999/Aug/08	071-260Mosaic-LandsatN-35N-35-30ETM-EarthSat-MrSID-19990808-20020617
8	Landsat ETM+	2000/Jun/30	WRS2p182r036-7x-20000630-ETM-EarthSat
9	Landsat MSS / Earth Sat	1975/Jul/26	LandsatWRS1p196r35-2m-19750726-MSS-EarthSat
10	Landsat TM / Earth Sat	1987/Jun/10	012-807LandsatWRS2p183r35-5t-19870610-TM-EarthSat
11	Landsat ETM+	2000/Jun/30	LandsatWRS2p182r036-7dx-20000630-ETM-GLS2000
12	Landsat ETM+	2005/Apr/09	LandsatWRS2p182r036L71182036 036-20050409-ETM-GLS2005

Table A.31: Available broadband Landsat satellite images covering the research area of Crete Island

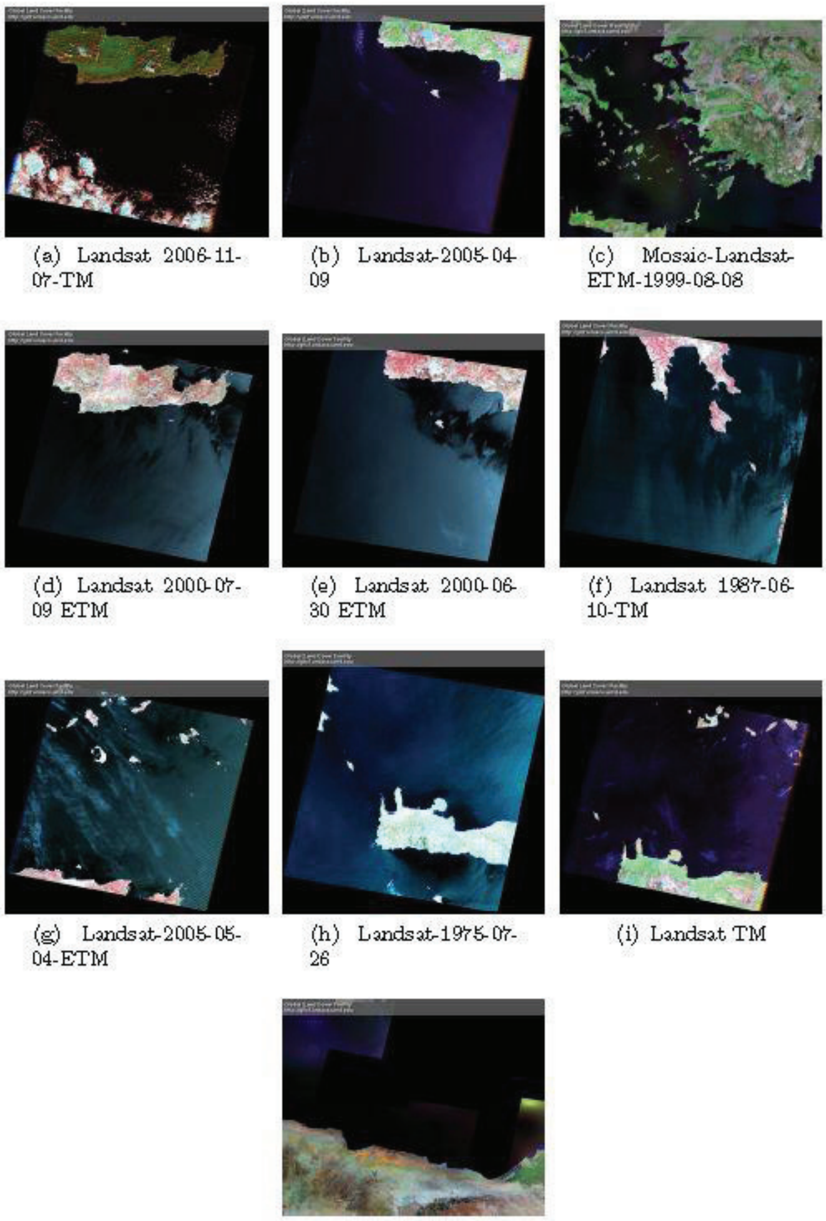

(a) Landsat 2006-11-07-TM

(b) Landsat-2005-04-09

(c) Mosaic-Landsat-ETM-1999-08-08

(d) Landsat 2000-07-09 ETM

(e) Landsat 2000-06-30 ETM

(f) Landsat 1987-06-10-TM

(g) Landsat-2005-05-04-ETM

(h) Landsat-1975-07-26

(i) Landsat TM

(j) Mosaic-Landsat-ETM-1999-08-08

Figure A.44: Landsat imagery, Crete Island. Previews

A.9. Analysis and classification of the satellite and aerial images

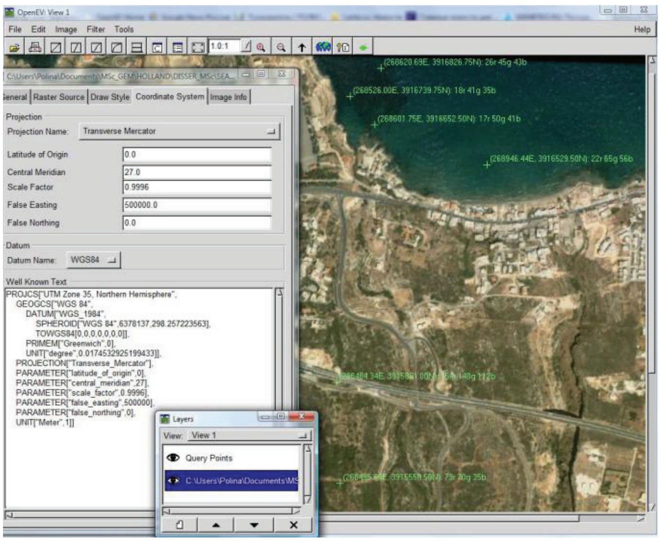

Figure A.45: The point querying shows the selected points and their coordinates within the area of seagrass meadow (green). <u>OpenEV</u>

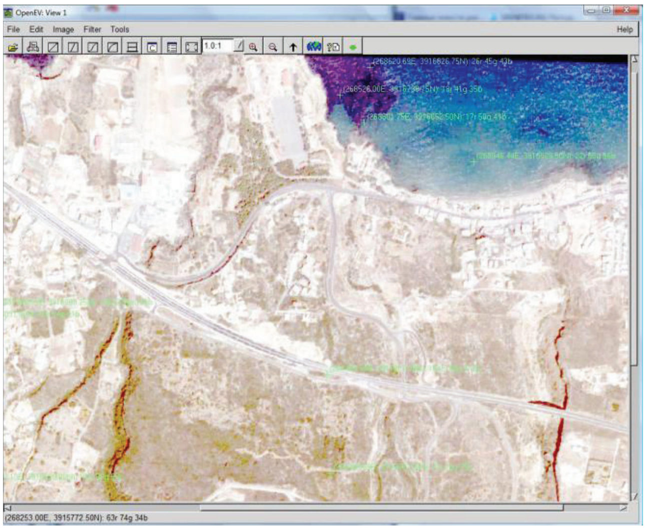

Figure A.46: Logarithmic Enhancment to Raster, applied to the aerial Google Earth image: the seagrass meadow can now be easily seen as a bright spot of purple color. <u>OpenEV</u>

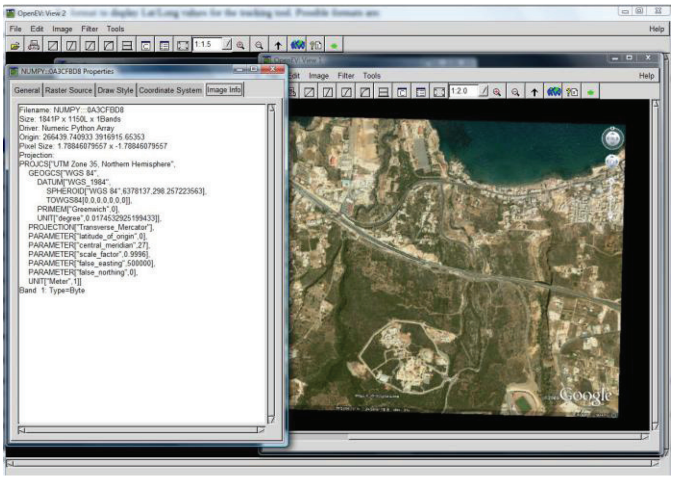

Figure A.47. Raster properties dialog: visualisation and spatial info about the image (projection UTM, zone 35, datum WGS-84, etc.) <u>OpenEV</u>.

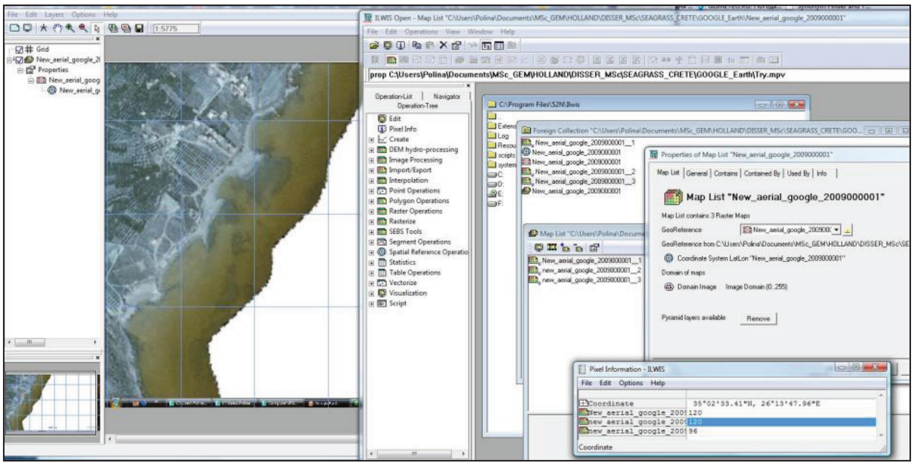

Figure A.48: Color composite image composed of 3 images of Cretan shelf, Google Earth. ILWIS.

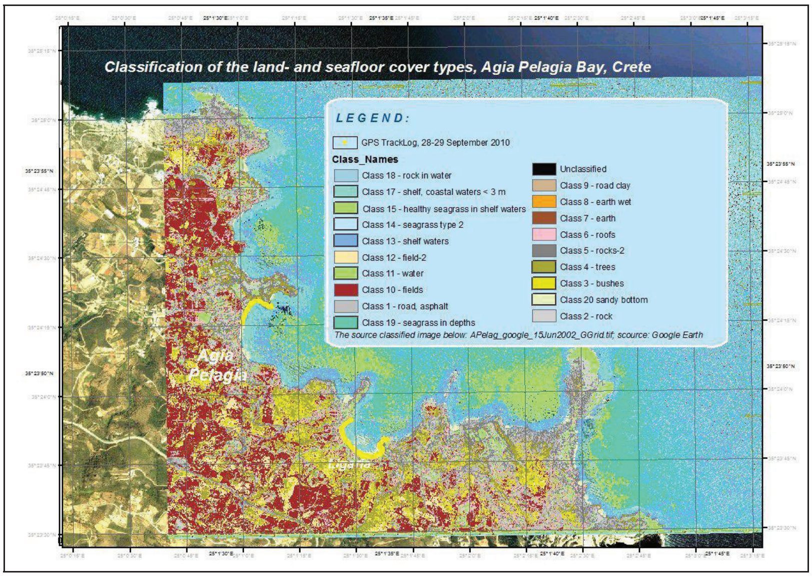

Figure A.49: Results of the unsupervised classification of the seafloor cover types and land structure, Agia Pelagia; raster layer read into the ArcGIS project

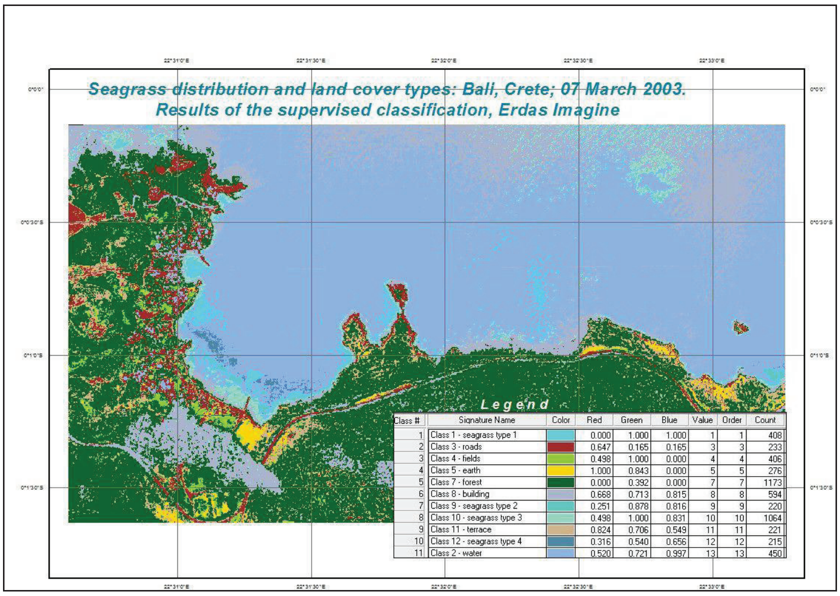

Figure A.50: Results of the image classification in Erdas Imagine: seagrass distribution in Bali area, Crete.

A.10. Accuracy assessment

Table A-32. Confusion matrix-2, between the classified Google Earth aerial image and fieldwork data, for Fig.A.43

Correctly classified	Rocky bottom	Shelf, < 3m	Healthy seagrass	Seagrass *P.oceanica*	Carbonate sand	Shelf waters, 0-3m	Shelf waters, 3-7m	Deep waters, > 7m	Field: corn, greens	Roads: asphalt+ground	Seagrass, other> 3m	Ground	Buildings (roofs)	Trees	Bushes	Total	κ producer accuracy
Rocky bottom	**14**	2	0	0	3	0	0	0	0	1	0	2	0	1	1	24	0.58
Shelf, < 3m	0	**12**	0	3	1	2	0	0	1	0	0	0	1	0	0	20	0.60
Healthy seagrass	0	1	**10**	3	2	0	0	0	1	0	2	0	0	0	0	19	0.52
Seagrass *P.oceanica*	0	1	1	**13**	0	1	0	0	1	0	2	0	0	1	1	21	0.62
Carbonate sand	2	0	0	0	**16**	0	0	0	0	0	0	2	0	0	0	20	0.80
Shelf waters, 0-3m	0	3	0	0	0	**9**	2	0	0	0	0	0	0	0	0	14	0.64
Shelf waters, 3-7m	1	2	0	0	0	3	**8**	1	0	0	0	0	0	0	0	15	0.53
Deep waters, > 7m	1	1	0	0	1	2	3	**16**	0	0	1	0	0	0	0	25	0.64
Fields: corn, greens	0	0	0	0	0	0	0	0	**14**	0	0	0	0	3	4	21	0.66
Roads: asphalt+ground	1	0	0	0	1	0	0	0	0	**5**	2	0	0	0	0	9	0.55
Seagrass, other> 3m	0	0	0	3	0	0	0	0	0	0	**24**	2	0	1	1	31	0.77
Ground	1	0	0	0	0	0	0	0	0	0	0	**11**	3	1	1	17	0.65
Buildings (roofs)	0	0	0	0	2	0	0	0	0	0	0	0	**9**	2	3	16	0.56
Trees	0	0	2	0	0	0	0	0	0	0	0	0	0	**7**	3	12	0.58
Bushes	0	0	0	0	0	0	0	0	0	0	0	0	0	2	**4**	6	0.66
Total	20	22	13	22	26	17	13	17	17	6	31	17	13	18	18	**270**	
κ user's accuracy	0.70	0.55	0.77	0.59	0.62	0.53	0.62	0.94	0.82	0.83	0.77	0.65	0.69	0.39	0.22	-	**0.64**

Overall Kappa (k) accuracy is calculated using the formula: ∑A/N, where A is number of correctly mapped points (172) and N is the total number of points (270). Thus, according to the results we received overall accuracy= 172/270= 0.6370, which is 64%. Overall k accuracy for unsupervised classification =64%.

Users accuracy (Reliability of classes) varies between 0.22 and 0.94 depending on class, which proves that supervised classification (see next table: Tab.A.33) has better results for seagrass mapping than the unsupervised classification.

Producer accuracy lies in interval between 0.52-0.77 according to class as well.

Table A-32. Confusion matrix-1, between the classified Google Earth aerial image and fieldwork data, for Fig.A.44

Correctly classified	Seagrass-1	Roads	Fields	Earth	Forest	Buildings	Seagrass-2	Seagrass-3	Terrace	Seagrass-4	Water	Total	κ producer accuracy
Seagrass *P.oceanica*	**22**	0	0	0	0	0	2	1	0	1	1	27	0.81
Roads	0	**18**	0	3	1	2	0	0	0	0	0	24	0.75
Fields	0	1	**10**	0	3	0	0	0	1	0	0	15	0.66
Earth	0	1	1	**13**	0	1	0	0	1	0	0	17	0.76
Forest	0	1	1	1	**9**	0	0	0	1	0	0	13	0.69
Buildings	0	0	2	0	1	**24**	0	0	1	0	0	28	0.85
Seagrass-2	3	0	0	0	0	0	**33**	2	0	2	2	42	0.78
Seagrass-3	1	0	0	0	0	0	1	**27**	0	1	1	31	0.87
Terrace	0	2	3	1	0	1	0	0	**19**	0	0	26	0.73
Seagrass-4	1	0	0	0	0	0	2	2	0	**37**	1	43	0.86
Water	2	0	0	0	0	0	1	1	0	1	**14**	19	0.74
Total	29	23	17	18	14	28	39	33	23	42	19	**285**	-
κ user's accuracy	0.76	0.78	0.59	0.72	0.64	0.86	0.85	0.82	0.83	0.88	0.74	-	**0.72**

Overall accuracy is calculated using the formula: $\sum$**A/N,** where A is number of correctly mapped points (226) and N is the total number of points (285). Thus, according to the results we received overall accuracy= 226/285= 0.79298, which is 72%. Overall accuracy=72%. User's accuracy (Reliability of classes) varies between 0.59 and 0.88. Producer accuracy lies in interval between 0.66-0.87.

A.11. Research general workflow.

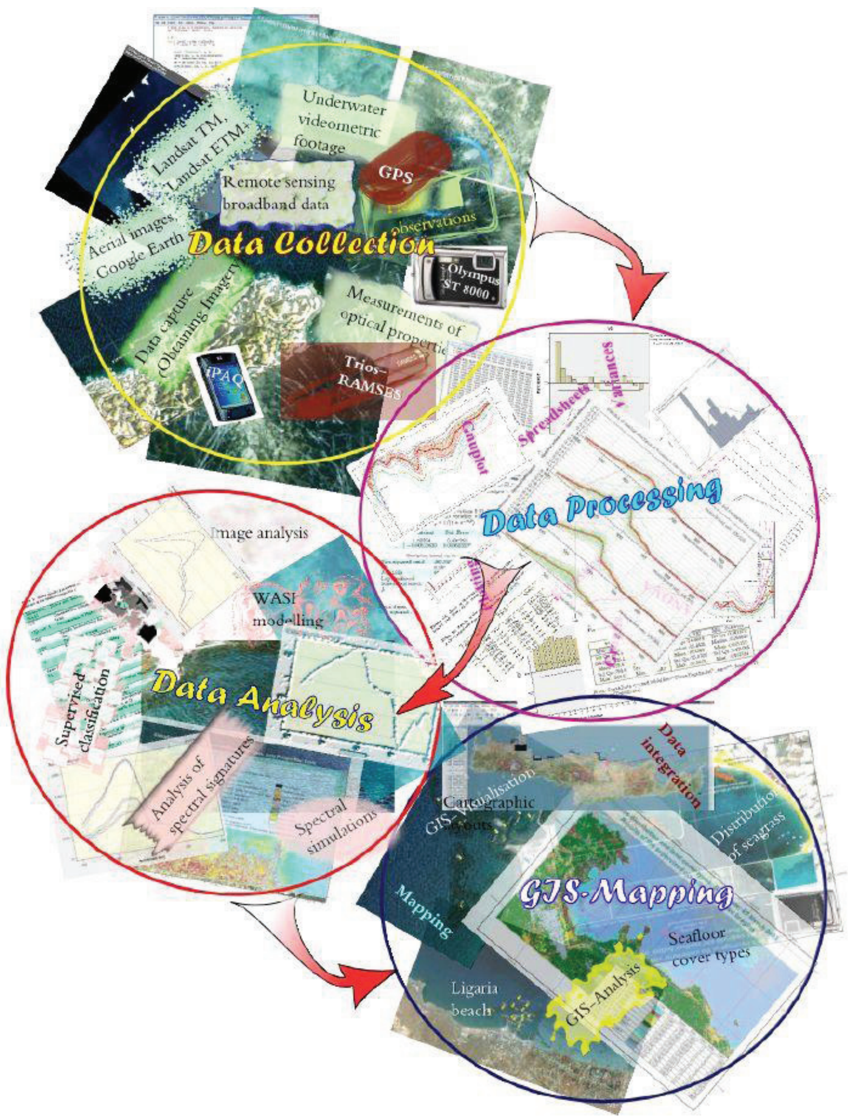

Figure A.51: General methodological research approach. Inkscape

A.12. Some snapshots of the working process

Figure A.52: Google Earth aerial imagery grabbing, Heraklion, the University of Crete

Figure A.53: Adjusting waterproof Olympus cameras for underwater seafloor videometric measurements.

Dr. Petros Lymberakis (left) and Dr. Bert Toxopeus (right)

Figure A.54: SCUBA gear diving equipment necessary for seagrass monitoring.
Source: Aquanauts.com.

Figure A.55: ...and it’s me, learning diving skills on Ligaria beach, Crete, 2010. On the photo: left.

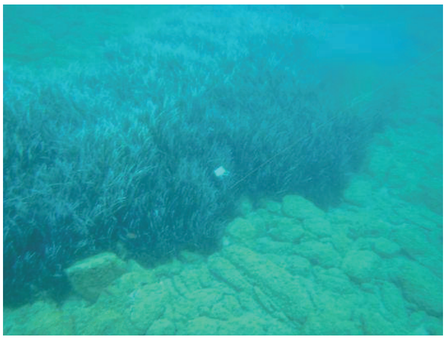

Figure A.56: Sticking the marker into the seafloor bottom in mattte of P.oceanica for depth measurements

Figure A.57: Placing the 0.5m circle and depth marker in the mattte of P.oceanica for photo capture

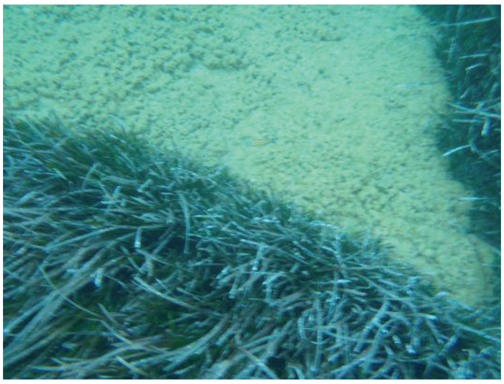

Figure A.58. Monitoring different seafloor cover types: matte of P.oceanica vs carbonate sand. Ligaria beach.

References

[1] Ackleson S. 2003. Light in shallow waters: A brief research review. Limnol. Oceanogr., 48(1, part 2), 2003, 323–328. American Society of Limnology and Oceanography, Inc. 19

[2] Alcoverro T., Romero J., Duarte C.M., Lopez N. 1997. Spatial and temporal variations in nutrient limitation of seagrass Posidonia oceanic growth in the NW Mediterranean. Marine ecology Progress Series.Vol.146: 155-161.

[3] Amoutzopoulou-Schina H and S.Haritonidis. 2005. Distribution and phenology of the marine phanerogam Posidonia oceanica in the Pagassitikos Gulf, Greece. Journal of Biological Research 4: 203 – 211, 2005 J. 4

[4] Arai K. and Tonooka H. 2005. Radiometric Performance Evaluation of ASTER VNIR, SWIR and TIR IEEE Transactions on Geoscience and Remote Sensing, Vol. 43, No. 12, Dec. 2005. 28

[5] Ardizzone G., Belluscio A. and Maiorano L. 2006. Long-term change in the structure of a Posidonia oceanica landscape and its reference for a monitoring plan. Marine Ecology. ISSN 0173-9565. 23

[6] Ball D., Soto-Berelov M., Young P. and Coots A. 2009. Baywide Seagrass Monitoring Program - Historical Seagrass Mapping. Fisheries Victoria Technical Report Series No. 70. 24

[7] Barille L., Robin M., Harin N., Bargain A., Patrick L. 2009. Increase in seagrass distribution at Bourgneuf Bay (France) detected by spatial remote sensing. Aquatic Botany. 24

[8] Bakran-Petricioli T., Antonic O., Bukovec D., Petricioli D., Janekovic I., Krizan J., Kusan V. and Dujmovic S. 2006. Modelling spatial distribution of the Croatian marine benthic habitats. Ecological Modelling 191, 96–105.

[9] Bell S.S., Robbins B.D. and Jensen S.L. 1999. Gap Dynamics in a Seagrass Landscape. Springer-Verlag. Ecosystems (1999) 2: 493–504. 125

[10] Bierwirth P. N., Lee T. J. and Burne R. V. 1993. Shalow sea-floor reflectance and water depth derived by unmixing multispectral imagery. Photogrammetric Engineering and Remote Sensing, vol. 59, No. 3, March, pp. 331-338. 27

[11] Blake S., Roob R. and Patterson E. 2000. Seagrass mapping of Victoria's Minor Inlets. Marine and Freshwater Resources Institute Report No. 28. 6

[12] Borum J., Duarte C.M., Krause-Jensen D. and Greve T.M. 2004. European seagrasses: an introduction to monitoring and management. The M and MS project. ISBN: 87-89143-21-3. Internet version: Available at http://www.seagrasses.org 7

[13] Brown C.J., Cooper K.M., Meadows W.J., Limpenny D.S., Rees H.L. 2002. Small scale mapping of sea bed assemblages in the eastern English Channel using

sonar and remote sampling techniques. Estuarine Coastal and Shelf Science, 54, 263-278. 10
[14] Boudouresque, C.F., Meinesz, A., Fresi, E. and Gravez, V., 1989. 2nd International Workshop on Posidonia oceanica Beds. G.I.S. Posidonie, Oceanica, 2, 322 pp. 7
[15] Bharathi A.M, Kumar S.C, Kalliappan S. 2003. Target Identification in multispectral images using *in-situ* hyperspectral reflectance. The Geospatial Resource Portal. Remote Sensing. www.gisdevelopment.net 28
[16] Buia M.C. and Mazzella L. 1991. Reproductive phenology of the Mediterranean seagrasses Posidonia oceanica (L.) Delile, Cymodocea nodosa (Ucria) Aschers., and Zostera noltii Hornem. Aquatic Botany, 40 (1991) 343-362. Elsevier Science Publishers B.V., Amsterdam. 7
[17] Butler 1987. Marine resource mapping: an introductory manual. 30
[18] Cappo, M., Alongi, D.M., Williams, D. and Duke, N. 1995. A Review and Synthesis of Australian Fisheries Habitat Research: Major threats, issues and gaps in knowledge of coastal and marine fisheries habitats. Fisheries Research and Development Corporation. 5
[19] Carter G.A., Criss G.A., Blossom G.A. and Biber P.D. 2008. Decadal-Scale Changes in Coverage on the Mississippi Barrier Islands, Northern Gulf of Mexico. http://precedings.nature.com/documents/3669/version/1/files/npre20093669-1.pdf 23
[20] Calvo S., Ciraolo G. and Loggia G. la. 2003. Monitoring Posidonia oceanica meadows in a Mediterranean coastal lagoon (Stagnone, Italy) by means of neural network and ISODATA classification methods. INT. J. REMOTE SENSING, 2003, VOL. 24, NO. 13, 2703–2716 8
[21] Cambridge M.L., Kendrick G.A. 2009. Contrasting responses of seagrass transplants (Posidonia australis) to nitrogen, phosphorus and iron addition in an estuary and a coastal embayment. Journal of Experimental Marine Biology and Ecology. 371, 34–41.
[22] Choo, C.K. 2006. Save our Seahorses. First Edition. www.sosmalaysia.org 10
[23] Clark, R.N., 1999. Spectroscopy of rocks and minerals and principles of spectroscopy. In: A.N. Rencz (ed.). Manual of Remote Sensing, Chapter 1, John Wiley and Sons, New York. 3-58. 10
[24] Connell J.H. 1978. Diversity in tropical rain forests and coral reefs. Science 199:1302– 10. 122
[25] Dehouck A., Martiny N., Froidefond J.-M., Sénéchal N. 2008. In-Water Reflectance Spectra Measured On Board a Jet-Ski Across a Complex Nearshore Zone of Case-2 Waters during the ECORS Experiment. Manuscript published in "Ocean Optics XIX, Barga: Italie (2008)" 23

[26] Dekker A.G., Brando V.E., Anstee J.M. 2005. Retrospective seagrass change detection in a shallow coastal tidal Australian lake. Remote Sensing of Environment 97:415-433. 8

[27] Dekker A., Brando V., Anstee J. 2005. Remote Sensing of Seagrass Ecosystems: Use of Spaceborne and Airborne Sensors. SVNL083-Larkum. 27

[28] Di Carlo G. 2004. The natural recolonisation process of the seagrass Posidonia oceanica (L.) Delile after the introduction of the Italo-Algerian methane pipeline in the SW Mediterranean sea. 15

[29] Diaz-Almela E., Marba N., Alvarez E., Santiago R., Holmer M., Grau A., Danovaro R., Argyrou M., Karakassis I, Duarte C.M. 2006. Benthic inputs as predictors of seagrass 1 (Posidonia 2 oceanica) fish farm-induced decline. http://arxiv.org/ftp/qbio/ papers/0611/0611006.pdf 5

[30] Dierssen H and Zimmerman R.C. 2003. Ocean color remote sensing of seagrass and bathymetry in the Bahamas Banks by high-resolution airborne imagery. Limnol. Oceanogr., 48(1, part 2), 2003, 444–455, by the American Society of Limnology and Oceanography. 28

[31] Dixon R, editor. 2005. Watching the Seagrass Grow – a guide for community seagrass monitoring in NSW (2nd Ed). Reference manual . The Community Environment Network, Ourimbah. 5

[32] Duarte, C.M. 2002. The future of seagrass meadows. Environmental Conservation 29 (2), 192–206. 5

[33] Dumay O., Fernandez C. and Pergent G. 2002. Primary production and vegetative cycle in Posidonia oceanica when in competition with the green algae Caulerpa taxifolia nd Caulerpa racemosa. J.Mar. Biol. Ass. UK, 82, 379-387. 4

[34] Dural B. 2010. Phenological observations on Posidonia oceanica (L.) Delile medows along the coast of Akkum (Sgack Bay, Aegean Sea, Turkey). J. Black Sea/Mediterranean Environment, Vol. 16 (1): 133-144. 7

[35] Edwards A.J. (ed.) 2000. Remote Sensing handbook for tropical coastal management. http://www.unesco.org/csi/pub/source/rs.htm 11

[36] Ferguson R.L. and Karl Korfmacher K. 1997 Remote sensing and GIS analysis of seagrass meadows in North Carolina, USA. Aquatic Botany 58 (1997) 241-258. 27

[37] Fletcher R.S., Pulich Jr. W. and Hardegree B. 2009. A Semiautomated Approach for Monitoring Landscape Changes in Texas Seagrass Beds from Aerial Photography. Coastal Education and Research Foundation doi: 10.2112/07-0882.1 28

[38] Fornes A., Basterretxea G., Orfila A., Jordi A., Alvarez A. and Tintore J. 2006. Mapping Posidonia oceanica from IKONOS. ISPRS Journal of Photogrammetry and Remote Sensing 60 (2006) 315–322. 8

[39] Francour, P., Magreau, J.F., Mannoni, P.A., Cottalorda, J.M., Gratiot, J., 2006. Management guide for Marine Protected Areas of the Mediterranean Sea, Permanent Ecological Moorings. Universite de Nice-Sophia Antipolis and Parc National de Port-Cros, Nice, 68 pp. 7

[40] Francour P., Ganteaume A. and M. Poulain. 1999. Effects of boats anchoring in Posidonia oceanica seagrass beds in the Port-Cross National Park (north-western Mediterranean Sea). Aquatic conservation: Marine and Freshwater Ecosystems: 9: 391-400. 5

[41] Fyfe S.K. 2003. Spatial and temporal variation in spectral reflectance: Are seagrass species spectrally distinct? Limnology and Oceanography 48: 464–479. 8

[42] Fyfe S.K. 2004. Hyperspectral studies of New South Wales with particular emphasis on the detection of light stress in Eelgrass Zostera capricorni. PhD Thesis. The University of Wollongong. Research Online, http://ro.uow.edu.au/theses/472/ 8

[43] Gege P. 2004. The water color simulator WASI: an integrating software tool for analysis and simulation of optical in situ spectra. Computers and Geosciences 30 (2004) 523–532. 63

[44] Gege, P. 2005. The Water Colour Simulator WASI. User manual for version 3. DLR Internal Report IB 564-01/05, 83 pp. 78

[45] Gobert S., Cambridge, M. L. Velimirov, B. Pergent, G. Lepoint, G. Bouquegneau, J. M. Dauby, P. Pergent-Martini, C. Walker, D. I. 2006. Biology of Posidonia. In Larkum A.W.D., Orth, R.J., Duarte C.M. (eds.), Seagrasses: Biology, ecology and conservation. Springer Verlag, Berlin, Pages 387–408. 5

[46] Gobert S., Defawe O, Lepoint G, Demoulin V and Bouquegneau J-M. 2001. Anthesis effects on Posidonia oceanica (L.) Delile phenology in the Bay of Calvi (Corsica, Mediterranean Sea). Hydrobiologia 455: 121–125. 7

[47] Green, E.P., P.J. Mumby, A.J. Edwards, and C.D. Clark, 1996. A review of remote sensing for the assessment and management of tropical coastal resources. Coast. Manag., 24(1):1-40. 8

[48] Green E.P., Short F.T. 2003. World Atlas of Seagrasses. University of California Press, Berkeley, USA.

[49] Guidetti P. 2008. Population dynamics of the seagrass Posidonia oceanica for evaluating meadow health status: a study case using reconstruction techniques. Laboratory of Zoology and Marine Biology, DiSTeBA, CoNISMa, University of Lecce. 7

[50] Gullstroom M.,, Lunden B., Bodin M., Kangwe J., Ohman M.C., Mtolera M.S.P. and Bjork M. 2006. Assessment of changes in the seagrass-dominated submerged vegetation of tropical Chwaka Bay (Zanzibar) using satellite remote sensing. Estuarine, Coastal and Shelf Science 67 (2006) 399-408. 27

[51] Haag S.M., Kennish M., Sakowicz G.P. 2008. Seagrass Habitat Characterization in Estuarine Waters of the Jacques Cousteau National Estuarine Research Reserve Using Underwater Videographic Imaging Techniques. Journal of Coastal Research, SI(55), 171– 179. West Palm Beach (Florida), ISSN 0749-0208. 8

[52] Den Hartog, C. 1970. The Seagrasses of the World. North Holland Publishing Company, Amsterdam, 275 pp. 31 plates. 6

[53] Den Hartog, C., 1977. Structure, function, and classification in seagrass communities. In: C.P. McRoy and C. Helfferich (Editors), Seagrass Ecosystems: a Scientific Perspective. Marcel Dekker, New York, pp. 89-121. 4

[54] Heege T., Bogner A., Pinnel N. 2003. Mapping of submerged aquatic vegetation with a physically based process chain. Proc. Remote Sensing, September 8-12 2–3/ Barcelona, Spain. Ed. by Kramer E. The International Society for Optical Engineering, Vol.5233. 28

[55] Hirose K., Syoji M., Hang H.T.M., Anh N.H., Triet T. and Nam V.N. 2004. Satellite data application for mangrove management. International Symposium on Geoinfomatics for Spatial Infrastructure Development in Earth and Allied Sciences. 28

[56] Hochberg, E.J., Atkinson, M.J. 2003a. Capabilities of remote sensors to classify coral, algae, and sand as pure and mixed spectra. Remote Sensing of Environment 85, 174–189. 29

[57] Hochberg, E.J., Atkinson, M.J., Andrefouet, S., 2003b. Spectral reflectance of coral reef bottom-types worldwide and implications for coral reef remote sensing. Remote Sensing of Environment 85, 159–173.

[58] Hogarth P. 2007. The Biology of Mangroves and Seagrasses. Oxford University Press. 1

[59] Holmer M., Marba N, Lamote M and Duarte C. 2009Deterioration of Sediment Quality in Seagrass Meadows (Posidonia oceanica) Invaded by Macroalgae (Caulerpa sp.). Estuaries and Coasts (2009) 32:456–466 DOI 10.1007/s12237-009-9133-4 1

[60] Holmer M, Argyrou M, Dalsgaard T., Danovaro R, Diaz-Almela E, Duarte C, Frederiksen M, Grau A, Karakassis I, Marbà N, Mirto S, Pérez M, Pusceddu A, Tsapakis M.2008 Effects of fish farm waste on Posidonia oceanica meadows: Synthesis and provision of monitoring and management tools. Marine Pollution Bulletin 56 (2008) 1618–1629. 5

[61] Iverson R.L. and Bittaker H.F. 1986. Seagrass Distribution and Abundance in Eastern Gulf of Mexico Coastal Waters. Estuarine, Coastal and Shelf Science, 22, 577-602. 19

[62] Jackson J., Nemeth D.J. 2007. A New Method to Describe Seagrass Habitat Sampled During Fisheries-Independent Monitoring. Estuaries and Coasts Vol. 30, No. 1, p. 171–178 February 2007 8
[63] Jensen S. and Bell S. 2001. Seagrass growth and patch dynamics: cross-scale morphological plasticity. Plant Ecology 155: 201–217, 2001. 125
[64] Jensen J.R., Rutchey K, Koch M.S, Narumalani S. 1995. Inland wetland change detection in the everglades water conservation area 2a using a time-series of normalized remotely-sensed data. Photogrammetric Eng Remote Sensing 61: 199–209 8
[65] Jerlov N.G. 1952. Influence of suspended and dissolved matter on the transparency of sea water. Wiley online Library. TellusVolume 5, Issue 1, Published online: 2010. 22
[66] Kalinowski A. and Oliver S. 2004 ASTER Mineral Index Processing Manual. Remote Sensing Applications. Geoscience Australia 28
[67] Kelly, M.G., 1980. Remote sensing of seagrass beds, Handbook of Seagrass Biology: An Ecosystem Perspective (R.C. Phillips and C.P. Mc Roy, editors), Garland STPM Press, New York, N.Y., pp. 69-86. 8
[68] Kendrick GA, Hegge BJ, Wyllie A, Davidson A, Lord DA. 2000. Changes in Seagrass Cover on Success and Parmelia Banks, Western Australia Between 1965 and 1995. Estuarine, Coastal and Shelf Science, 50:341-353. 8
[69] Kirk J.T.O. 1994. Light and photosynthesis in aquatic ecosystems, pp 1–509. University Press, Cambridge, UK. 23
[70] Kirkman H. 1996. Baseline and Monitoring Methods for Seagrass Meadows. Journal of Environmental Management (1996) 47, 191–201. 10
[71] Kuo J, McComb AJ, 1989. Seagrass taxonomy, structure and development. In: Larkum AWD, McComb AJ, Shepherd, eds. Biology of seagrasses: a treatise on the biology of seagrasses with special reference to the Australian region. Elsevier, The Netherlands: 6-73. 4
[72] Leoni V., Pasqualini V., Pergent-Martini Ch., Vela A., Pergent G. 2006. Morphological responses of Posidonia oceanica to experimental nutrient enrichment of the canopy water. Journal of Experimental Marine Biology and Ecology xx (2006) xxx–xxx. 5
[73] Leoni V., Pasqualini V., Pergent-Martini Ch., Vela A., Pergent G. 2007. Physiological responses of Posidonia oceanica to experimental nutrient enrichment of the canopy water. Journal of Experimental Marine Biology and Ecology 349, 73–83. 5
[74] Leoni V., Vela A., Pasqualini V., Pergent-Martini Ch., Pergent G. 2008. Effects of experimental reduction of light and nutrient enrichments (N and P) on

seagrasses: a review. Aquatic Conservation: Marine and Freshwater Ecosystems, 18: 202–220.
[75] Lewis M. 2001. Discriminating Vegetation with Hyperspectral Imagery - What is Possible? http://www.ieeexplore.ieee.org/stamp/stamp.jsp?arnumber=00978199 Proceedings, International Geoscience and Remote Sensing Symposium, 9-13 July 2001, Sydney, Australia. ISBN 0-7803-7031-7 23
[76] Louchard E.M., Reid R.P., Stephens F.C., Davis C.O., Leathers R.A., Downes T.V. 2003. Optical remote sensing of benthic habitats and bathymetry in coastal environments at Lee Stocking Island, Bahamas: A comparative spectral classification approach. Limnology and Oceanography (2003) 48:511-521. 23
[77] Luque A. and Templado J.A. 2004. Praderas y bosques marinos de Andalucia Consejeria de Medio Ambiente, Junta de Andalucia (in press).
[78] Lyzenga D.R. 1981. Remote sensing of bottom reflectance and water attenuation in shallow water using aircraft and Landsat data. International Journal of Remote Sensing 2, 71-82. 8
[79] Maffione R.A. and Dana D.R. 1997 Instruments and methods for measuring the backward-scattering coefficient of ocean waters. Optical Society of America 63
[80] Maffione R.A. 2001a. Evolution and Revolution in Measuring Ocean Optical Properties. Oceanography, Vol.14, No.3. 22
[81] Maffione R.A. 2001b.Hyperspectral Optical Properties, Remote Sensing, and Underwater Visibility. Hydro-Optics, Biology, and Instrumentation Laboratories. 22
[82] Malthus T.J. and Karpouzli E. 2003. Integrating field and high spatial resolution satellite based methods for monitoring shallow submersed aquatic habitats in the Sound of Eriskay, Scotland, UK. Int Journal Remote Sensing 24: 2585–2593. 8
[83] Matarrese R., Acquaro M., Morea A., Tijani K., Chiaradia M.T. 2008. Applications of remote sensing techniques for mapping Posidonia oceanica meadows. Geoscience and Remote Sensing Symposium. ISBN:978-1-4244-2807-6. 14
[84] Matarrese R., Acquaro M., Morea A., Khalid T., Chiaradia M.T. 2006 Applications of remote sensing techniques for mapping Posidonia oceanica meadows. http://www.igarss08.org/Abstracts/pdfs/3888.pdf 8
[85] McKenzie L.J., Campbell S.J. 2002. Manual for Community (citizen) Monitoring of Seagrass Habitat. Western Pacific Edition. Marine Plant Ecology Group, QDPI, Northern Fisheries Centre, Cairns. 43 pp. 1
[86] McKenzie L.J., Campbell S.J. and Roder C.A. 2003. Seagrass-Watch: Manual for Mapping and Monitoring Seagrass Resources by Community (citizen) Volunteers. 2nd Edition. QFS, NFC, Cairns. 100pp. 8

[87] McKenzie L.J. 2003. Guidelines for the rapid assessment of seagrass habitats in the Western Pacific. Marine Plant Ecology Group, QDPI, Northern Fisheries Centre, Cairns, http://www.seagrasswatch.org 19
[88] McKenzie L.J., Campbell S.J. and F.Lasi 2006. Seagrasses and Mangroves. In: Green A.P. Lokani W., Atu P., Ramonia P., Thomas P. and Almanmy J (eds). 2006 Solomon Islands Marine Assessment. Technical report of survey conducted May 13 to June 17 2004. The Nature Conservancy, Indo-Pacific Resource Centre. Report No 1/06 6
[89] McKenzie L.J. and Yoshida R. 2007. Seagrass-Watch: Guidelines for Monitoring Seagrass Habitats in the Fiji Islands. Proceeding of a training workshop. Corpus Christi Teachers College Laucala Bay, Suva, Fiji, 16th June 2007. Seagrass-Watch HQ Cairns, 42pp. 6
[90] McKenzie L.J. 2008. Seagrass-Watch. Proceedings of a Workshop for Mapping and Monitoring Seagrass Habitats in North East Arnhem Land, Northern Territory. 18-20 October 2008. Seagrass-Watch HQ, Cairns, 49pp. 1
[91] McKenzie L.J., Yoshida R. 2009. Seagrass Watch. Proceedings of a Workshop for Monitoring Seagrass Habitats in Indonesia. The Nature Conservancy, Coral Triangle Centre, Sanur, Bali, Indonesia. 78
[92] Meinesz, A., Lefevre, J.R., Astier, J.M., 1991. Impact of coastal development on the infralittoral zone along the south-eastern Mediterranean shore of continental France. Marine Pollution Bullettin 23, 343–347. 5
[93] Mellors J. and McKenzie L. 2009(a). Seagrass-Watch: Guidelines for Monitoring Seagrass Habitats. Proceedings of a workshop held on Thursday Island, Torres Strait 4- 8.03.2009. 23
[94] Mellors J and McLenzie L. 2009(b). Seagrass-Watch: Seagrass Monitoring Guidelines for Torres Strait Communities. Meer Island. Proceedings of a workshop held on Meer Island, Torres Strait 14-15 September 2009. 58 pp. 6
[95] Micheli C., Paganin P, Peirano A., G. Caye, Meinesz A. and Bianchi C.N. 2005. Genetic variability of Posidonia oceanica (L.) Delile in relation to local factors and biogeographic patterns. Aquatic Botany 82 (2005) 210–221 5
[96] Montefalcone M. 2009.Ecosystem health assessment using the Mediterranean seagrass Posidonia oceanica: A review. Ecological indicators 595 – 604 7
[97] Montefalcone M., Albertelli G., Morri C. and Bianchi C.N. 2010. Patterns of wide-scale substitution within meadows of the seagrass Posidonia oceanica in NW Mediterranean Sea: invaders are stronger than natives. Aquatic Conserv: Mar. Freshw. Ecosyst. 20: 507–515. 125
[98] Montefalcone M., Albertelli G., Bianchi C.N., Mariani M., Morri C. 2006. A new synthetic index and a protocol for monitoring the status of Posidonia oceanica

meadows: a case study at Sanremo (Ligurian Sea, NW Mediterranean). Aquatic Conservation: Marine and Freshwater Ecosystems, 16, 29–42. 10

[99] Mount R. 2003. The application of digital aerial photography to shallow water seabed mapping and monitoring – how deep can you see? Coastal GIS 2003: and integrated approach to Australian coastal issues, 7th - 8th July 2003. Wollongong, University of Wollongong, pp. 139-156. 8

[100] Mumby P.G., Green E.P., Edwards A.J. and Clark C.D. 1999. The cost-effectiveness of remote sensing for tropical coastal resources assessment and management. Journal of Environmental Management Volume 55, Issue 3, March 1999, Pages 157-166 24

[101] Mumby, P. J. and Edwards, A. J. 2002. Mapping marine environments with IKONOS imagery: Enhanced spatial resolution can deliver greater thematic accuracy. Remote Sensing of Environment, 82, 248–257 27

[102] Mumby P.J. Skirving W., Strong A.E., Hardy J.T., LeDrew E.F., Hochberg E.J., Stumpf R.P. and David L.T. 2004. Remote sensing of coral reefs and their physical environment. Marine Pollution Bulletin, 48:219-228. 19

[103] Nagelkerken I., van der Velde G., Gorissen M.W., Meijer G.J., van't Hofc T. and den Hartog C. 2000. Importance of Mangroves, Seagrass Beds and the Shallow Coral Reef as a Nursery for Important Coral Reef Fishes, Using a Visual Census Technique. Estuarine, Coastal and Shelf Science 51, 31–44 doi:10.1006/ecss.2000.0617, online: http://www.idealibrary.com 4

[104] Noralez S. 2010. Exploring the Limits of Mapping Seagrass. A case study for P. oceanica. MSc Thesis. ITC. Netherlands. 4

[105] Norris J.G., Wyllie-Echeverria S., Mumford T., Bailey A. and Turner T. 1997. Estimating basal area coverage of subtidal seagrass beds using underwater videography. Aquatic Botany 58 (1997) 269-287 4

[106] SPOT, Official Website http://www.spotimage.com/web/en/172-spot-images.php 27

[107] Orth R. J., Carruthers T.J.B., Dennison W.C., Duarte C. M., Fourqurean J.W. , Heck Jr. K. L. , Hughes A. R., Kendrick G. A., Kenworthy W. J., Olyarnik S., Short F.T., Waycott M. and Williams S. L. 2006. A Global Crisis for Seagrass Ecosystems. Vol. 56 No. 12, BioScience 987. 6

[108] Palandro D., Andréfouët S., Muller-Karger F. E., Dustan Ph., Hu Ch., and Hallock P. 2003. Detection of changes in coral reef communities using Landsat-5 TM and Landsat-7 ETM+ data. Can. J. Remote Sensing, Vol. 29, No. 2, pp. 201–209. 28

[109] Pasqualini V., Pergent-Martini C. and Pergent, G. 1998(a). Use of remote sensing for the characterization of the Mediterranean coastal environment – the case

of Posidonia oceanica. Journal of Coastal Conservation 4: 59-66, 1998, EUCC; Opulus Press Uppsala. 30
[110] Pasqualini V., Pergent-Martini C., Clabaut P., Pergent G. 1998(b). Mapping of Posidonia oceanica using aerial photographs and side scan sonar: Application off the island of Corsica (France). Estuarine Coastal Shelf Sci 47:359–367. 8
[111] Pasqualini V, Pergent-Martini C, Pergent G. 1999. Environmental impact identification along the Corsican coast (Mediterranean Sea) using image processing. Aquatic Botany, 65:311-320. 8
[112] Pasqualini V., Pergent-Martini C, Clabaut P, Marteel H., and Pergent G. 2001. Integration of Aerial Remote Sensing, Photogrammetry, and GIS Technologies in Seagrass Mapping. Photogrammetric Engineering and Remote Sensing Vol. 67, No. 1, January 2001, pp. 99-105. 8
[113] Pasqualini V., Pergent-Martini C, Pergent G., Agreila M., Skoufas G., Sourbes L. and Tsirika A. 2005. Use of SPOT 5 for mapping seagrasses: An application to Posidonia oceanica. Remote Sensing of Environment, 94:39-45. 27
[114] Peneva E., Griffith J.A. and Carter G.A. 2008. Seagrass Mapping in the Northern Gulf of Mexico using Airborne Hyperspectral Imagery: A Comparison of Classification Methods. Journal of Coastal Research, Number 244:850-856. 2008. Published By: Coastal Education and Research Foundation DOI: 10.2112/06-0764.1 29
[115] Peneva E.I., Griffith J.A. and Carter G.A. 2007. Mapping seagrass distribution on Horn Island, MS using hyperspectral imagery. ftp://ftp.ecn.purdue.edu/jshan/proceedings/asprs2005/Files/0134.pdf 29
[116] Pergent G. 1990. Lepidochronological analysis of the seagrass Posidonia oceanica (L.) Delile: a standardized approach. Aquatic Botany, 37 (1990) 39-54 39 Elsevier Science Publishers B.V., Amsterdam – Printed in The Netherlands
[117] Pergent-Martini C., Pasqualini V., Ferrat L and Pergent G. 2006. Ecological Data in Integrated Coastal Zone Management: Case Study of Posidonia oceanica Meadows Along the Corsican Coastline (Mediterranean Sea). Environ Manage (2006) 38:889–895 DOI 10.1007/s00267-005-0056-y. 8
[118] Pergent-Martini C, Leoni V., Pasqualini V., Ardizzone G.D., Balestri E., Bedini R., Belluscio A., Belsher T., Borg J., Boudouresque C.F., Boumaza S., Bouquegneau J.M., Buia M.C., Calvo S., Cebrian J., Charbonnel E., Cinelli F., Cossu A., Di Maida G., Dural B., Francour P., Gobert S., Lepoint G., Meinesz A., Molenaar H., Mansour H.M., Panayotidis P., Peirano A., Pergent G., Piazzi L, Pirrotta M, Relini G, Romero G, Sanchez-Lizaso J.L, Semroud R., Shembri P., Shili A., Tomasello A., Velimirov B. 2005. Descriptors of Posidonia oceanica meadows: Use and application. Ecological Indicators 5, 213–230. 5

[119] Phinn S, Roelfsema C, Dekker A, Brando V, Anstee J. 2008. Mapping seagrass species, cover and biomass in shallow waters: An assessment of satellite multi-spectral and airborne hyperspectral imaging systems in Moreton Bay (Australia). Remote Sensing of Environment, 112:3413-3425. 29
[120] Ralph P.J., Macinnis-Ng C.M.O., Frankart C. 2005. Fluorescence imaging application: effect of leaf age on seagrass photokinetics. Aquatic Botany 81 (2005) 69–84. 8
[121] Rasib A.W. and Hashim M. 1997. Mapping Seagrass From Satellite Remote Sensing Data. Proceedings of Asian Conference on Remote Sensing. http://eprints.utm.my/2161/ 27
[122] Ribed P.S. 2002. Submarine vegetation studies using remote sensing: importance in beach measurements. Journal of Environmental Protection and Ecology, 3 No 4, 953-958 (2002) 8
[123] Richardson L.L., LeDrew Ellesworth F. 2006. Remote Sensing of Aquatic Costal Ecosystems Processes. Springer. Science and Management Applications.
[124] Robbins B.D., Bell S.S. 1994. Seagrass landscapes: a terrestrial approach to the marine subtidal environment. TREE vol.9, no 8, doi:10.1016/0169-5347(94)90041-8 119
[125] Sabins F. 1997. Remote Sensing, Principles and Interpretation. W.H. Freeman and Company, New York.
[126] Schmidt K. and Skidmore A.K. 2003. Spectral discrimination of vegetation types in a coastal wetland. Remote Sensing of Environment. 85:92-108. 28
[127] Schmieder K. 1997. Littoral zone - GIS of Lake Constance: a useful tool in lake monitoring and autecological studies with submersed macrophytes. Aquatic Botany 58 (1997) 333-346 19
[128] Schultz S.T. 2008. Seagrass monitoring by underwater videography: Disturbance regimes, sampling design, and statistical power. Aquatic Botany 88 (2008) 228–238. 23
[129] Short F.T. and Coles R.G. (eds). 2001. Global Seagrass Research Methods, p 482. Elsevier Publishing Co., Amsterdam 8
[130] Shortis M., Harvey E., Seager J. 2007. A Review of the Status and Trends in Underwater Videometric Measurement. SPIE Conference 6491, Videometrics IX,IS and T/SPIE Electronic Imaging, San Jose, California, U.S.A., 28 January–1 February 2007 45
[131] Stephens F.C., Louchard E.M., Reid R.P., Maffione R.A. 2003. Effects of microalgal communities on reflectance spectra of carbonate sediments in subtidal optically shallow marine environments. Limnology and Oceanography, 48:535-546. 23

[132] Thorhaug, A., Richardson, A. D. and Berlyn, G. P. 2007. Spectral reflectance of the seagrasses: Thalassia testudinum, Halodule wrightii, Syringodium filiforme and five marine algae. International Journal of Remote Sensing, 28: 7, 1487 — 1501. 8
[133] Toole D.A., Siegel D.A., Menzies D.W., Neumann M.J. and Smith R.C. 2000. Remote-sensing reflectance determinations in the coastal ocean environment: impact of instrumental characteristics and environmental variability. Applied Optics 39(3), 456-469. 75
[134] Vahtmae E, Kutser T, Martin G, Kotta J. 2006. Feasibility of hyperspectral remote sensing for mapping benthic macroalgal cover in turbid coastal waters - a Baltic Sea case study. Remote Sensing of Environment (2006) 101:342-351. 23
[135] Vahtmae E. and Kutser T. 2007. Mapping bottom type and water depth in shallow coastal waters with satellite remote sensing. Journal of Coastal Research, SI 50 (Proceedings of the 9th International Coastal Symposium), 185 – 189. Gold Coast, Australia, ISSN 0749.0208 29
[136] Villegas P. P. 2006. Magnitude of herbivory in Posidonia oceanica (L.) Delile and factors responsible for spatial variation. Available on web: http://www.tesisenxarxa.net/ 19
[137] Wabnitz C.C., Andréfouët S., Torres-Pulliza D., Müller-Karger F. E. and Kramer P.A. 2008. Regional-scale seagrass habitat mapping in the Wider Caribbean region using Landsat sensors: Applications to conservation and ecology. Remote Sensing of Environment Vol. 112, Issue 8, 15 August 2008, Pages 3455-3467 Earth Observations for Marine and Coastal Biodiversity and Ecosystems Special Issue. 27
[138] Walker, D.I., 1989. Methods for monitoring seagrass habitat. Proceedings Rep. Workshop, 20-22 June 1988, Melbourne, Australia, VIMS Working Paper 18, pp. 1-26. 8
[139] Werdell P.J. and Roesler C.S. 2003. Remote assessment of benthic substrate composition in shallow waters using multispectral reflectance. Limnol. Oceanogr., 48 (1, part 2), 557– 567 23
[140] Yang Ch., Yang D., Cao W., Zhao J., Wang G., Sun Zh., Xu Zh., Kumar M. S. R. 2010. Analysis of seagrass reflectivity by using a water column correction algorithm. International Journal of Remote Sensing. 31: 17, 4595 — 4608. 59

Index of Concepts

Index of People